UNCLASSIFIED

AD NUMBER:	AD0835379

LIMITATION CHANGES

TO:

Approved for public release; distribution is unlimited.

FROM:

Distribution authorized to U.S. Gov't. agencies and their contractors; Export Control; 1 Apr 1968. Other requests shall be referred to The Air Force Materials Laboratory, Metals and Ceramics Division, Wright-Patterson AFB, OH 45433

AUTHORITY

AFML, USAF LTR, 12 JAN 1972

THIS PAGE IS UNCLASSIFIED

AFML-TR-68-64

AD835579

ADVANCED METHODS TO TEST
THIN GAGE MATERIALS

F. K. Rose and J. L. Stokes

Solar Division of International Harvester Company

Technical Report AFML-TR-68-64

April 1968

Air Force Materials Laboratory
Air Force Systems Command
Wright-Patterson Air Force Base, Ohio

108
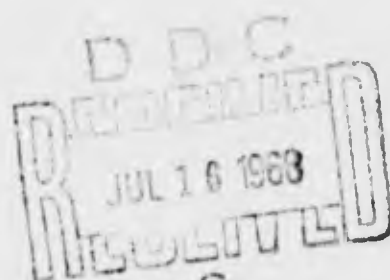
DOCUMENT CONTROL DATA - R & D

(Security classification of title, body of abstract and indexing annotation must be entered when the overall report is classified)

1 ORIGINATING ACTIVITY (Corporate author)	2a. REPORT SECURITY CLASSIFICATION
Solar Division of International Harvester Co. 2200 Pacific Highway San Diego, California 92112	UNCLASSIFIED
	2b. GROUP

3. REPORT TITLE

ADVANCED METHODS TO TEST THIN GAGE MATERIALS

4. DESCRIPTIVE NOTES *(Type of report and inclusive dates)*

Final Report - 1 August 1966 through 31 October 1967

5. AUTHOR(S) *(First name, middle initial, last name)*

Rose, F. K. and Stokes, J. L.

6. REPORT DATE	7a. TOTAL NO. OF PAGES	7b. NO. OF REFS
April 1968	110	15

8a. CONTRACT OR GRANT NO. AF 33(615)-1709	9a. ORIGINATOR'S REPORT NUMBER(S)
b. PROJECT NO. 7351	RDR 1440-19
c. TASK NO. 735106	9b. OTHER REPORT NO(S) *(Any other numbers that may be assigned this report)*
d.	AFML-TR-68-64

10. DISTRIBUTION STATEMENT This document is subject to special export controls and each transmittal to foreign governments or foreign nationals may be made only with prior approval or the Metals and Ceramics Division (MAM), Air Force Materials Laboratory, Wright-Patterson Air Force Base, Ohio 45433.

11. SUPPLEMENTARY NOTES	12. SPONSORING MILITARY ACTIVITY
	Metals and Ceramics Division Air Force Materials Laboratory Wright-Patterson AFB, Ohio

13. ABSTRACT

This report describes work performed during the final year of a three-year program. The overall objective of the program was to develop equipment and methods for measuring the mechanical properties of thin gage alloys (less than 0.015-inch thick). Elastic moduli, fracture toughness, tear resistance, and the mechanical properties of composites are discussed in this third-year report.

A method is described for the measurement of dynamic shear moduli in thin gage materials. Specimens were induced to resonate in torsion, and the moduli were calculated from the equations of Pickett and Spinner. The results indicate that this technique is applicable to materials at least as thin as 0.010 inch An ultrasonic-pulse technique was used on selected alloys to determine dynamic Young's moduli in short-traverse direction, but was not capable of measuring shear moduli. Static shear moduli were determined from shear panels, torsion of thin-wall cylinders, and uniaxial tensile tests.

The fracture characteristics of TZM molybdenum alloy sheet were investigated, and values of fracture toughness were obtained for thinner material because of its tendency to delaminate during testing. The effect of side grooves on the fracture surfaces of symmetrical edge notch specimens and measuring their notched strengths in uniaxial tension.

Three different tear tests were evaluated on selected thin gage alloys which included Type 321 stainless steel (full hard, very brittle), and Type 430 (very ductile). The tests gave a good indication of the tear resistance of both types of material.

The tensile properties of Ti-B composite tapes were measured at room temperature, and at elevated temperatures up to 1500°F. The tensile properties of individual boron filaments were measured at room temperature and 1000°F. The elastic modulus and stress-relaxation properties of the Ti-75A matrix were determined at 1000°F for comparison with the creep data.

DD FORM 1 NOV 65 **1473**

Security Classification

KEY WORDS	LINK A		LINK B		LINK C	
	ROLE	WT	ROLE	WT	ROLE	WT
Extensometry for thin materials						
Thin gage tensile testing						
High temperature tensile testing						
Fracture toughness testing						
Tear testing						
Composite testing						
Fiber testing						

Security Classification

NOTICES

ADVANCED METHODS TO TEST
THIN GAGE MATERIALS

F. K. Rose and J. L. Stokes

FOREWORD

This technical report was prepared by the Research Laboratories of Solar Division of International Harvester Company, San Diego, California, under U.S. Air Force Contract AF33(615)-1709. This contract was initiated under Project No. 7351, "Metallic Materials", Task No. 735106, "Behavior of Metals". The work was administered under the direction of the Metals and Ceramics Division of the Air Force Materials Laboratory, Air Force Systems Command, with Mr. A.W. Brisbane, MAMD, acting as project engineer.

Mr. F.K. Rose, Senior Research Engineer, was principal investigator for the program. Mr. J.L. Stokes made major contributions to the fracture toughness and tear test studies. Work was performed under the supervision of Dr. A.G. Metcalfe, Associate Director of Research.

This report covers work performed from 1 August 1966 through 31 October 1967. Solar's report number is RDR 1440-19.

The manuscript of this report was released by the authors February 1968 for publication.

This technical report has been reviewed and is approved.
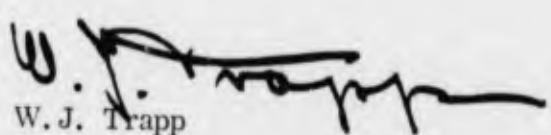
W.J. Trapp
Chief, Strength and Dynamics Branch
Metals and Ceramics Division

ABSTRACT

This report describes work performed during the final year of a three year program. The overall objective of the program was to develop equipment and methods for measuring the mechanical properties of thin gage alloys (less than 0.015-inch thick). Elastic moduli, fracture toughness, tear resistance, and the mechanical properties of composites are discussed in this third-year report.

A method is described for the measurement of dynamic shear moduli in thin gage materials. Specimens were induced to resonate in torsion, and the moduli were calculated from the equations of Pickett and Spinner. The results indicate that this technique is applicable to materials at least as thin as 0.010 inch. An ultrasonic-pulse technique was used on selected alloys to determine dynamic Young's moduli in short-transverse direction, but was not capable of measuring shear moduli. Static shear moduli were determined from shear panels, torsion of thin-wall cylinders, and uniaxial tensile tests.

The fracture characteristics of TZM molybdenum alloy sheet were investigated, and values of fracture toughness were obtained for 0.030-inch and 0.060-inch material. Reliable values were not obtained for thinner material because of its tendency to delaminate during testing. The effect of "side grooves" on the fracture behavior of TZM and L-605 alloys was studied by machining grooves across the surfaces of symmetrical edge notch specimens and measuring their notched strengths in uniaxial tension.

Three different tear tests were evaluated on selected thin gage alloys which included Type 301 stainless steel (full hard, very brittle), and Type 430 stainless steel (very ductile). The tests gave a good indication of the tear resistance of both types of material.

The tensile properties of Ti-B composite tapes were measured at room temperature, and at elevated temperatures up to 1500 F. The tensile properties of individual boron filaments were measured at room temperature and 1000 F. Creep tests were performed on Ti-B composites and boron filaments at 1000 F. The elastic modulus and stress-relaxation properties of the Ti-75A matrix were determined at 1000 F for comparison with the creep data.

CONTENTS

CONTENTS (Cont)

ILLUSTRATIONS

ILLUSTRATIONS (Cont)

ILLUSTRATIONS (Cont)

ILLUSTRATIONS (Cont)

TABLES

I. INTRODUCTION

The need for strong, lightweight structures in space flight applications has created considerable interest in foil gage metals and composite materials. However, before these materials can be used intelligently by the design engineer, their mechanical properties must be measured accurately over the useful temperature range. Unfortunately, the standard test methods for sheet metal are not entirely satisfactory for materials thinner than about 0.015 inch.

This report describes work accomplished during the third year of a three-year program. The overall objective of the program was to develop methods and equipment to accurately measure the mechanical properties of ...'s and composites in thicknesses from 0.015 inch to 0.002 inch.

The first two years of the program were devoted to the design and construction of specialized equipment for tensile and creep testing thin gage materials. This included a tensile machine for testing at temperatures up to 5000 F in high vacuum, an electromechanical extensometer for measuring gage-length strain at elevated temperatures, and a highly successful method for gripping thin gage materials during tensile loading. This equipment was used extensively in the third year of the program.

The tensile testing system developed during the first year (Ref. 1) is shown in Figure 1. It consists of a screw-driven tensile machine designed to accommodate two vacuum chambers. The upper chamber, which contains the load cell, is isolated from the lower chamber and maintained at a low vacuum. This double-chamber design is essential for accurate testing of thin materials in vacuum because it eliminates errors in load measurement resulting from atmospheric pressure effects.

The double-beam extensometer developed during the second year (Ref. 2) is shown in Figure 2 installed in the tensile machine and attached to a thin gage specimen.

The third year of the program had three objectives:

1. To develop methods for the determination of elastic shear moduli in thin sheet.

2. To develop methods for fracture toughness and tear testing of thin sheet.

3. To develop methods for testing thin-gage composites.

The work completed in these areas is discussed in the following sections.

1
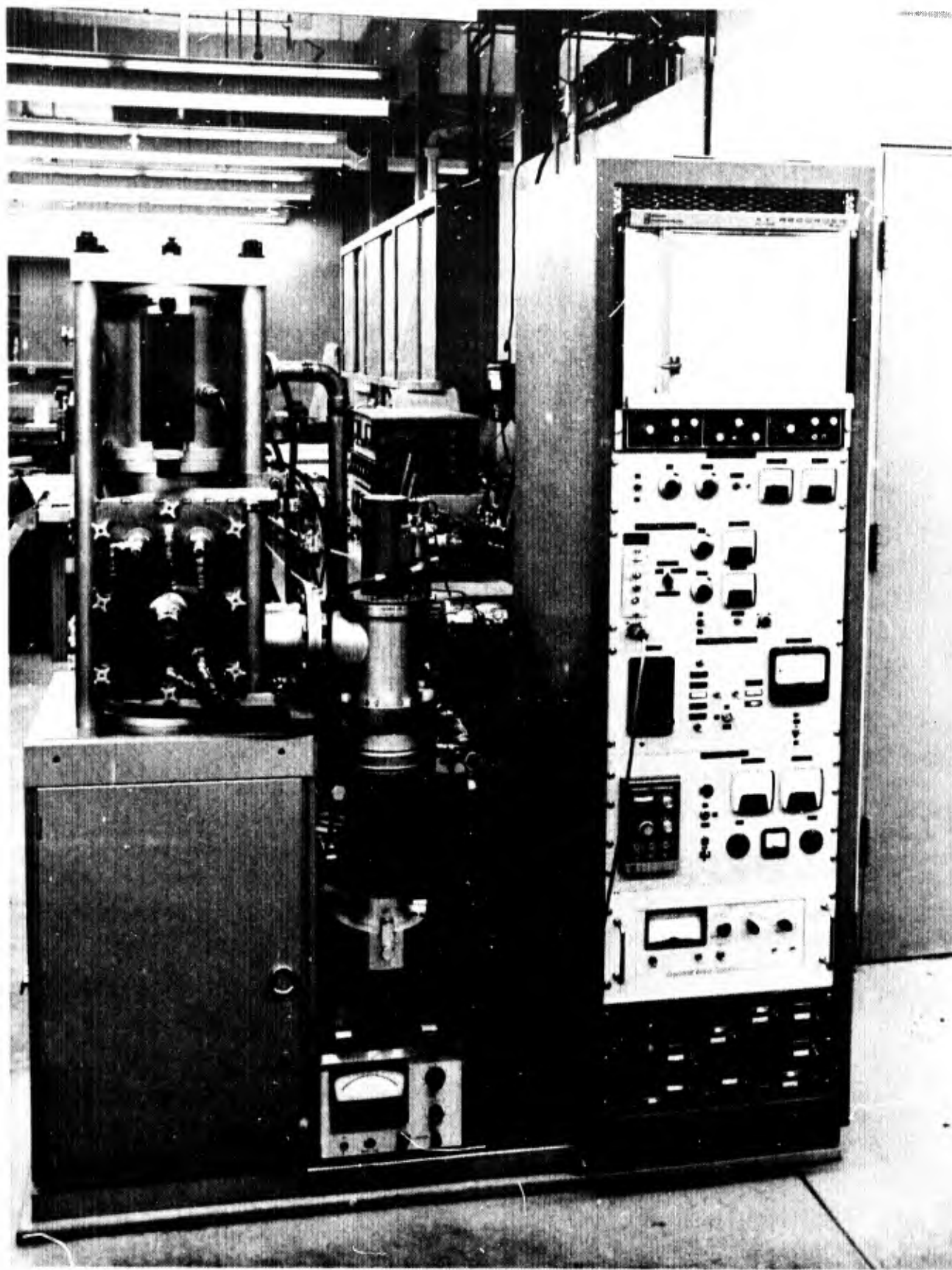
FIGURE 1. THIN GAGE TENSILE TESTING MACHINE

2
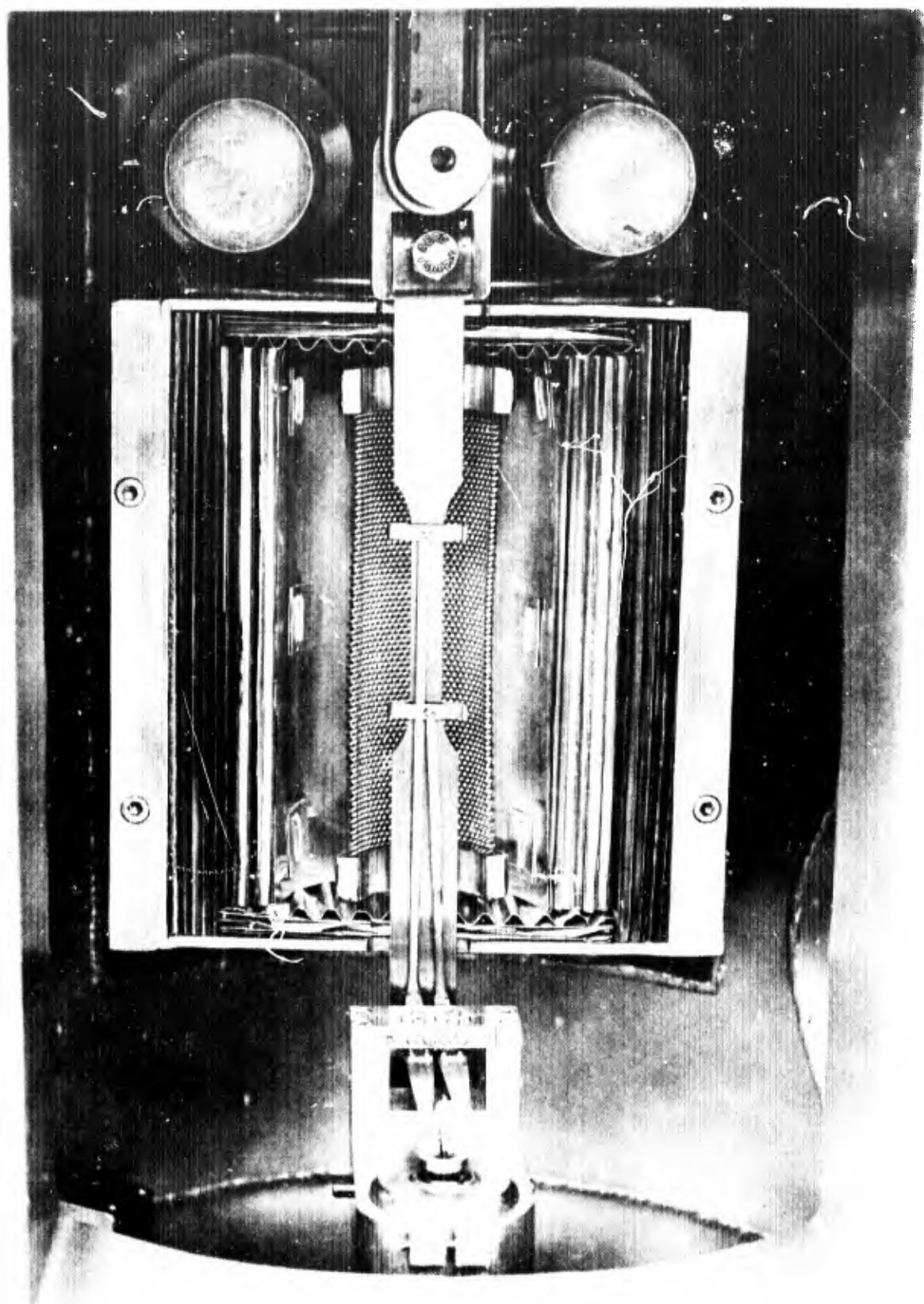
FIGURE 2. DOUBLE-BEAM EXTENSOMETER ATTACHED TO
THIN GAGE SPECIMEN

II. METHODS FOR MEASURING SHEAR MODULUS
OF THIN GAGE MATERIALS

Several methods to determine shear modulus of thin gage materials have been examined. The anisotropic character of many foils makes it essential that the values and methods be related to the generalized theory of elasticity. This theory is discussed first and is followed by description and discussion of the various methods.

2.1 GENERALIZED HOOKE'S LAW

In its most general form Hooke's Law states that each stress component is a linear function of the components of the strain tensor. This relationship can be expressed as follows:

$$\sigma_z = C_{11}\epsilon_z + C_{12}\epsilon_y + C_{13}\epsilon_i + C_{14}\gamma_{zy} + C_{15}\gamma_{zi} + C_{16}\gamma_{yi}$$
$$\sigma_y = C_{21}\epsilon_z + C_{22}\epsilon_y + C_{23}\epsilon_i + C_{24}\gamma_{zy} + C_{25}\gamma_{zi} + C_{26}\gamma_{yi}$$
$$\sigma_i = C_{31}\epsilon_z + C_{32}\epsilon_y + C_{33}\epsilon_i + C_{34}\gamma_{zy} + C_{35}\gamma_{zi} + C_{36}\gamma_{yi}$$
$$\tau_{zy} = C_{41}\epsilon_z + C_{42}\epsilon_y + C_{43}\epsilon_i + C_{44}\gamma_{zy} + C_{45}\gamma_{zi} + C_{46}\gamma_{yi}$$
$$\tau_{zi} = C_{51}\epsilon_z + C_{52}\epsilon_y + C_{53}\epsilon_i + C_{54}\gamma_{zy} + C_{55}\gamma_{zi} + C_{56}\gamma_{yi}$$
$$\tau_{yi} = C_{61}\epsilon_z + C_{62}\epsilon_y + C_{63}\epsilon_i + C_{64}\gamma_{zy} + C_{65}\gamma_{zi} + C_{66}\gamma_{yi}$$

The 36 coefficients C_{ij} are called elastic constants, or coefficients of stiffness. In general, these coefficients are not constants but may depend on location in the body, time and temperature. Actually, the generalized Hooke's Law is not a law but an approximation that is valid for small strains since any continuous function is linear over a sufficiently small range of variables. However, for a given temperature, time, and location in the body, the coefficients are constants and are characteristic of the material.

If the material has two mutually orthogonal planes of elastic symmetry, it can be shown that $C_{14} = C_{24} = C_{34} = C_{56} = 0$. Under these conditions the required elastic constants are:

5

$$
(C_{ij}) = \begin{matrix}
C_{11} & C_{12} & C_{13} & 0 & 0 & 0 \\
C_{21} & C_{22} & C_{23} & 0 & 0 & 0 \\
C_{31} & C_{32} & C_{33} & 0 & 0 & 0 \\
0 & 0 & 0 & C_{44} & 0 & 0 \\
0 & 0 & 0 & 0 & C_{55} & 0 \\
0 & 0 & 0 & 0 & 0 & C_{66}
\end{matrix}
$$

If the elastic constants of a body are invariant under any rotation of coordinates, the material is elastically isotropic. For this special case,

$$C_{11} = C_{22} = C_{33}, \quad C_{12} = C_{21} = C_{13} = C_{31} = C_{32},$$

and $C_{44} = C_{55} = C_{66}$. Therefore, only three elastic constants are required to describe an isotropic solid: C_{11}, C_{12}, and C_{44}.

In engineering notation, $C_{11} = 2G + \lambda$

$C_{44} = G$, and $C_{12} = \lambda$.

where
- E = Young's Modulus
- G = Shear Modulus
- μ = Poisson's Ratio
- λ = Lame's Constant,

$$\text{and} \quad \lambda = \frac{\mu E}{(1 + \mu)(1 - 2\mu)}$$

From these relationships, $E = 2G(1 + \mu)$. Therefore, an isotropic material has only two independent elastic constants.

Unfortunately, most thin gage alloys are not isotropic. Even if the properties do not vary in the plane of the sheet, they are almost always different in the short-transverse direction. If the properties vary from the rolling direction to the transverse direction, as is often the case, the material will have 12 elastic constants. For this reason one must be aware of which modulus is being measured when testing rolled sheet material.

2.2 STATIC METHODS FOR MEASURING ELASTIC MODULI

In order to determine a particular elastic modulus, two quantities must be known: (1) the stress in the material, (2) the strain resulting from that stress. Because, in general, the relationship between stress and load is not simple, any test to determine elastic constants must be carefully designed so that the stress

6

distribution in the specimen is accurately known. If the stress can be computed from the applied load, the strain can be measured experimentally and the elastic constant computed.

An additional difficulty is encountered in attempting to determine a shear modulus from a static test. Even if the shear stress is known, shear strain cannot be measured directly because very small angular changes are involved. Shear strain can only be determined indirectly from linear strains.

2.2.1 Shear Moduli From Uniaxial Tensile Tests

Because the tensile test was considered the most reliable method for determining elastic constants of thin gage materials, static values were first measured by means of uniaxial tensile tests. The results of these tests were then used as an guide in judging the accuracy of other types of tests.

The elastic moduli of five specimens of TD Nickel were determined at room temperature, 500 C, 800 C, and 1100 C. At room temperature, strain was measured in longitudinal and transverse directions with foil-type bonded strain gages. At the elevated temperatures, elongations were measured with the thin gage double beam extensometer. Baseline tensile properties of materials tested are presented in Table I.

Table II summarizes the room-temperature elastic constants which were computed from strain-gage data. These data show marked preferred orientation that varies with the thermomechanical processing of the TDNi sheet, as discussed previously in Section 2.6 of Reference 2, G was computed from the relationship

$$G = \frac{E}{2(1 + \mu)} \cdot \qquad (1)$$

The elevated temperature elastic properties are listed in Table III. Room temperature values of Poisson's ratio were used to compute G. These data are shown in Figure 3 as plots of elastic moduli versus temperature.

Although smooth curves have been fitted to the limited amount of data available, there may be serious deviations from these curves near the ferromagnetic Curie temperature of Nickel (358 C).

2.2.2 Shear Moduli From Thin Gage Panels

Theoretically, it should be possible to produce a condition of pure shear stress in a small square panel by reinforcing the edges with beams of heavier material, pinning the beams at the four corners, and loading the specimen in uniaxial tension across a diagonal. This assumes that no significant bending of the beams will occur.

7

TABLE I

ROOM TEMPERATURE TENSILE PROPERTIES OF TD NICKEL

Specimen	Direction In Sheet	Yield Stress (psi) (0.2%)	Ultimate Tensile Strength	Percent Elongation
0.012-inch TD Ni Heat TDN-C-707	R.D.	71.2	96.2	11.1
0.012-inch TD Ni Heat TDN-C-707	T.D.	73.0	92.1	7.9
0.012-inch TD Ni Heat TDN-948	R.D.	42.3	61.0	9.1
0.012-inch TD Ni Heat TDN-948	T.D.	41.3	60.3	7.8
0.006-inch TD Ni Heat TDN-706	T.D.	69.7	85.5	7.2

Note: R.D. = Rolling Direction
      T.D. = Transverse Direction

TABLE II

ROOM TEMPERATURE ELASTIC MODULI OF TD NICKEL

Specimen	Direction In Sheet	Tensile Modulus, E, (psi x 10^6)	Poisson's Ratio	Shear Modulus, G, (psi x 10^6)
0.012-inch TD Ni Heat TDN-C-707	R.D.	34.0	0.21	14.1
0.012-inch TD Ni Heat TDN-C-707	T.D.	36.1	0.22	14.8
0.012-inch TD Ni Heat TDN-948	R.D.	18.1	0.34	6.74
0.012-inch TD Ni Heat TDN-948	T.D.	18.2	0.34	6.80
0.006-inch TD Ni Heat TDN-706	T.D.	33.6	0.27	13.2

Note: R.D. = Rolling Direction
      T.D. = Transverse Direction

TABLE III

ELEVATED-TEMPERATURE ELASTIC MODULI OF TD NICKEL*

Material	Direction In Sheet	Room Temperature		Temperature					
				500 C		800 C		1100 C	
		E	G	E	G	E	G	E	G
0.012-inch TDN-C-707	R.D.	34.0	14.1	23.4	9.5	18.0	7.5	14.9	6.2
	T.D.	36.1	14.8	27.9	11.4	22.6	9.3	15.9	6.5
0.012-inch TDN-948	R.D.	18.1	6.7	12.1	4.5	9.3	3.5	6.5	2.4
	T.D.	18.2	6.8	12.6	4.7	11.1	4.1	7.4	2.8
0.006-inch TDN-706	T.D.	33.6	13.2	24.0	9.5	18.2	7.2	-	-

* All values in million psi

Note: R.D. = Rolling Direction
T.D. = Transverse Direction
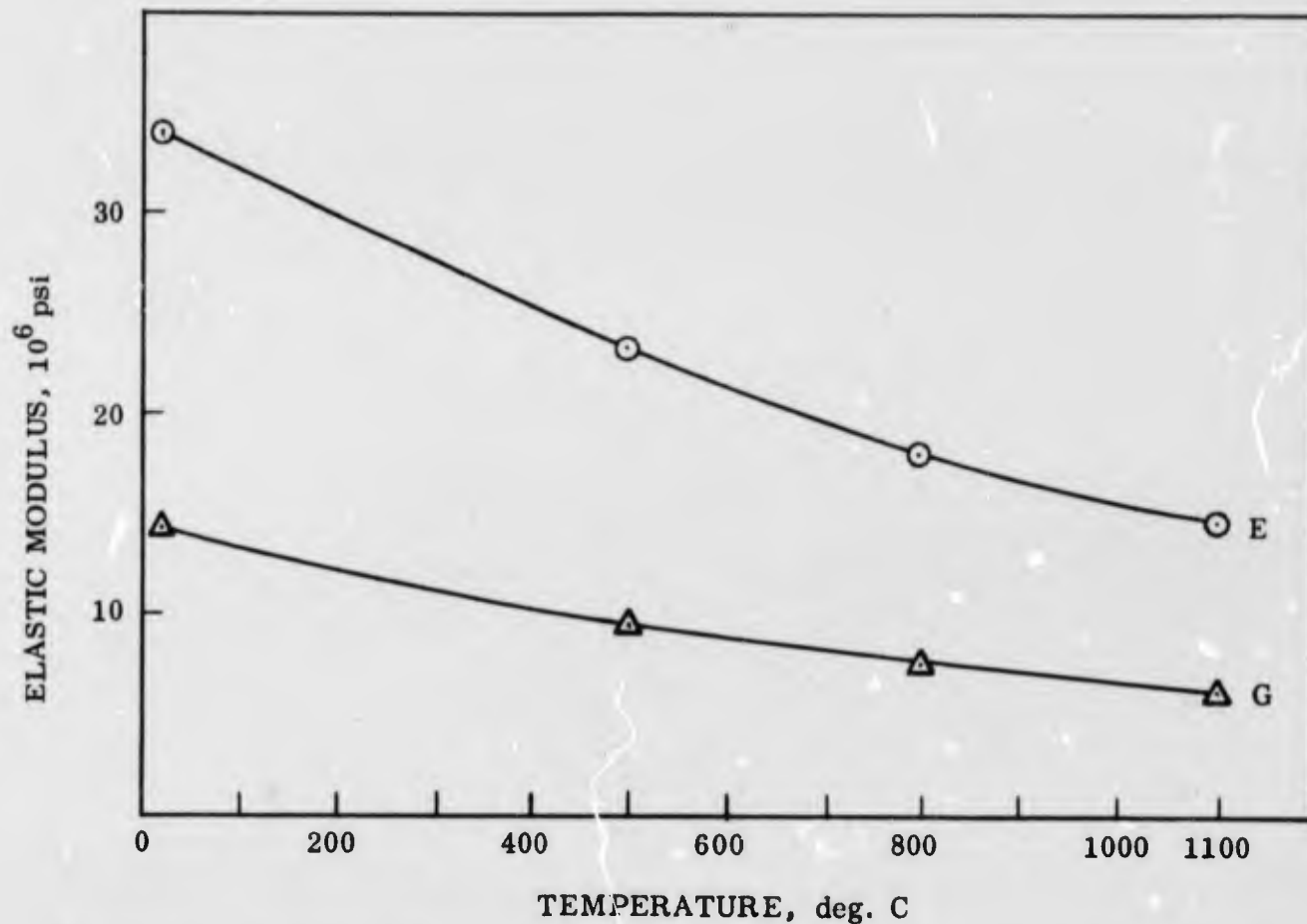
FIGURE 3. ELASTIC MODULI VERSUS TEMPERATURE FOR 0.012-INCH THICK TD NICKEL SHEET (Rolling Direction)

9

Small panels were made from 0.012-inch thick TD Nickel by diffusion bonding the beams to the sheet, and from 17-7 PH stainless steel by spot welding (using a row of overlapping spots along the beam). The diffusion-bonded TD Nickel specimen is shown in Figure 4. The panel is 2-3/4 inches square and the beams are 0.060-inch thick x 1/4-inch wide x 2-1/2 inches long. The effective area after bonding is 1-3/4-inches square.

The panels were loaded in uniaxial tension, and strain was measured by means of strain-gage rosettes (3 gages at 45°) mounted at the centers of the panels. The orietation of the gages is shown in Figure 5.

The stainless steel specimen was tested with a rosette on one side only, and the strain was found to be very non-linear due to bending of the panel. Therefore, the TD Nickel specimen was tested with a rosette on each side with the gages in a bridge circuit. The strain-gage data are plotted versus load in Figure 6.
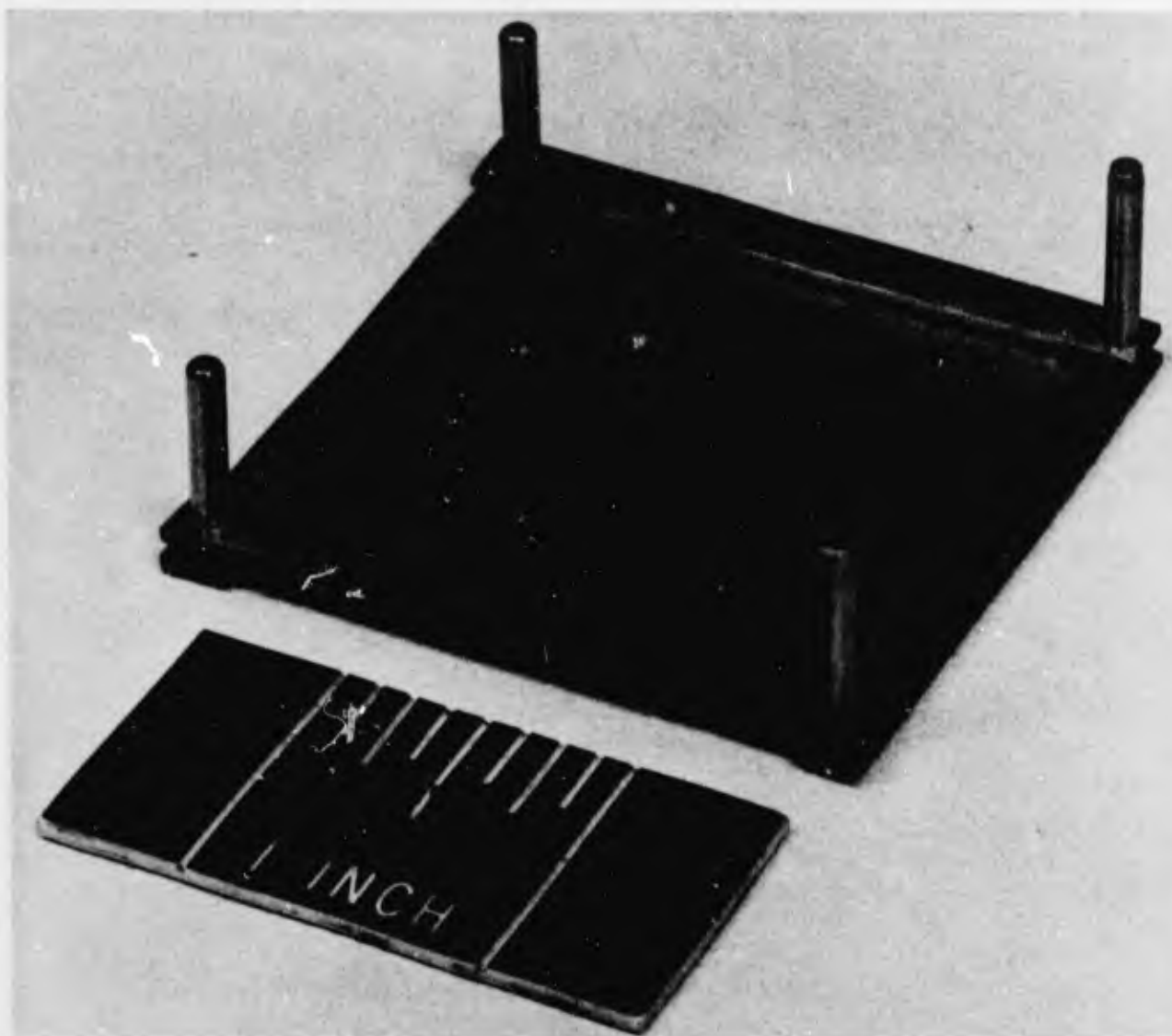
FIGURE 4. DIFFUSION BONDED TD NICKEL SHEAR PANEL

10
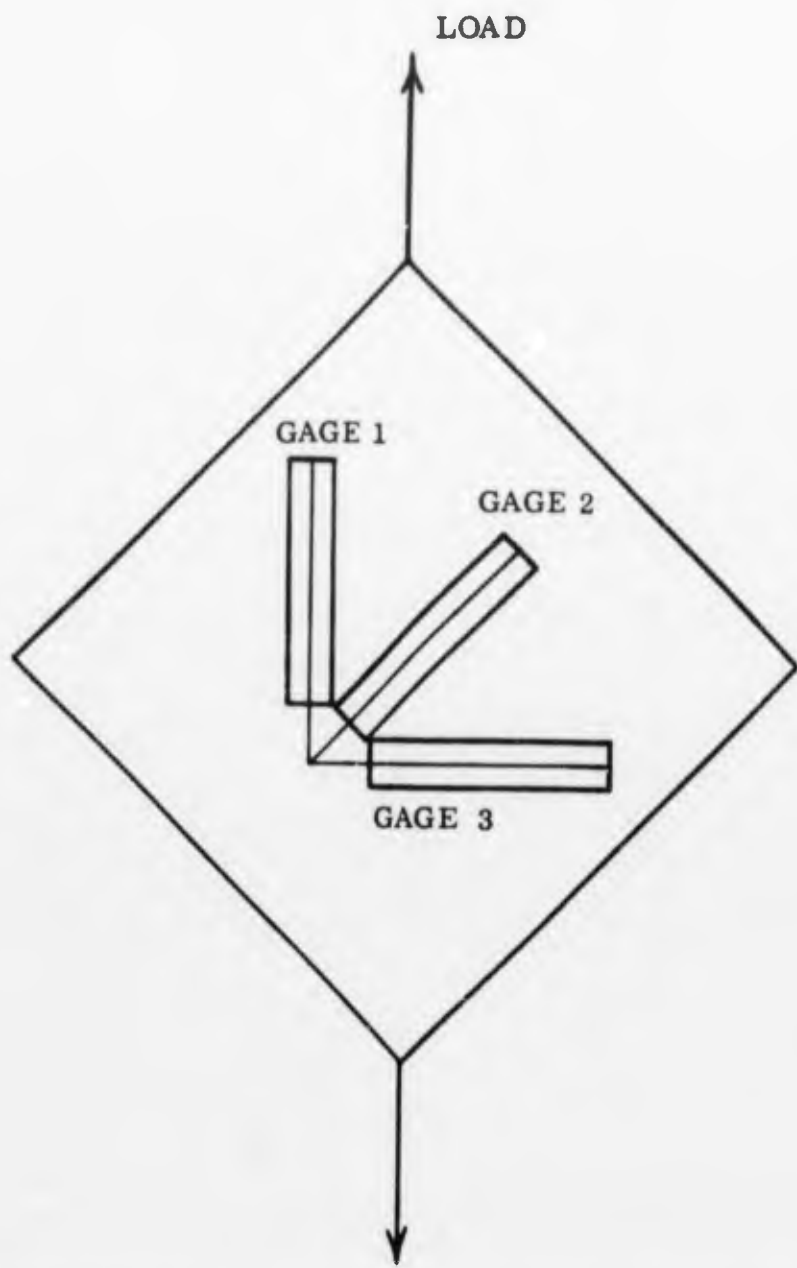
LOAD

FIGURE 5. ORIENTATION OF 45-DEGREE STRAIN-GAGE ROSETTE ON SHEAR
PANEL

These strain data were then plotted on a Mohr's circle to determine a value
of shear strain at maximum load. A load of 160 pounds was found to produce a
shear strain of 484 μ-radians. The resolved shear stress resulting from this load
was calculated to be 5380 psi. This results in a shear modulus of 11.1×10^6 psi.
The shear modulus from tensile data was found to be 14.1×10^6 psi for the same
material (Heat TDN-C-707). This discrepancy may be due to a nonuniform stress
distribution in the shear panel caused by bending of the beams, or due to anisotropy
of the material.
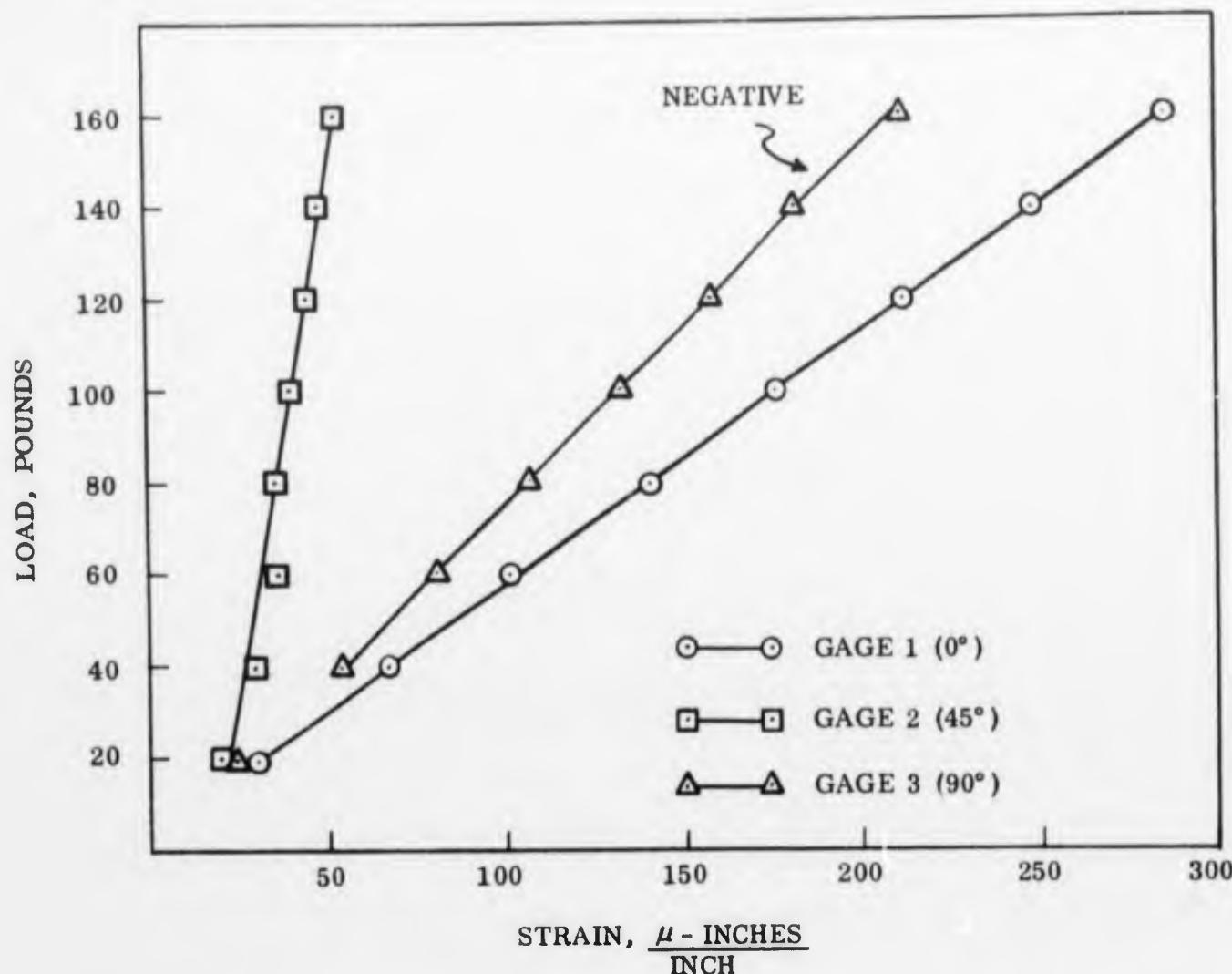
FIGURE 6. LOAD VERSUS STRAIN FOR 0.012-INCH THICK TD NICKEL SHEAR
PANEL

2.2.3 Shear Moduli From Torsion of Thin Wall Cylinders

Small thin wall cylinders were made from TD Nickel and Type 17-7 PH
stainless steel by wrapping the sheet material around a rod of the desired diameter
and heating at approximately 2000 F for 15 minutes. Several one-half-inch diameter
cylinders made this way are shown in Figure 7.

Strain gage rosettes were mounted on the specimens, and they were loaded
in torsion on the small fixture shown in Figure 8. The orientation of the rosettes is
shown in Figure 9. Shear strain was determined by Mohr's circle analyses of the
measured linear strains. Shear stress was calculated by means of the following
relationships which are based on St. Venant's elastic-membrane analogy (Ref. 3):

12

FIGURE 7. THIN WALL CYLINDER MADE FROM 0.012-INCH THICK SHEET

13
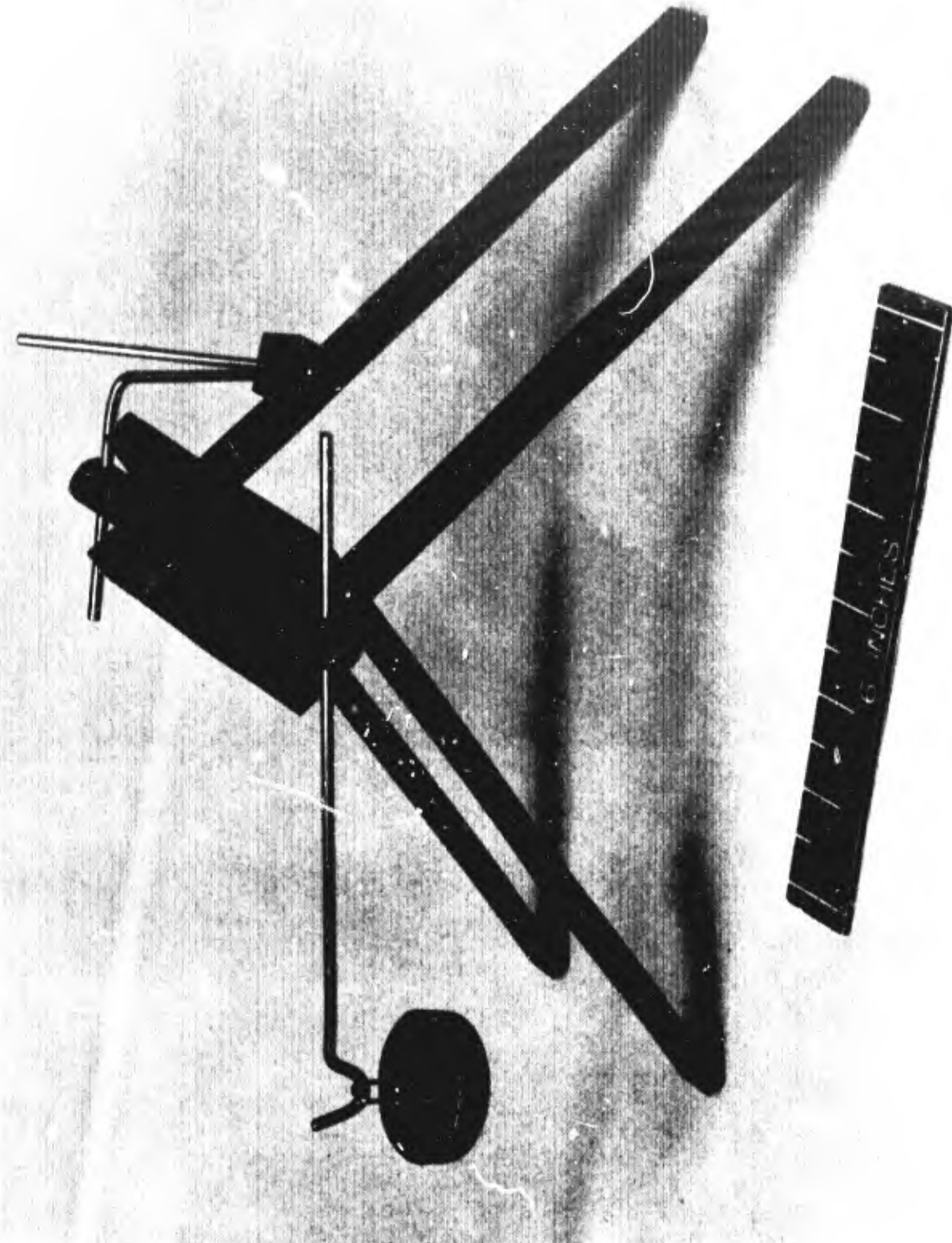
FIGURE 8. FIXTURE FOR TORSION TESTING OF THIN WALL CYLINDERS

14
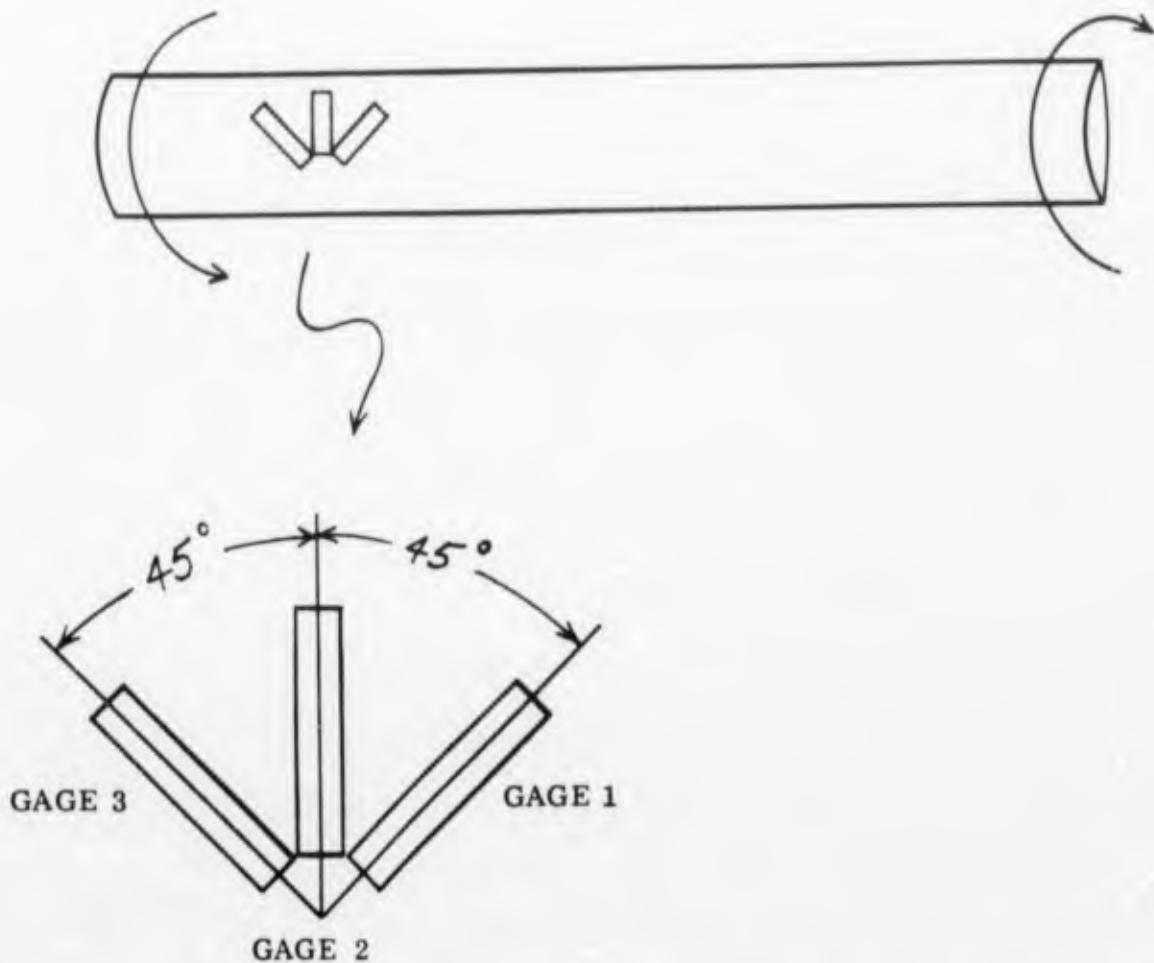
FIGURE 9. ORIENTATION OF STRAIN-GAGE ROSETTES ON THIN WALL CYLINDERS

For a Split Cylinder

$$\tau = \frac{3T}{2\pi rt^2}$$
where T = Torque
       r = radius
       t = thickness   (2)

$$G = \frac{3T}{2\pi rt^3} \cdot \frac{1}{\theta}$$
where θ = angle of twist per unit length   (3)

For a Closed Cylinder

$$\tau = \frac{3T}{2\pi r^2 t}$$ (4)

$$G = \frac{T}{2\pi r^3 t} \cdot \frac{1}{\theta}$$ (5)

To compare split versus closed cylinders, a $\frac{1}{2}$-inch-diameter stainless steel cylinder was closed by electron-beam welding the longitudinal seam. This does not produce an ideal specimen, however; because the properties of the welded zone are not identical to those of the parent material.

No closed cylinders were made from TD Nickel because this material does not lend itself to welding.

Plots of torque versus strain for the four cylinders which were tested are shown in Figures 10 through 13. Specimen dimensions and calculated values of stress, shear strain, and shear moduli are summarized in Table IV.
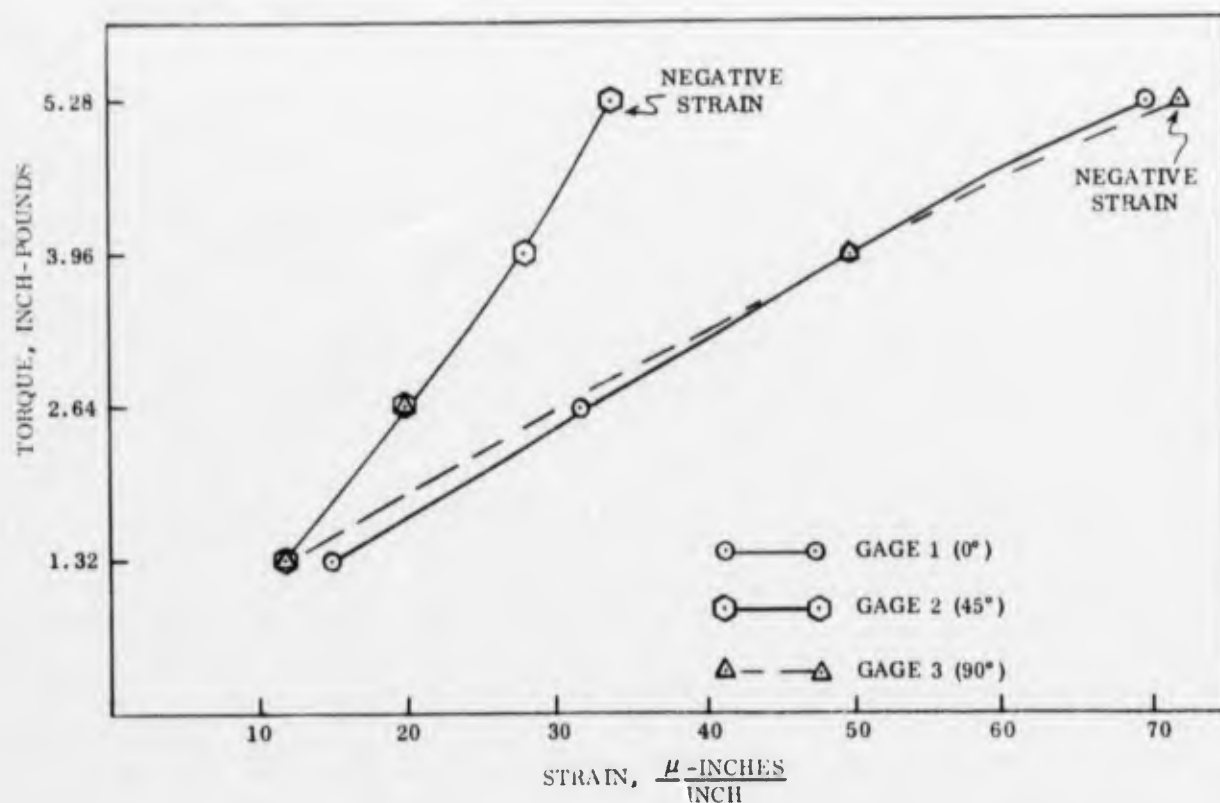
FIGURE 10. TORQUE VERSUS STRAIN FOR 1/2-INCH DIAMETER 0.012-INCH THICK 17-7 PH STAINLESS STEEL CYLINDER CLOSED BY ELECTRON BEAM WELDING

16
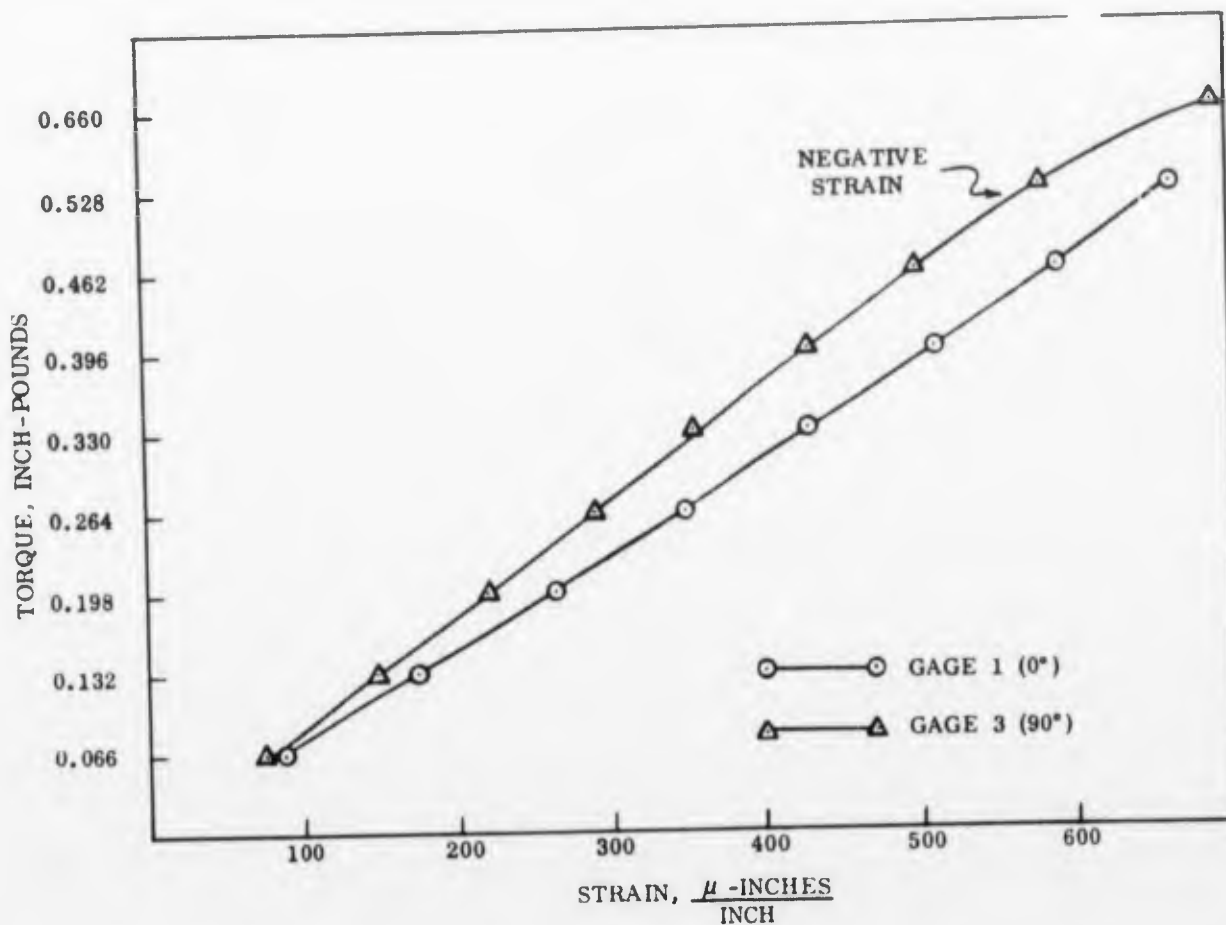
FIGURE 11. TORQUE VERSUS STRAIN FOR 1/2-INCH DIAMETER 0.012-INCH THICK TD NICKEL SPLIT CYLINDER

2.3 DYNAMIC METHODS FOR MEASURING ELASTIC MODULI

2.3.1 Shear Modulus by Torsional Resonance

The elastic properties of bulk solids have been determined for about 20 years by the method developed by Pickett (Ref. 4). The method of Pickett related the elastic modulus to the resonant frequency by

$$E = D \, m \, f^2 \tag{6}$$

where E is either Young's modulus or the shear modulus, depending upon the mode of vibration,

D is a geometrical shape factor

m is the mass of the specimen

f is the fundamental resonant frequency of either flexural or torsional vibration.

17
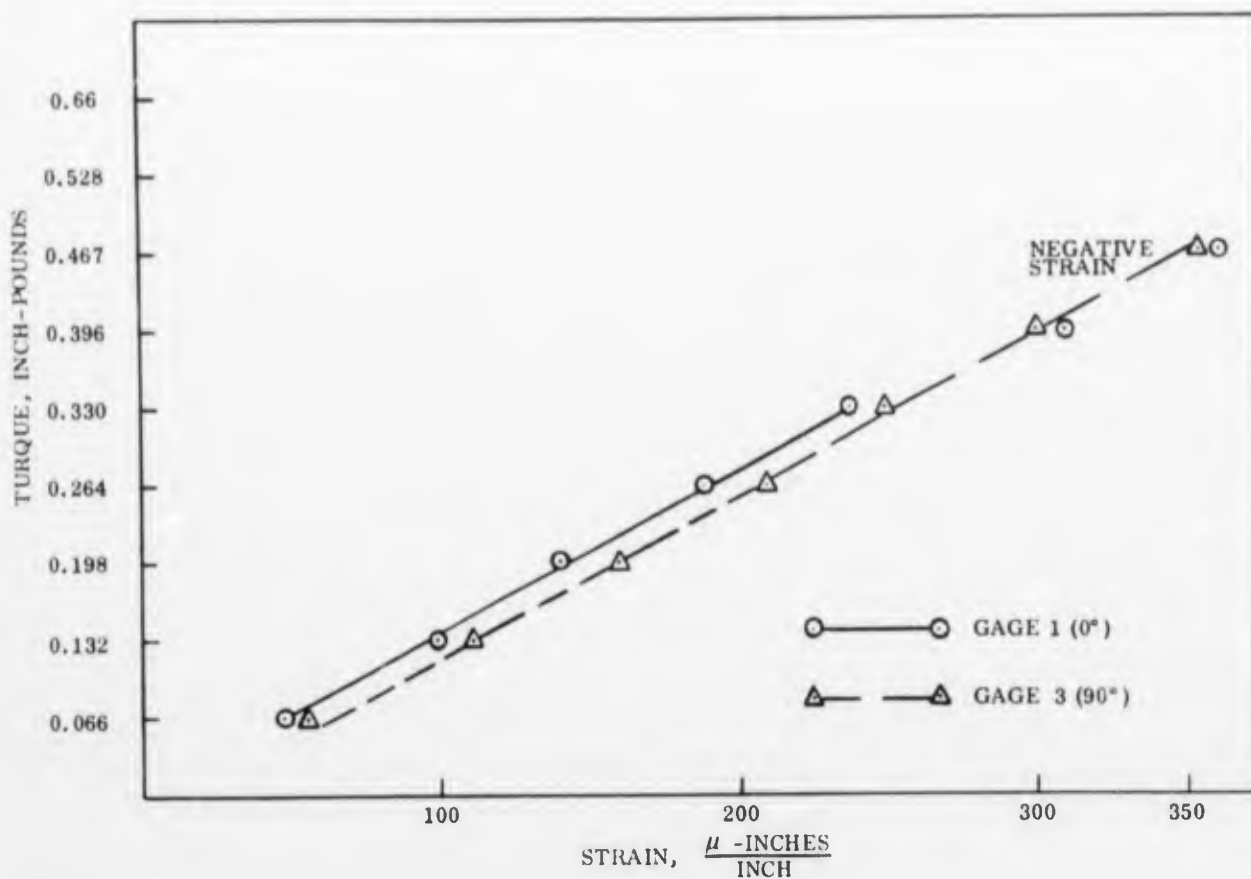
FIGURE 12. TORQUE VERSUS STRAIN FOR ONE-INCH DIAMETER 0.012-INCH THICK TD NICKEL SPLIT CYLINDER

For the shear modulus determination from torsional vibration of a prixm, the

For the shear modulus determination from torsional vibration of a prism, the shape factor

$$D = \frac{4RL}{S} \tag{7}$$

where L is the length, S is the cross-sectional area of the specimen, and for a rectangular prism

$$R = \frac{a/b + b/a}{4a/b - 2.51(a/b)^2 + 0.21(a/b)^6} \tag{8}$$

where a is the thickness and b is the width.

The applicability of equation (8) to thin materials was questionable as R rapidly approaches infinity as thickness decreases.

For bulk materials, the width-to-thickness ratio need not exceed 2 and the corresponding R value is a minor shape factor correction close to unity (1.376); how-ever, thin gage specimens of convenient size must have a width to thickness ratio of at least 10, the power terms in the denominator of equation (8) become negligible, and the shape factor correction becomes very large.

18
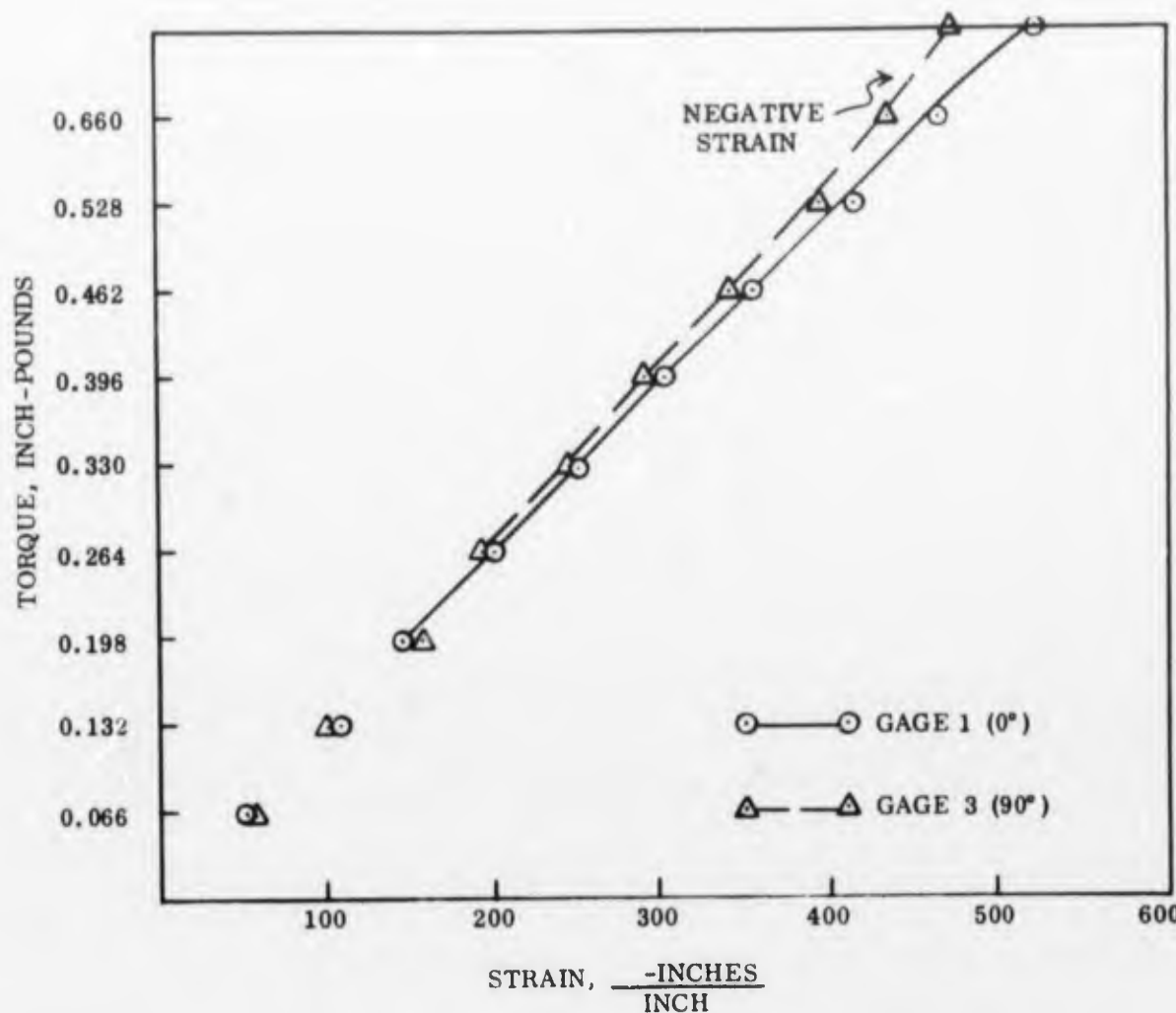
FIGURE 13. TORQUE VERSUS STRAIN FOR ONE-INCH DIAMETER 0.012-INCH
THICK 17-7 PH STAINLESS STEEL SPLIT CYLINDER

To determine the validity of the above expressions for the calculation of
shear modulus of thin materials a series of specimens was prepared from stainless
steel sheet. The thickness of the specimens was varied from 0.063 to 0.011 inch,
while maintaining a b/a ratio greater than 10. The fundamental frequencies for
torsional vibration were measured using the well known double wire suspension
technique shown in Figure 14A. Changes in specimen thickness, width, and length
were progressively made moving from 0.063 to 0.019 inch thick sheet. The effect
of each size change on the calculated shear modulus is shown in Table V. The modu-
lus values were slightly affected by size as specimens of the same thickness were
made from the same sheet, and thus should have identical moduli.

Difficulties were encountered when the double suspension technique was
applied to 0.010-inch-thick material: the low mass of the specimen would not
straighten the 0.004-inch-diameter nickel wires; the mode of vibration was difficult
to determine; and the resonant frequencies were not sharply defined and varied with
amplitude which indicated loading of the specimen by the suspension.

19

TABLE IV

SHEAR MODULI DETERMINED FROM TORSION
TESTS ON THIN-WALL CYLINDERS

Specimen Description	Computed Shear Stress (psi)	Shear Strain (μ-Radians)	G* (10^6 psi)	G (10^6 psi) Based on Angular Deflection
0.012 In. TD Nickel $\frac{1}{2}$"-D. Split Cylinder 5 Inches Long Heat TDN-C-707	6720	700	9.6	11.4
0.012 In. TD Nickel 1"-D. Split Cylinder 8 Inches long Heat TDN-C-707	4240	460	9.21	9.35
0.012 In. 17-7 PH s.s. $\frac{1}{2}$"-D Closed Cylinder 5 Inches long	560	80	7.0	—
0.012 In. 17-7 PH s.s. 1"-D Split Cylinder 8 Inches long	4380	536	8.17	9.83

* Strain-Gage Data

These difficulties were eliminated by using the specimen shape and suspension method shown diagrammatically in Figure 14B. A square specimen, approximately 1 inch per side, was supported rigidly at its midpoint by two opposed cone-point clamps. The specimen was induced to resonate in torsion by means of a 0.004-inch-diameter nickel wire connected between the electrodynamic shaker and the specimen. The wire was spotwelded to the specimen at a position halfway between the support clamp and one corner. Resonance was detected by means of a phonograph "cutter" head coupled lightly to the specimen with a 1/16-inch-diameter aluminum oxide "stylus".

The experimental set-up for the evaluation and development of this dynamic method is shown in Figure 15. The specimen was excited to resonate by the small electrodynamic shaker which was mounted in the tripod stand above the specimen. The shaker was driven at frequencies from 20 cps to 20,000 cps by an amplifier and audio-oscillator. The oscillator frequency was fed to the horizontal amplifier of the oscilloscope and output of the phonograph "cutter" head to the vertical amplifier of the 'scope. In-phase resonance was indicated by the 45° Lissajou figure appearing on the 'scope in Figure 15. By probing the specimen with the stylus, as shown in Figure 16, the mode of vibration was easily determined. An electronic counter was used to measure the frequency of resonance.

Suspension Wire from Vibrator

Suspension Wire
to Phono Pick-up

A. RECTANGULAR SPECIMEN
WITH DOUBLE WIRE SUSPENSION

Coupling Wire from Vibrator

Rigid Cone-Point Suspension

Aluminum Oxide
Stylus

B. SQUARE SPECIMEN WITH
RIGID SUPPORT AT CENTER
NODE

Phono Cutter Head
Pick-up
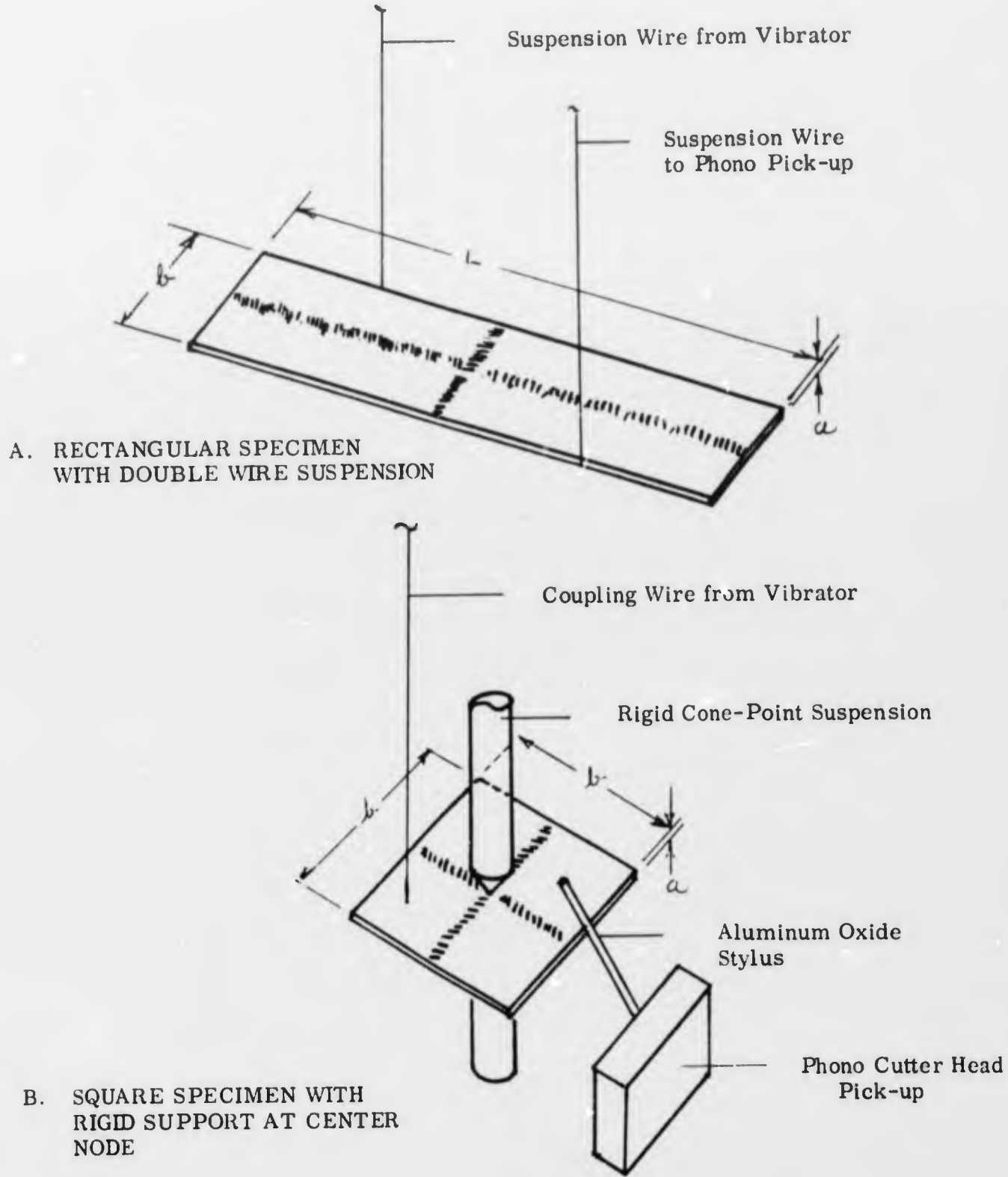
FIGURE 14. DYNAMIC SHEAR MODULUS SPECIMENS AND SUSPENSION SYSTEMS

21

TABLE V

SHEAR MODULUS DETERMINATIONS ON STAINLESS STEEL (T-321)

RECTANGULAR BEAM SPECIMENS SUSPENDED FROM TWO 0.004-INCH WIRES (Fig. 14A)

a Thickness (Inch)	b Width (Inch)	L Length (Inch)	m Mass (Gms)	$\frac{b}{a}$	R	f Resonant Frequency (cps)	G Shear Modulus $(\times 10^6$ psi)
0.0627	0.7565	6.025	36.436	12.07	38.60	1626	10.74
0.0627	0.7445	4.00	23.754	11.87	37.46	2470	10.62
0.0406	0.7521	4.00	15.543	18.53	88.90	1596	10.67
0.0406	0.4113	4.00	8.504	10.13	27.60	2899	10.95
0.0189	0.4007	3.00	2.882	21.2	116.1	6148	10.37

FIGURE 15. EQUIPMENT FOR SHEAR MODULUS DETERMINATION BY TORSIONAL RESONANCE OF THIN SHEET

22
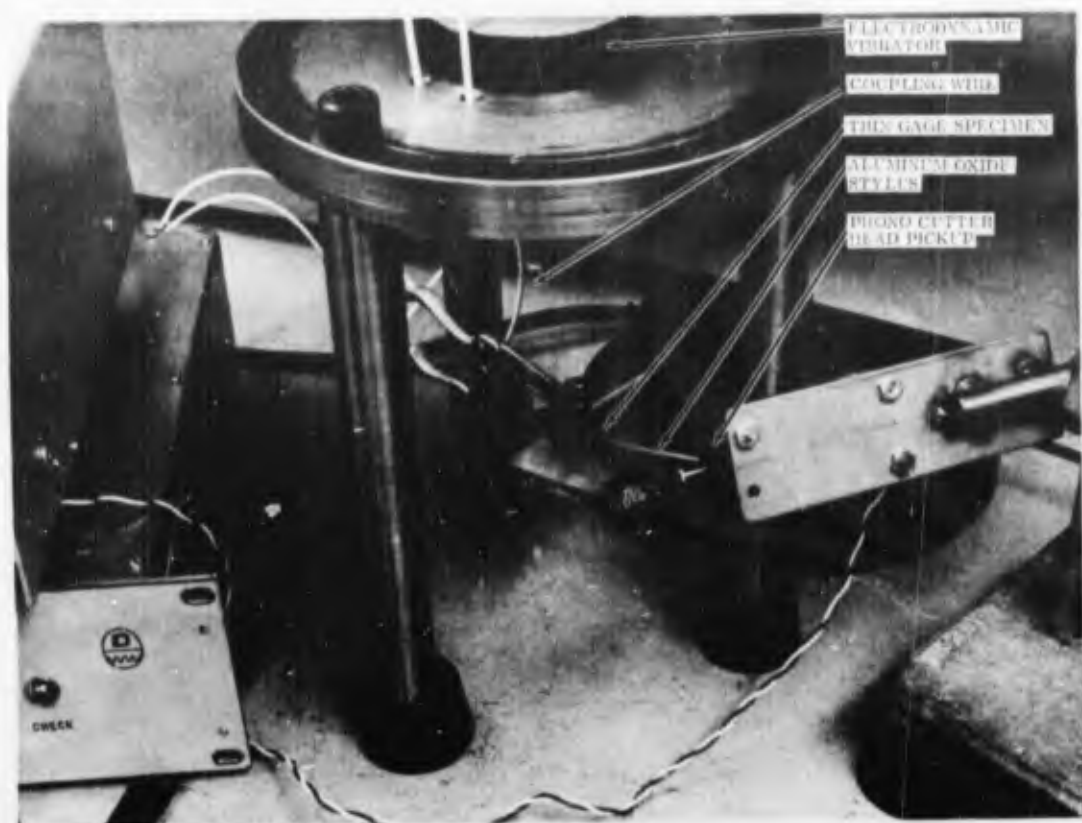
FIGURE 16. CLOSEUP VIEW OF THIN SHEET SPECIMEN POSITIONED FOR VIBRATION IN TORSIONAL MODE

The shear modulus values were determined for four thin gage alloys and are presented in Table VI. These alloys were selected to test this dynamic method over a very wide range of elastic properties. All of the specimens had very sharply defined resonant frequencies that were reproducible within about 2 cps when the specimens were removed and then reinstalled in the cone-point clamps. The values obtained for the shear modulus for the stainless steel, columbium, and molybdenum alloys are in good agreement with values for thicker materials.

The shear modulus value of 9.57×10^6 psi for TD Nickel is in disagreement with the static values reported earlier for the same material (Heat TDN-C-707) in Table II. The mode of resonant vibration of this specimen was slightly abnormal and differed from that of the other materials which are known to be more isotropic. The modes of torsional resonance that were determined by probing the thin gage specimens is shown in Figure 17. The circles indicate the oscilloscope traces obtained at various locations on the specimen. A horizontal trace indicated a node or lack of vibration; a 45 degree line with a positive slope indicated vibrations in-phase with the wire attachment point; and a 45 degree line with a negative slope indicated vibrations 180 degrees out of phase with the attachment point. The TD Nickel specimen at resonance had two opposite quadrants in-phase while the other two quadrants were inactive.

23

TABLE VI

SHEAR MODULUS DETERMINATIONS ON SEVERAL THIN GAGE ALLOYS

SQUARE PLATE SPECIMENS CLAMPED AT MIDPOINT (Fig. 14B)

Material	a Thickness (Inch)	b Width (Inch)	L Length (Inch)	m Mass (Gms)	$\frac{b}{a}$	R	f Resonant Frequency (cps)	G Shear Modulus ($\times 10^6$ psi)
Stainless Steel (T-321)	0.0117	1.606	1.606	3.800	137.2	4715	573	11.45
Cb752	0.0122	1.203	1.203	2.599	98.7	2445	672	5.36
TZM	0.0121	1.202	1.202	2.8503	99.4	2463	1126	16.82
TD Nickel	0.0123	1.104	1.104	2.1973	89.9	2020	1078	9.57

2.3.2 Elastic Moduli From Sound-Velocity Measurements

In principle, the ultrasonic technique is relatively simple. The velocity of sound in a solid is related to the elastic constants as follows:

$$V^2 \text{ (longitudinal wave)} = \frac{E}{\rho} \frac{(1-\mu)}{(1+\mu)(1-2\mu)} \tag{9}$$

$$V^2 \text{ (shear wave)} = \frac{G}{\rho} \tag{10}$$

E = Young's Modulus

G = Shear Modulus

μ = Poisson's Ratio

ρ = Density

An investigation of the applicability of ultrasonic techniques for the determination of the elastic moduli of thin gage alloys was made possible through the fine cooperation of the Los Alamos Scientific Laboratories. A Solar engineer went to the Los Alamos Laboratories and conducted measurements of sound velocity in thin gage alloys.

The setup shown schematically in Figure 18 was used to measure the velocity of sound in four alloys: 0.0118-inch thick Type 17-7PH stainless steel, 0.0105-inch thick L-605, 0.0125-inch thick TZM, and 0.010-inch thick Ti-6Al-4V. The following equipment was used:

24
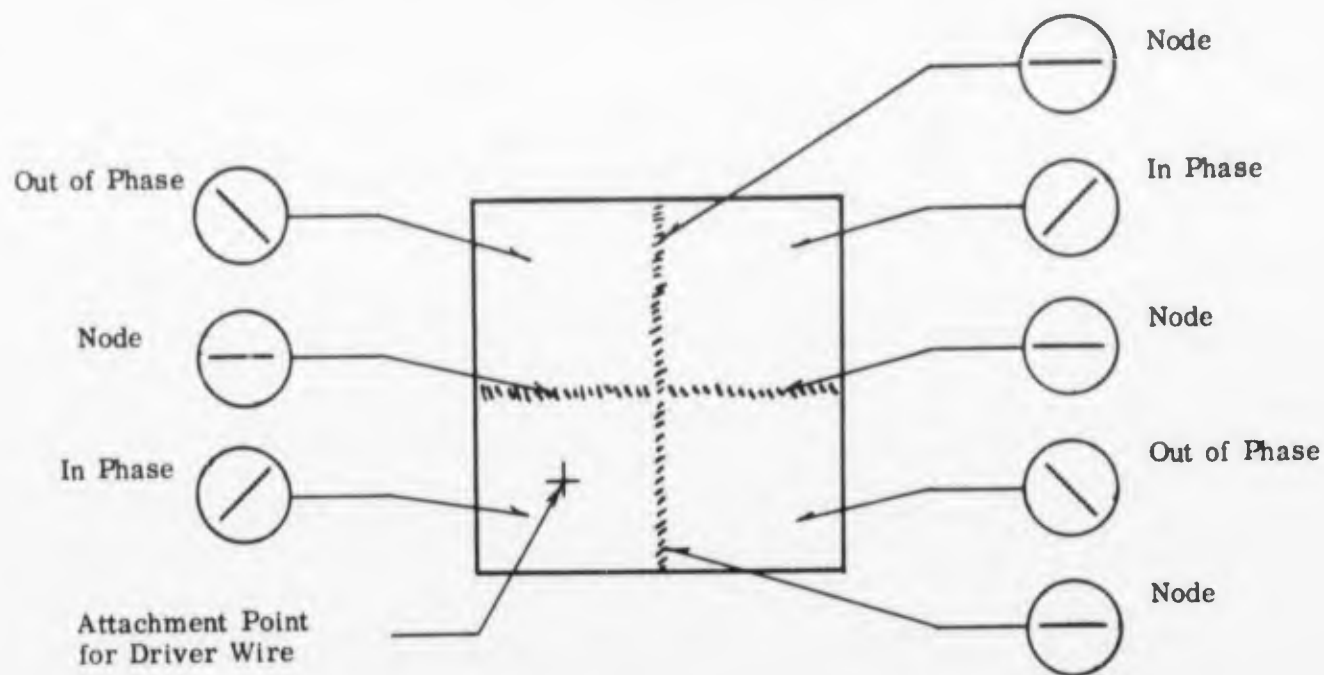
A. Normal Torsional Mode
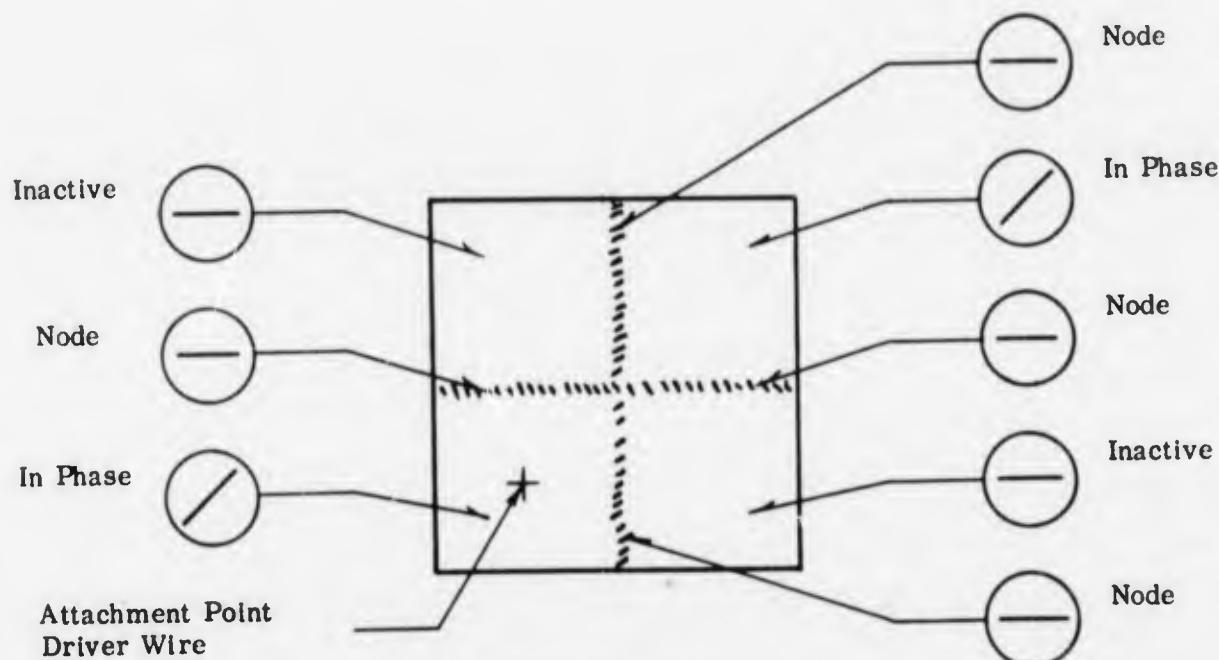
B. Torsional Mode for TD Nickel

FIGURE 17. MODE FOR TORSIONAL RESONANCE FOR THIN GAGE SPECIMENS
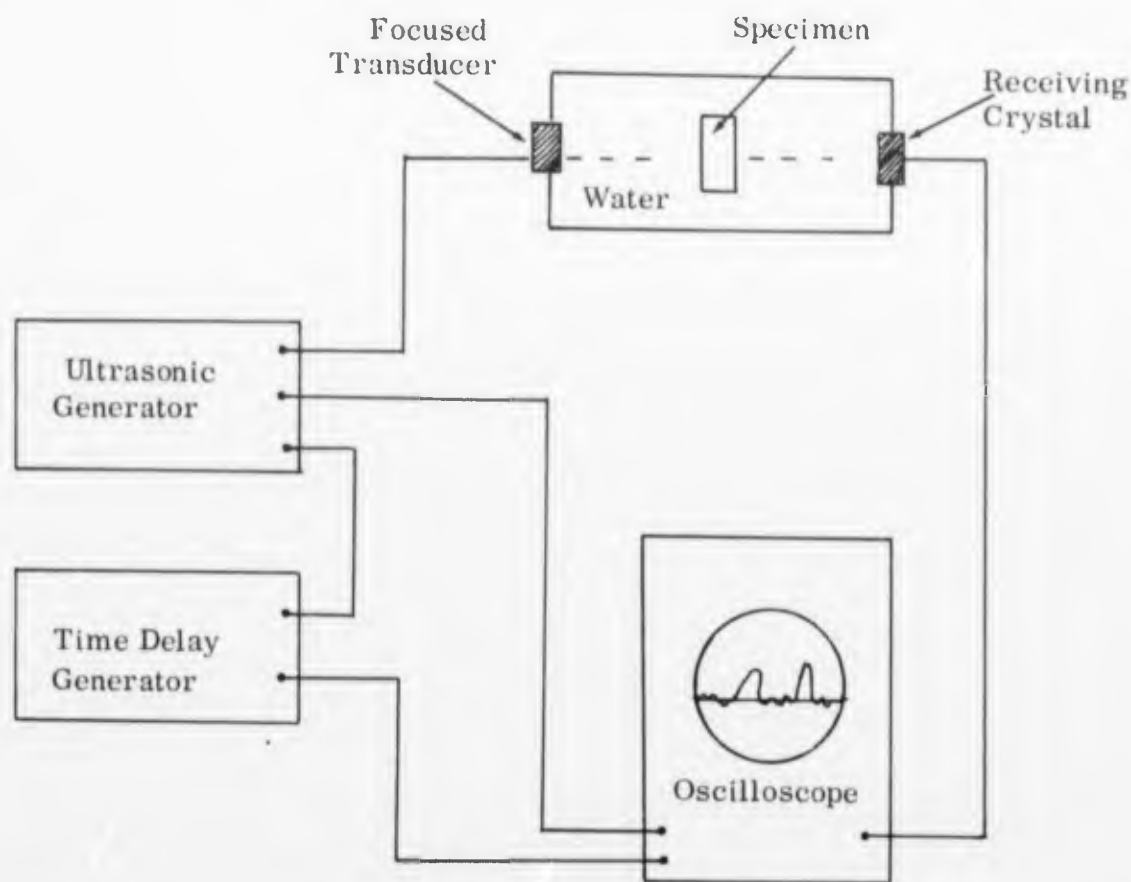
FIGURE 18. EXPERIMENTAL SETUP FOR SOUND VELOCITY MEASUREMENTS
IN THIN GAGE ALLOYS

Ultrasonic Generator:	Don Erdman Company High Res System Model 1177 2 μ-sec pulse with 2×10^{-9} sec rise time at 22 mc.
Transducer:	Erdman focused crystal with 0.050-inch-diameter beam.
Electronic Accessories:	3 Hewlett-Packard 10 db wide-band amplifiers, Type 46-AR 1 General Radio Company time-delay generator. 1 Tektronix Type 585 oscilloscope

The ultrasonic generator was used to deliver a short pulse of high-frequency
sound to the specimen by means of a focusing transducer. The pulse passed through
the sample and was picked up by a receiving crystal on the other side. The time for
the pulse to pass through the specimen was measured with an oscilloscope. The test
was conducted in water to achieve efficient coupling between transducer and specimen.

26

The velocities of the longitudinal waves were measured with the beam perpendicular to the specimen surfaces. Young's moduli calculated from these velocities are, therefore, short-transverse moduli. Each specimen was then rotated slowly with respect to the beam in an attempt to obtain a shear wave in the material. In the thicker materials the conversion from longitudinal mode to shear mode occurs when the specimen surface is at an angle of approximately 30° to the ultrasonic beam. Unfortunately, it was not possible to obtain pure shear waves in the thin gage alloys tested. Instead, the longitudinal waves tended to convert to Lamb waves at the critical angle.

The velocities of longitudinal sound waves, and the calculated moduli of the 4 alloys tested are listed in Table VII. A Poisson's ratio of 0.3 was assumed in all calculations.

TABLE VII

YOUNG'S MODULI CALCULATED FROM SOUND VELOCITIES
IN FOUR SELECTED THIN GAGE ALLOYS

Alloys	Thickness Inches	Velocity of Longitudinal Sound wave, cm/sec x 10^5	Young's Modulus In Short-Transverse Direction, psi x 10^6
17-7 PH s.s.	0.0118	5.12	30.2
L-605	0.0105	5.93	33.3
TZM	0.0125	6.14	41.3
Ti-6-4	0.010	5.95	17.1

Another approach to this problem has been developed by Panametrics, Inc., of Waltham, Massachusetts. Experiments conducted by Panametrics on material supplied by Solar indicate that their technique is capable of measuring shear moduli in 0.012-inch-thick TD Nickel at room temperature and at elevated temperatures.

The Panametrics' system consists of an ultrasonic pulse generator and readout instrument, an extensional or shear wave transducer, a lead-in wire, and the specimen, as shown in Figure 19. Normally the lead-in wire is about 1 mm in diameter and the specimen is about 0.5 mm in diameter by 50 mm long. For these tests with 0.012 inch thick TD Nickel sheet, the specimen was made 0.012 x 0.012 x 2.0 inches long.

In operation, an ultrasonic pulse is sent from the transducer down the lead-in wire to the specimen. An "echo" or reflection of the pulse will occur at both the beginning and end of the specimen. The velocity of sound in the specimen is calculated knowing the time delay between the two "echos" and the length of the specimen.
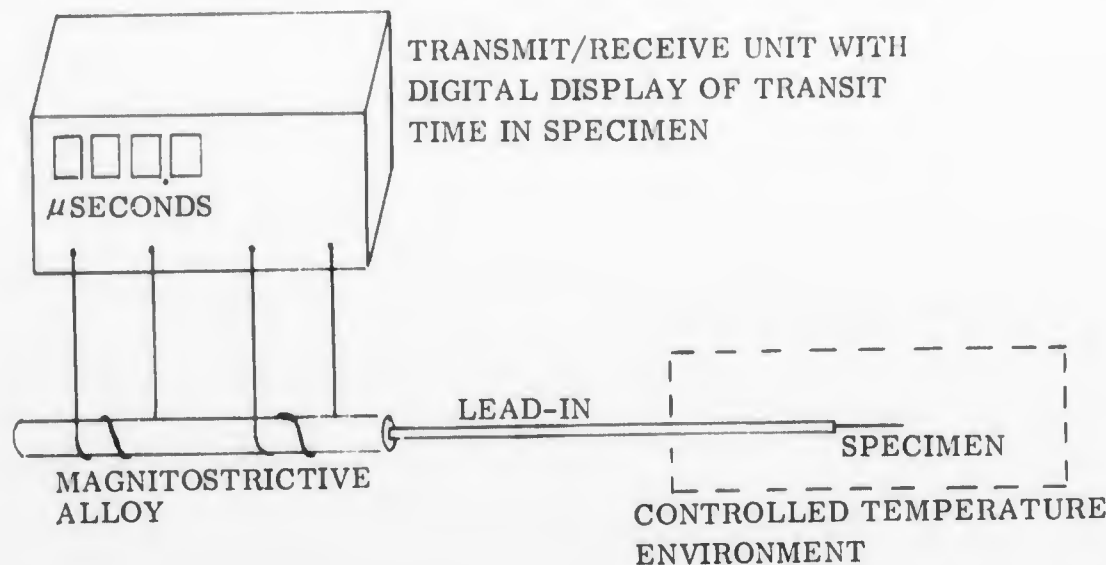
FIGURE 19. SCHEMATIC OF ULTRASONIC METHOD USED BY PARAMETERS TO MEASURE MODULI OF THIN-GAGE TD NICKEL ALLOY

Panametrics reported a room temperature value of 10×10^6 psi. This agrees well with the value of 9.57×10^6 psi which was obtained from the torsional resonance technique. They also reported a value of 5.6×10^6 psi at some elevated temperature ("glowing red"), but they did not measure the temperature.

One possible disadvantage of this technique is that the specimen must be in the form of a thin rod or wire. To prepare a specimen it is necessary to shear a strip with a width equal to the thickness of the sheet. For example, the TD Nickel specimen mentioned above was in the form of a bar 0.012-inch square by 2 inches long. It would be difficult to prepare a similar specimen from 0.002-inch thick sheet.

It is to be noted that the above experimental results by Parametrics are to be considered only preliminary. The purpose merely was to determine feasibility of a method, and not to establish accurate data. Parametrics claims that with careful measurement of specimen length, and test temperature, moduli accuracy of one percent is attainable in specimens a few inches long.

Discussion of Methods to Measure Shear Modulus

Three static and three dynamic methods have been examined to measure shear modulus. These methods are:

- Uniaxial tension test
- Shear panel
- Torsion of cylinder

28

- Torsional resonance
- Transverse sound velocity (focused transducer)
- Longitudinal sound velocity (pulse method)

Experimental difficulties were encountered with several of the methods that would make routine determination difficult and make extrapolation to thinner gages than those studied extremely unlikely. These difficulties are summarized below:

Shear panel: Difficult to make and to preserve flatness of panel. (Mechanical fastening gave an initially flat panel, but load transfer was uneven; diffusion bonding tended to leave distortion as a result of heating.)
Bending of beams could not be ignored and operation at pins was not satisfactory.

Torsion of cylinder: Uniform, closed cylinders could not be made without affecting the properties of the material.
Torsion loading at ends was not satisfactory and uniform loading was not achieved.

Torsional resonance: Appears to be an excellent method, resonance was readily obtained with normal materials.

Transverse velocity: Shear wave could not be induced in thin sheets.

Longitudinal velocity Appears to be an excellent method, but specimen preparation for small gages (e.g., 0.002 x 0.002 x 2 inches) would be prohibitive.

In addition to these experimental differences, it is necessary to consider the relevance of the shear moduli to the sheet properties. Figure 20 attempts to illustrate simply the principal finite element that is distorted by shear in each of these tests. For isotropic materials, these differences are not critical, but for anisotropic material the difference is critical. It is apparent that the distortion of the finite cube differs and must be related to the type of shear experienced in the application for which the sheet is intended.

For the cases of uniaxial tensile and torsion of a thin walled cylinder, only shear moduli in the plane of the sheet are involved in the distortion of the finite element. In the case of torsion of a flat plate, the determination of shear moduli involves the thickness direction as well. With anisotropic materials the analysis can be extremely comples. The modulus value for anisotropic sheet, computed from the equations of Pickett, gives a shear modulus of intermediate value.

29

A. UNIAXIAL TENSILE
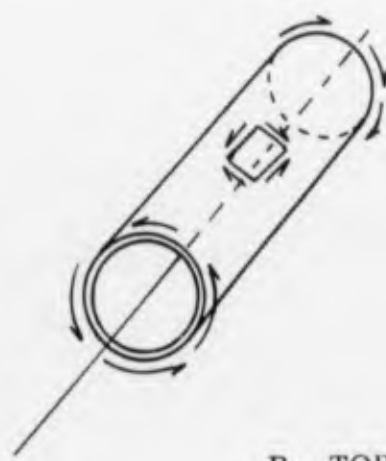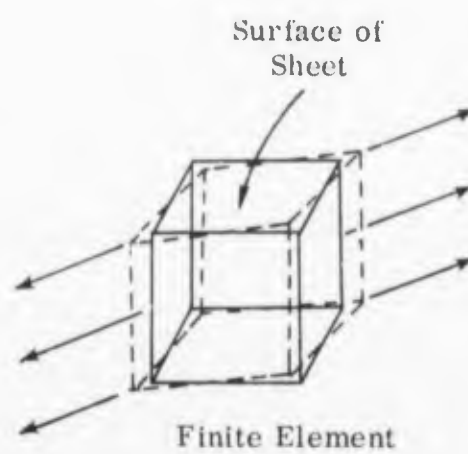
B. TORSION OF CYLINDER
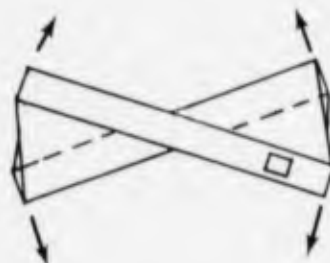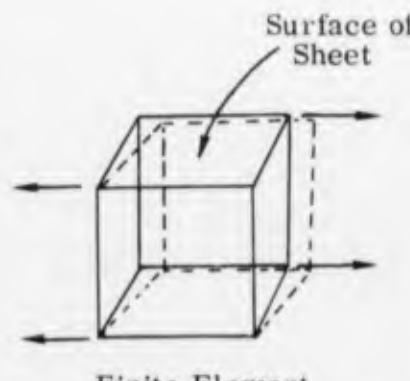
C. TORSIONAL RESONANCE
OF FLAT PLATE
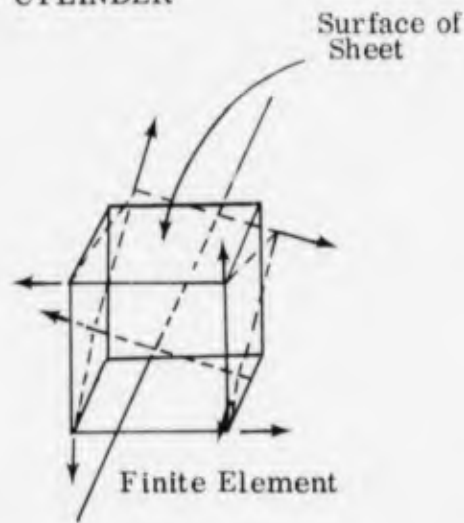
FIGURE 20. SHEAR STRAIN PRODUCED IN FINITE ELEMENTS BY VARIOUS
TEST METHODS

30

III. FRACTURE TOUGHNESS TESTING

In principle, the requirements of a fracture toughness test seem relatively modest, i.e., the test should predict the largest crack a material can tolerate without fracturing when loaded to the yield stress. In practice, however, it is very difficult to determine values of fracture toughness which are useful from a design standpoint. This is especially true of thin materials which typically exhibit a plane-stress condition. In spite of considerable progress being made in this area, fracture toughness tests on thin gage metals are likely to be very subjective. This is not surprising when one considers that fracture mechanics is based on the theory of linear elasticity. Any such mathematical analysis assumes a homogeneous, isotropic material. Unfortunately, most metals and alloys do not satisfy this requirement. It appears, therefore, that even under optimum experimental conditions, approximate values of fracture toughness are the best that can be anticipated. The one consolation in this regard is that the present analyses usually yield conservative values.

3.1 SHARP CRACK FRACTURE MECHANICS

Much of the literature on fracture toughness is confusing because of the seemingly arbitrary restrictions placed on specimen design. Authors frequently do not make it clear why these restrictions are necessary or what the consequences will be if they are violated. It seems appropriate, therefore, to discuss the analyses on which fracture toughness testing is based before discussing the testing of thin gage materials specifically.

It can be shown by means of a simple calculation that the theoretical cohesion strength of a crystal is from 10 to 1000 times larger than the observed fracture strength of metals. Griffith (Ref. 5) explained this discrepancy on the basis of micro-cracks in brittle materials. He suggested that the theoretical cohesive strength might be exceeded at a crack root at a much lower average stress. He also formulated a theory of minimum energy to explain crack propagation. This states that the equilibrium state of a deformed body is one in which the potential energy of the system is a minimum. This means that when the surface energy of a solid increases due to crack extension, there must be a corresponding decrease in strain energy to maintain the energy balance. Griffith stated it as follows: "A crack will propagate when the decrease in elastic strain energy is at least equal to the energy required to create the new surface."

Using this concept, an expression was developed for the stress necessary to cause an existing crack to propagate:

$$\sigma = \left[\frac{2E\gamma}{\pi a} \right]^{\frac{1}{2}}$$

$2a$ = crack length
E = elastic modulus
γ = surface energy

This theory satisfactorily predicts the behavior of brittle materials such as glass, but does not allow for the plastic deformation which always accompanies crack extension in metals.

Orowan (Ref. 6) modified the above expression to include a term P, representing the plastic energy required to extend a crack in a metal:

$$\sigma = \left[\frac{2E(\gamma + P)}{\pi a} \right]^{\frac{1}{2}}$$

Since P is much larger than γ, γ is usually ignored in this expression.

The first practical use of this theory was made by Irwin (Ref. 7). Irwin replaced the term for energy ($\gamma + P$) by an experimentally determined parameter $\mathcal{G}$. $\mathcal{G}$ is commonly known as the crack-extension force or energy release rate. This represents the fraction of total work which is irreversibly absorbed in local plastic flow and cleavage to create a unit area of new surface. The units of $\mathcal{G}$ are $\frac{\text{in-lbs}}{\text{in}^2}$.

3.1.1 The Westergaard Method of Stress Analysis of Cracks

Westergaard's analysis follows the pattern common to most problems in elasticity, i.e., he formulated a stress function which satisfied (1) equilibrium conditions, (2) compatability conditions, (3) boundary conditions. These conditions are stated as follows:

Equilibrium
$$\begin{cases} \dfrac{\partial \sigma_x}{\partial x} + \dfrac{\partial \tau_{xy}}{\partial y} = 0 \\[2ex] \dfrac{\partial \tau_{xy}}{\partial x} + \dfrac{\partial \sigma_y}{\partial y} = 0 \\[2ex] \tau_{xy} = \tau_{yx} \end{cases}$$

Compatibility
$$\nabla \left(\sigma_x + \sigma_y \right) = 0$$

The boundary conditions depend, of course, on the problem being solved.

32

The equilibrium conditions are automatically satisfied if a stress function, ϕ, is defined so that:

$$\sigma_x = \frac{\partial^2 \phi}{\partial y^2}$$

$$\sigma_y = \frac{\partial^2 \phi}{\partial x^2}$$

$$\tau_{xy} = \frac{\partial^2 \phi}{\partial x \, \partial y}$$

Substituting 3 into 2 gives:

$$\nabla^4 \phi = 0 \quad \text{which is the basic requirement of an Airy}$$
$$\text{Stress Function.}$$

Westergaard used complex variables to solve the problem of a sharp crack, and arrived at the following expressions for stresses at the tip of a crack:

$$\sigma_x = \frac{K}{(2\pi r)^{\frac{1}{2}}} \quad \cos\frac{\theta}{2}\left[1 - \sin\frac{\theta}{2}\,\sin\frac{3\theta}{2}\right]$$

$$\sigma_y = \frac{K}{(2\pi r)^{\frac{1}{2}}} \quad \cos\frac{\theta}{2}\left[1 + \sin\frac{\theta}{2}\,\sin\frac{3\theta}{2}\right]$$

$$\tau_{xy} = \frac{K}{(2\pi r)^{\frac{1}{2}}} \quad \sin\frac{\theta}{2}\,\cos\frac{\theta}{2}\,\cos\frac{3\theta}{2}$$

Solving for K gives the "tangent equation" which is commonly used in fracture toughness testing:

$$K = \sigma \left[W \, \tan\frac{\pi a}{W}\right]^{\frac{1}{2}}$$

σ = gross stress
2a = crack length
W = specimen width

K is known as the stress-intensity factor, and is related to $\mathcal{G}$ and the elastic modulus E as follows:

$$K = \sqrt{\mathcal{G} E}$$

The units of K are psi $\sqrt{\text{in.}}$

3.1.2   Plane Strain versus Plane Stress

A value of fracture toughness determined for sheet material will be either plane strain or plane stress, depending on the thickness of the sheet. Thick material which is constrained in the short-transverse direction will exhibit a plane-strain condition throughout most of the thickness, although shear tips indicate lack of constraint at the surface. As the thickness decreased, transition of the principal fracture mode occurs with mixed fractures in the transition range. Finally, a thickness will be reached below which only plane stress is possible. Some factors which determine the transition thickness range of a metal are: crack size, crack shape, temperature, heat treatment, deformation history, rate of loading, etc.

The significance of the transition in fracture toughness testing is that plane strain fracture toughness is apparently independent of specimen dimensions and provides an invariant fracture characteristic of the materials. Plane stress fracture toughness, on the other hand, depends on specimen shape and size. This is due primarily to the large size of the plastically deformed zone at the crack tip. For a small plastic zone, the linear analysis is reasonably accurate, but the accuracy decreases with increasing plastic deformation.

Srawley and Brown (Ref. 8) have pointed out that the controlling factor in the transition from plane stress to plane strain is the ratio of plastic zone size to thickness. The size of the plastic zone can be estimated from Westergaard's equations by setting $\sigma_y = \sigma_{ys}$, which gives

$$r_p = \frac{K^2}{2\pi \sigma_{ys}^2} \qquad 2$$

This is the correction factor usually used in the tangent equation as follows:

$$K^2 = \sigma^2 \operatorname{Tan} \frac{\pi}{W}\left[a + r_p\right] = \sigma^2 \operatorname{Tan} \frac{\pi a}{W} + \frac{K^2}{2W \sigma_{ys}^2}$$

Boyle, Sullivan and Krafft (Ref. 9) in their work on 7075-T6 aluminum, found that a plane strain condition prevailed when the thickness was greater than approximately four times the plastic zone. Srawley and Brown have adopted this criterion, but point out that this condition is not always sufficient to insure plane strain.

Because of the relationship between thickness and plastic zone size, the ASTM Special Committee on Fracture Testing has defined a constraint factor β, to indicate a "relative" plastic zone size (Ref. 10).

$$\beta = \frac{K^2}{B \sigma_{ys}^2} \qquad \text{where} \quad B \quad \text{is the thickness.}$$

34

Substituting Srawley and Brown's criterion $B = 4r_p = \dfrac{2K^2}{\pi \sigma_{ys}^2}$ in the above expression gives $\beta \leq \dfrac{\pi}{2}$ for plane strain.

The following notation is usually used to distinguish between plane strain and plane stress fracture toughness:

$\mathcal{G}_c$ - plane stress $\left.\vphantom{\begin{array}{c}a\\b\end{array}}\right|$ Critical value of strain-energy release rate at point of instability.

$\mathcal{G}_{Ic}$ - plane strain

K_c - plane stress $\left.\vphantom{\begin{array}{c}a\\b\end{array}}\right|$ Critical value of stress-intensity factor at point of instability.

K_{Ic} - plane strain

$$K_c^2 = E\,\mathcal{G}_c \quad \text{and} \quad K_{Ic}^2 = \dfrac{E\,\mathcal{G}_{Ic}}{1 - \nu^2}$$

E = elastic modulus

ν = Poisson's ratio

3.1.3 Errors Due to Plastic Deformation

At the onset of fracture when $K = K_c$ the error introduced by plastic flow will be approximately:

$$\frac{r_p}{a} = \frac{1}{2\pi a}\left(\frac{K_c}{\sigma_{ys}}\right)^2$$

But according to Irwin:

$$\sigma^2 = \frac{E\,\mathcal{G}}{a}$$

or $\quad K = \sigma(\pi a)^{\frac{1}{2}}.$

Substituting this into the above equation gives:

$$\frac{r_p}{a} = \frac{1}{2}\left(\frac{\sigma}{\sigma_{ys}}\right)^2$$

where σ is the gross fracture stress.

35

This shows that in order to keep r_p small, the specimen must be designed to give a low value of $\frac{\sigma}{\sigma_{ys}}$. If the net section stress at instability exceeds the uniaxial yield strength of the material, the test is not represented even approximately by a linear elastic-stress-field model and does not provide a useful measure of fracture toughness.

The ASTM has suggested that the analysis will be sufficiently accurate if the net fracture stress does not exceed $0.8 \, \sigma_{ys}$. They state, however, that the inaccuracy will be less than 10 percent when $\sigma_n = \sigma_{ys}$. Based on a limited number of tests, the committee has determined that $\mathcal{G}_c$ will be independent of specimen width and crack length when the $0.8 \, \sigma_{ys}$ condition is met.

Substitution of $\sigma_{net} = 0.8 \, \sigma_{ys}$ in the tangent equation gives the maximum value of $\mathcal{G}_c$ which can be measured accurately for a given specimen:

$$\mathcal{G}_{c \text{ max.}} = 0.64 \, \frac{\sigma_{ys}}{E} \cdot W \left[1 - \frac{2 \, a_m}{W} \right] \, \text{Tan} \, \frac{\pi a}{W}$$

where a_m is the crack half-length at instability and $a = a_m + r_p$. The constant 0.64 was introduced by Srawley and Brown based on experimental results.

From this expression, it is seen that the most efficient specimen will have the value of $\frac{2 \, a_m}{W}$ for which the quantity $0.64 \left[1 - 2 \, a_m \right]^2 \, \text{Tan} \, \frac{a}{W}$ is greatest. Srawley and Brown show that this quantity is a maximum in the range of $\frac{2 \, a_m}{W}$ between 0.3 and 0.4, and that the useful range of $\frac{2 \, a_m}{W}$ extends up to about 0.6. They recommend that if $\frac{2 \, a_m}{W}$ exceeds 0.6 in any test, the results not be used.

Although the above discussion was developed on the basis of center-notched specimens, it should apply equally to symmetrical edge-notched specimens. There is a slight difference in the tangent equation for edge-notched specimens, however. For symmetrical edge notches:

$$K_c^2 = \sigma^2 W \, \text{Tan} \, \frac{\pi a}{W} + 0.1 \, \text{Sin} \, \frac{2 \pi a}{W}$$

where a = average crack length at maximum load + r_p.

Up to the present time no expression for K in closed form has been derived for single-edge-notched tensile specimens.

3.1.4 Summary of Specimen Design Requirements

In order for a fracture toughness test to be accurately described by a linear elastic stress analysis, the following conditions must be met:

1. $\sigma_{net} \leq 0.8 \sigma_{ys}$

2. Initial crack length, $2a_0 = 0.3W$

3. Crack length at instability, $2a_m \leq 0.6W$.

It has also been suggested that the width to thickness ratio, $\frac{W}{B}$, should be between 16 and 45 for plane stress testing. This is not a consequence of the elastic stress analysis, however, and the upper limit of 45 can be exceeded if precautions are taken to prevent buckling. Below $\frac{W}{B} = 16$ the test will be plane strain.

Assuming that an acceptable specimen has been designed, two experimental quantities are needed in order to calculate the fracture toughness:

1. Crack length at instability

2. Load at instability

The criterion for the point of instability is that the load P as a function of elongation reaches either a maximum (plane stress), or a point of inflection of zero slope (plane strain "pop-in").

3.2 EXPERIMENTAL WORK

3.2.1 Materials Selection

In order to determine the degree of brittleness necessary for meaningful fracture toughness testing, screening tests were performed on 3 alloys varying in nature from ductile to brittle. These were:

- Type 430 stainless steel (ductile)
- TD Nickel (intermediate)
- TZM (brittle)

For these tests, specimens 0.006-inch thick by 0.75-inch wide by 5-inches long were used. Symmetrical edge notches approximately 1/8-inch long were made in each specimen by shearing. This resulted in $\frac{2a}{W} = 0.33$, which satisfies the ASTM requirement.

On testing in tension, all materials failed in a ductile manner, indicating a plane-stress condition. The net fracture stresses and σ_{net} to σ_{ys} ratios are tabulated below in Table VIII.

TABLE VIII

FRACTURE TOUGHNESS DATA FROM THREE SELECTED ALLOYS

Alloy	σ_{net}	σ_{net}/σ_{ys}
430 s.s.	65 ksi	1.85
TD Nickel	97	1.38
TZM	125	0.76

Table VIII shows that only TZM met the requirement that $\sigma_{net} \leq \sigma_{ys}$. For this reason TZM was chosen as specimen material for subsequent fracture-toughness studies.

3.2.2 Test Specimens

Figure 21 is a photograph of typical specimens used in the study. All specimens were 3/4-inch wide and either 5 or 10 inches long. The 5-inch-long specimens were used for testing thicker gages of TZM (0.030 and 0.060 inch), and were tested on the MTS tensile testing unit. The 10-inch long specimens were used for thinner gages and were tested using the thin-gage tensile tester and double beam extensometer which were developed during the first two years of this program.

Center notches were produced in the specimens by drilling a small hole, notching the hole with a 3-cornered file, and sharpening the notch with a jeweler's saw having a 0.006-inch wide blade. Some of the specimens were also fatigue cracked, as discussed below.

3.2.3 Effect of Thickness on Fracture Toughness of TZM

To investigate the effect of thickness on fracture toughness, specimens of four different thicknesses were tested. These were: 0.060 inch, 0.030 inch, 0.012 inch and 0.006 inch.

The effect of delamination became very apparent during these tests. TZM is normally very brittle and exhibits low fracture toughness. This behavior was observed in the 0.030 inch and 0.060 inch specimens and was characterized by completely brittle failure with no slow crack growth. However, in several instances it was observed that apparently identical specimens failed in a ductile manner with the crack growing slowly across almost the entire specimen width before failure. This type of failure was accompanied by necking in the short-transverse direction, which indicates a plane stress condition. This apparent increase in toughness is due to the large amount of energy absorbed in creating new surface area when the specimen delaminates. Fracture surfaces of specimens with and without delamination are shown in Figure 22. All test results in delamination were considered invalid and were not used to calculate fracture toughness. Since brittle failure was

38

TOP: Five-inch Specimen for testing on MTS unit

BOTTOM: Ten-inch Specimen for testing on thin gage tensile machine

6 INCHES

FIGURE 21. TZM FRACTURE TOUGHNESS SPECIMENS

A.

Top – Almost complete delamination

Bottom – No apparent delamination

Magnification: 5X
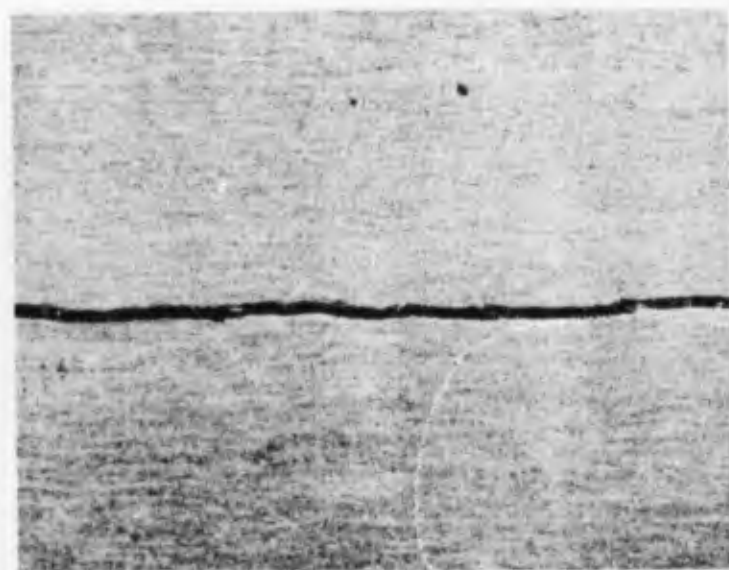
B.

Photomicrograph of delaminated
surface

Magnification: 100X

FIGURE 22.   FRACTURE SURFACES OF TZM FRACTURE
TOUGHNESS SPECIMENS

not observed in 0.006-inch or 0.012-inch material, no values are presented in Table IX.

TABLE IX

FRACTURE TOUGHNESS OF TZM

Thickness	Notch Lengths 2_a	Gross Stress at Failure	K_{IC}
0.030 inch	0.220 inch	74,300 psi	46,000 psi $\sqrt{in}$
0.060 inch	0.200 inch	52,200 psi	30,100 psi $\sqrt{in}$

3.2.4 Fatigue Cracking of TZM Specimens

Weiss and Yukawa (Ref. 11) suggest that the maximum notch-root radius be less than 1/10 the specimen thickness, i.e., $\frac{B}{\rho} > 10$, (ρ = notch-root radius). The most effective means of meeting this requirement in thin gage alloys is by fatigue cracking. Theoretically, this should produce a notch radius of atomic dimensions.

It was initially planned to fatigue crack all specimens before testing as recommended by the ASTM. Fatigue cracks were produced in 30-mil-thick TZM specimens by cycling them in tension-tension loading between 15,000 psi and 75,000 psi for approximately 25,000 cycles. It appears that the fatigue cycles caused the specimens to delaminate because, in general, the fatigue crack specimens failed in a more ductile manner than those without fatigue cracks. Based on this observation, it is suggested that materials having a tendency to delaminate not be fatigue cracked prior to testing.

Because of the faint appearance of the cracks on the specimen surface, fatigue cracking of this material is a very tedious and time-consuming operation. The operator must observe the specimen closely during the test because the crack propagates rapidly once it is initiated. If the test is not stopped in time, the specimen will break and the time required to set up and run the test will have been wasted.

Figure 23 shows the appearance of fatigue cracks in 0.030-inch thick TZM.

3.2.5 Calibration Curves for Determining Crack Length in Fracture Toughness Specimens

The two quantities necessary to calculate a value of fracture toughness are: (1) load at instability, and (2) crack length at instability. Since the load can easily be measured, the problem is essentially that of determining the crack length.

Compliance Gage Method

One way of measuring crack length is by means of an extensometer (compliance gage) attached to the specimen on each side of the notch. As the specimen is loaded in tension it will first elongate elastically and produce a straight line on the

41
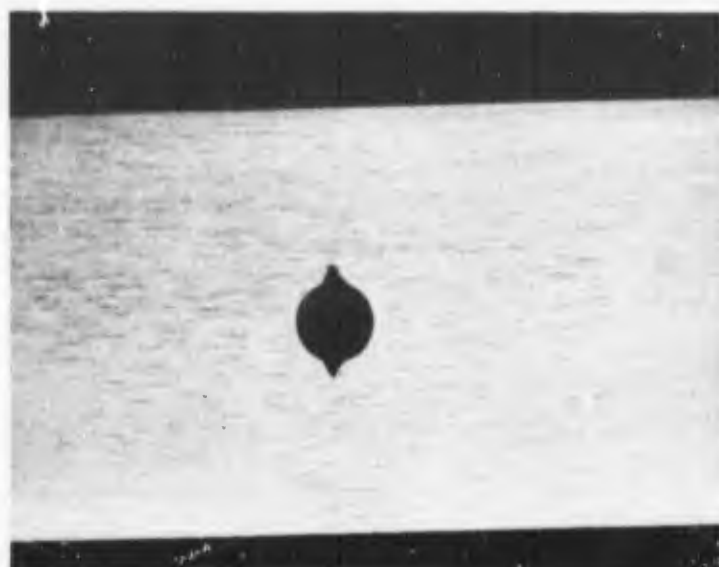
A.

Magnification: 3X

B.
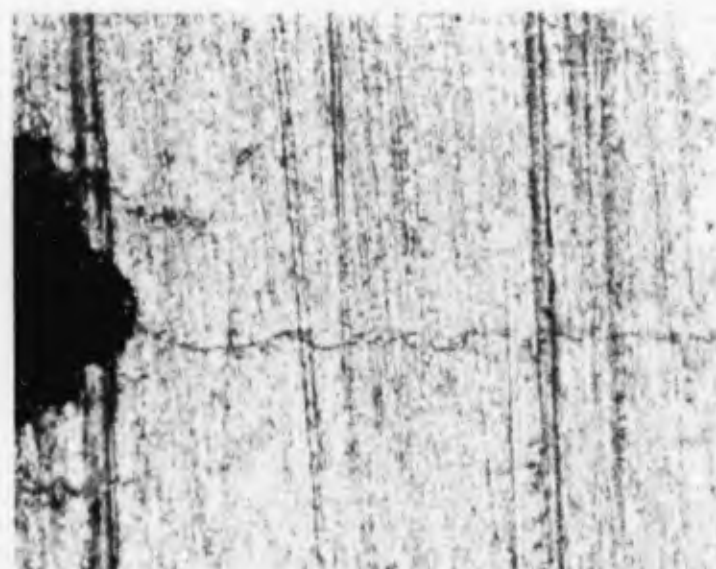
Magnification: 100X

FIGURE 23. FATIGUE CRACKS IN TZM FRACTURE
TOUGHNESS SPECIMEN

42

load-elongation curve. At some critical load the crack will start to grow slowly and the curve will deviate from linearity (a very brittle material will fracture at this point and the initial crack length can be used in the fracture toughness calculation). A load-deflection curve obtained with a compliance gage resembles a typical stress-strain curve. The essential difference is that the nonlinear portion is due primarily to crack growth rather than plastic deformation. If a straight line is drawn from the point of instability on the curve (either the maximum load or "pop-in" load) to the origin, the slope of this line will be related to the crack length at instability.

An inherent advantage of a compliance gage is that it provides an automatic correction for the effect of plastic deformation at the crack tip. On unloading, the load-deflection curve should always return to the origin. Actually, the curve does not return exactly to zero because of the small amount of plastic deformation. If the slope of the unloading curve is adjusted to return to zero, the crack length corresponding to this slope will include the plastic zone correction factor. This value can, therefore, be used in the tangent equation directly. Furthermore, the relative amounts of elastic and plastic work expended in crack extension will be represented by the areas enclosed by the curve. This is illustrated in Figure 24.

In order to establish the relationship between crack length and slope (or compliance) it is necessary to determine a calibration curve by testing several specimens with different crack lengths and plotting compliance versus crack length. The curve shown in Figure 25 was determined in this manner, with the double-beam extensometer. To use this curve, the initial compliance and notch length of each test specimen is first determined. This gives one point on the curve. If it does not fall on the curve, the curve is shifted up or down as required until the point is on the curve. The important characteristic of the curve is, therefore, its shape rather than precise location with respect to the axes.

It has been suggested that such a curve will be independent of specimen's size if dimensionless ratios are plotted as was done in Figure 25. The considerable scatter of data from these tests indicates that this may not be true for thin-gage materials. The most serious source of error in a test of this kind is specimen bending. Because of this effect, the compliance-gage technique is not the most accurate method for measuring crack extension in thin-gage materials. The data from which Figure 25 was plotted are tabulated in Table X.

Electrical Potential Method

Another way to determine crack length is by passing a current through the specimen and measuring the potential drop across the crack. Again a series of specimens must be tested, and a dimensionless curve plotted relating potential drop to crack length. The curve in Figure 26 was determined in this way. Figure 27 is a sketch of the test setup, and Figure 28 is a photograph showing a typical specimen with electrodes attached. A constant current of 1 amp was passed through the

43
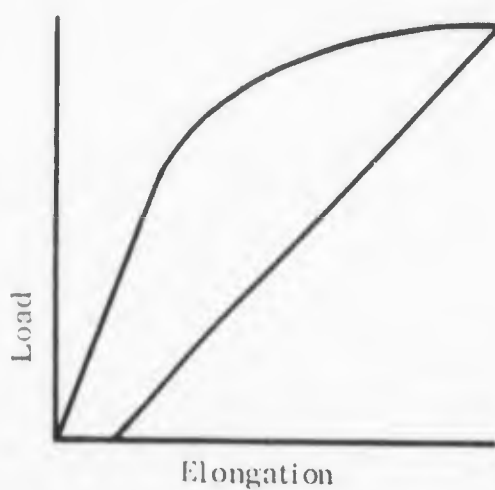
Actual unloading curve
(Total energy expended
in crack extension)
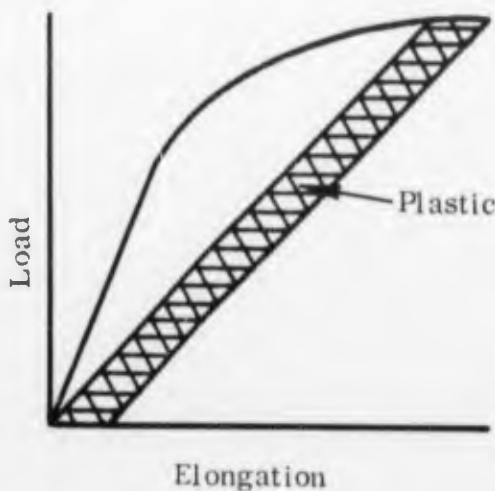
Relative amounts of
elastic and plastic
energy.
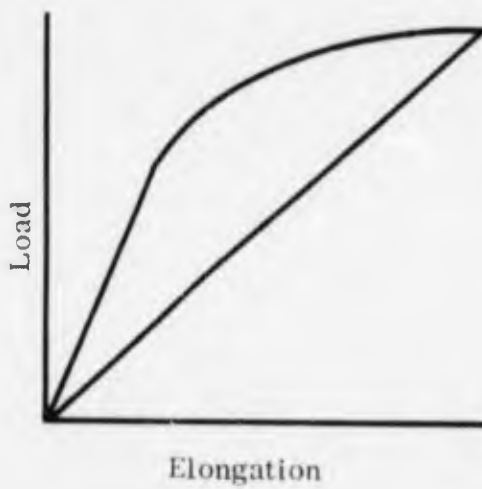
Unloading curve corrected
to pass through origin.

FIGURE 24. LOAD-ELONGATION CURVES OBTAINED WITH COMPLIANCE
GAGE (Idealized)

44
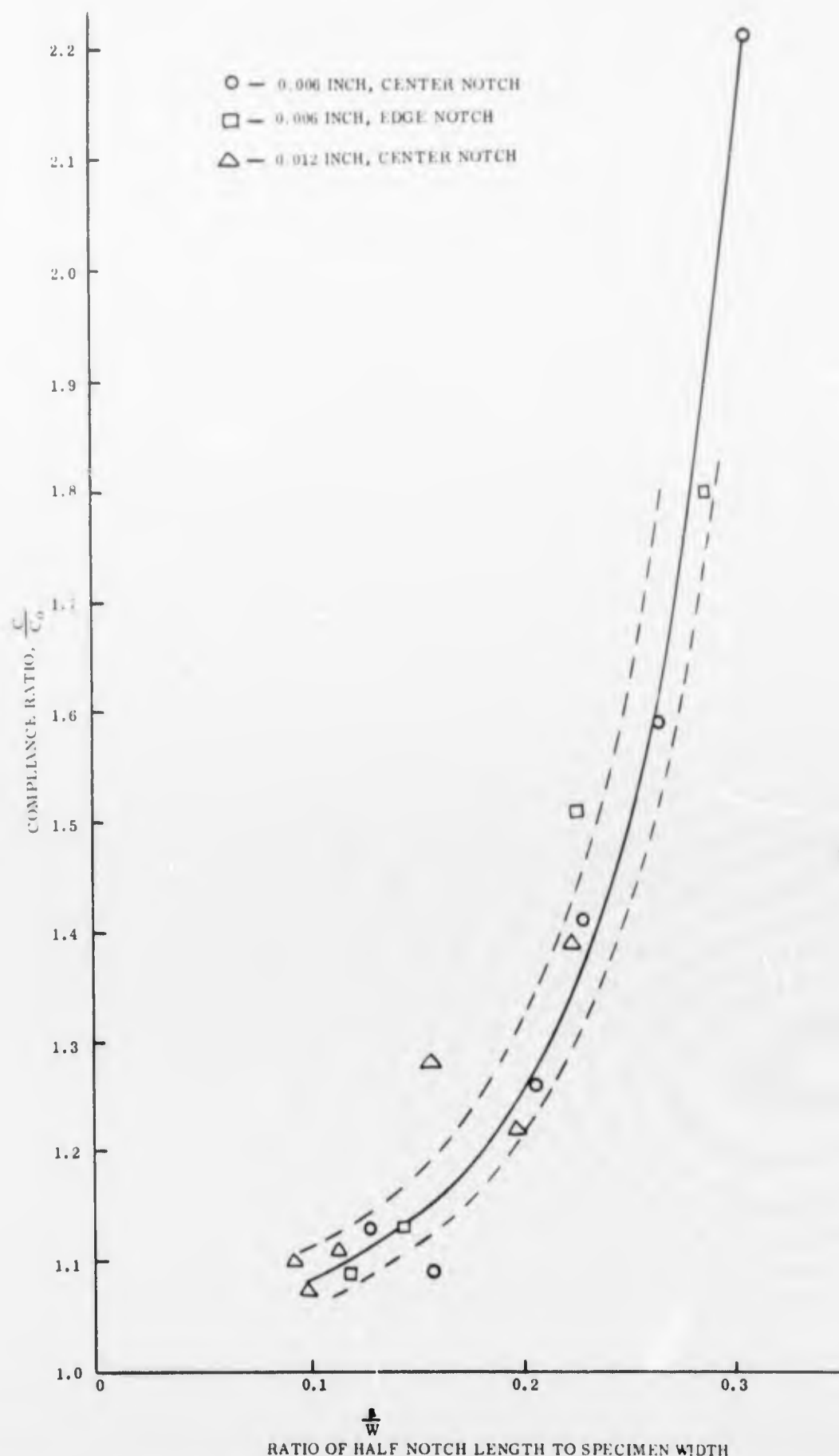
FIGURE 25. RELATIONSHIP BETWEEN COMPLIANCE RATIO AND NOTCH LENGTH
FOR TZM FRACTURE TOUGHNESS SPECIMENS

TABLE X

COMPLIANCE DATA FOR TZM FRACTURE TOUGHNESS SPECIMENS

Specimen	Notch Length Ao (in.)	Compliance $C = e/P$	Compliance Ratio, C/C_o	$\dfrac{Ao}{W}$
0.006 Inch Center Notch	0	5.55 μ-in/lb	1	0
	0.150	5.36	0.965	0.0981
	0.193	6.30	1.13	0.129
	0.237	6.05	1.09	0.159
	0.311	7.02	1.26	0.205
	0.342	7.85	1.41	0.227
	0.394	8.82	1.59	0.264
	0.459	12.25	2.21	0.303
0.006 Inch Edge Notch	0	5.0	1	0
	0.178	5.47	1.09	0.119
	0.218	5.64	1.13	0.145
	0.336	7.58	1.51	0.224
	0.428	9.0	1.8	0.286
0.012 Inch Center Notch	0	2.44 μ-in/lb	1	0
	0.136	2.69	1.1	0.0915
	0.147	2.63	1.075	0.099
	0.170	2.70	1.11	0.114
	0.233	3.12	1.28	0.157
	0.295	2.96	1.22	0.199
	0.330	3.40	1.39	0.222
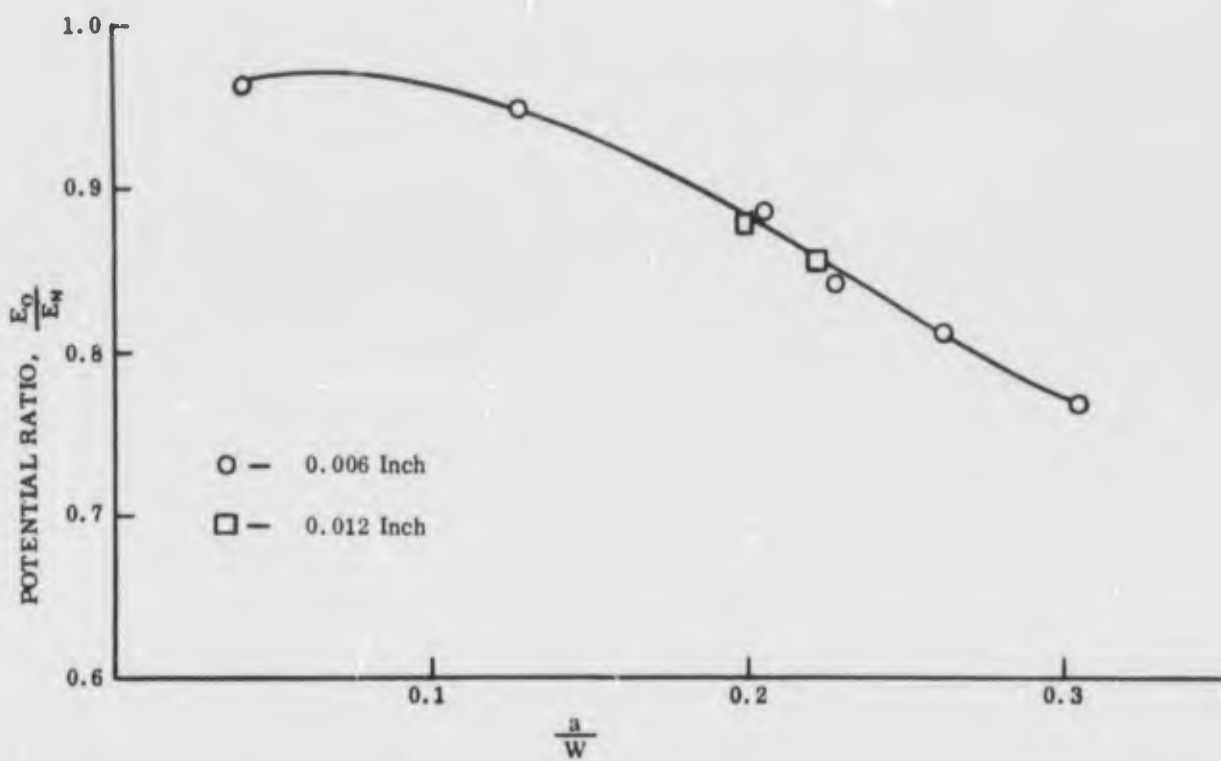
FIGURE 26.   CALIBRATION CURVE RELATING ELECTRICAL POTENTIAL AND
NOTCH LENGTH FOR CENTER NOTCHED TZM SPECIMENS
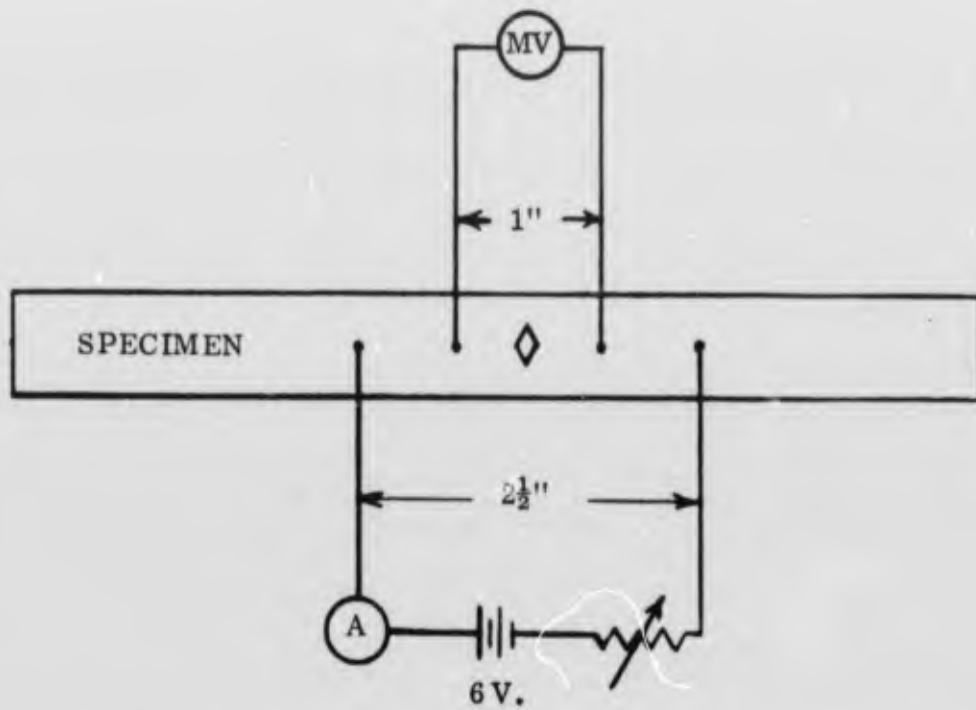
FIGURE 27.   ARRANGEMENT FOR MEASURING POTENTIAL DROP IN FRACTURE
TOUGHNESS SPECIMENS

47
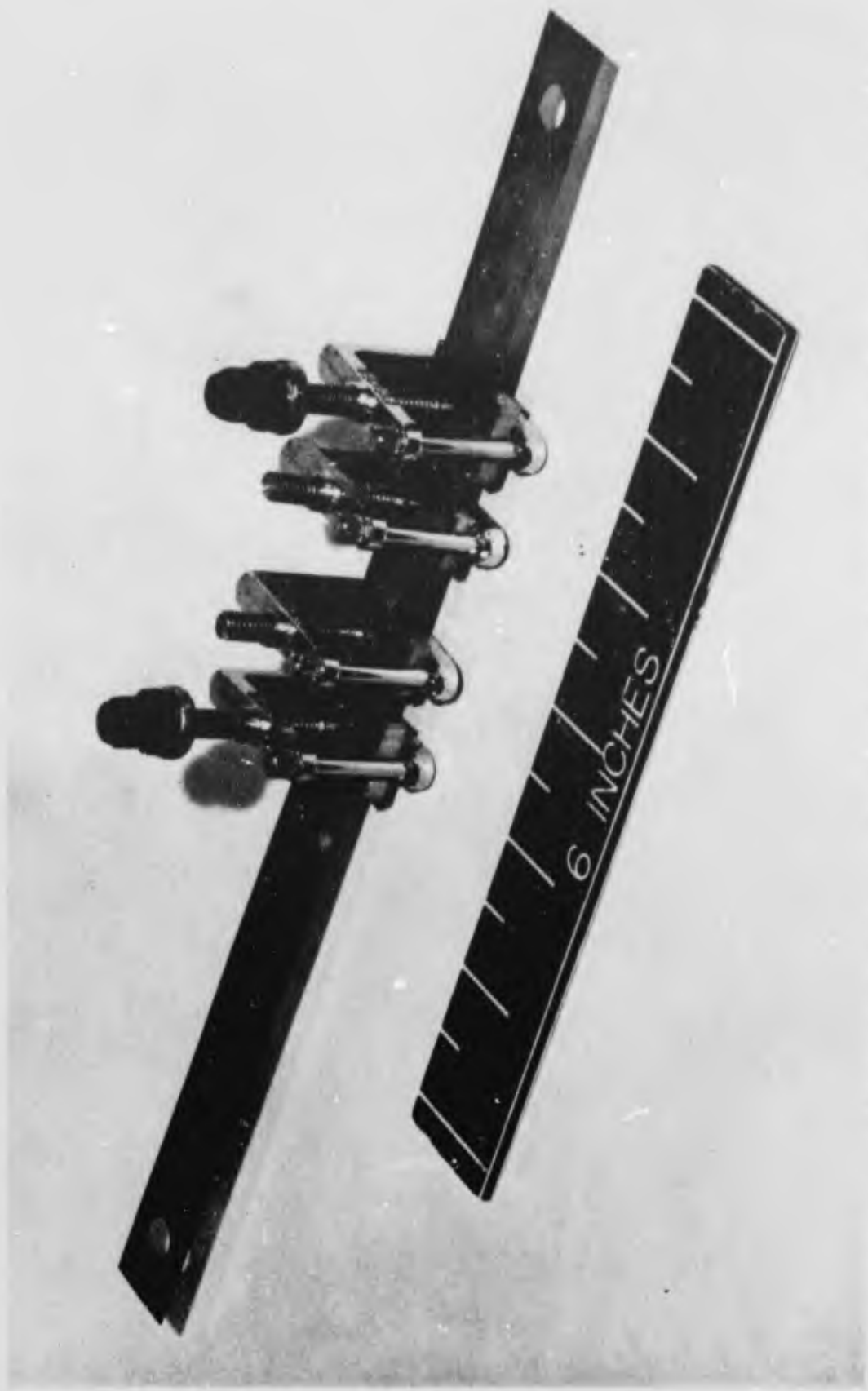
FIGURE 28. FRACTURE TOUGHNESS SPECIMEN WITH ELECTRODE ATTACHED FOR POTENTIAL DROP MEASUREMENTS

specimen via the outer electrodes and the potential drop measured across the inner electrodes which were placed $\frac{1}{2}$ inch on each side of the notch. The electrodes were made by modifying hose clamps of the type normally found in the chemistry laboratory. It can be seen from the figure that although a reasonably smooth curve was obtained, the sensitivity of this set-up was not too great. The data from which Figure 26 was plotted are presented in Table XI.

It must be pointed out that the technique described here can be used to determine the nature of the calibration curve but it cannot be used to actually test a specimen to failure. In order to test a specimen using this technique, it would be necessary to use a constant current source such as the milli-ohmmeter described by Anctil, Kula and DiCesare (Ref. 12).

3.2.6 Side Groove Studies

As the thickness of a thin-gage metal is increased, the apparent fracture toughness of the material will undergo a transition from plane stress, K_C, to plane strain, K_{IC}, and will finally reach a constant value which will not be changed by further increases in thickness. This plane-strain value of fracture toughness can then be used to describe the fracture behavior of the material.

TABLE XI

ELECTRICAL POTENTIAL DATA OBTAINED FROM
TZM FRACTURE TOUGHNESS SPECIMENS

Specimen	Notch Length $2a_O$	Potential Difference		Potential Ratio E_O/E_N	$\dfrac{a_O}{W}$
		E_O	E_N		
0.006" Center Notch	0.150 in.	0.59 mv	0.613	0.962	0.0981
" "	0.193	0.592	0.624	0.95	0.129
" "	0.311	0.60	0.676	0.887	0.205
" "	0.342	0.595	0.71	0.839	0.227
" "	0.394	0.605	0.748	0.81	0.264
" "	0.459	0.665	0.863	0.768	0.303
0.012" Center Notch	0.295	0.286	0.326	0.878	0.199
" "	0.330	0.286	0.335	0.854	0.222

All materials will undergo a transition from plane stress to plane strain. The thickness at which this transition occurs will depend, of course, on the toughness of the particular material being tested. In the present study, for instance, plane strain fracture was observed in 0.003-inch thick Type 301 stainless steel in the full hard condition (320 ksi yield strength). For a very ductile material the transition thickness may be on the order of 1/8 inch or more.

Freed and Krafft (Ref. 13) have described a technique for inducing plane strain fractures in normally ductile materials and thereby lowering the transition thickness. They accomplished this by machining "side grooves" in standard edge-notch specimens. A sketch of their specimen is shown in Figure 29. To obtain a value of K_{IC} from such a specimen, a "nominal" value of K is calculated without considering the side grooves. This nominal value is then corrected by the ratio of ungrooved to grooved thickness raised to a power which should be on the order of 0.5, i.e.,

$K_{IC} = K_{nom} \left(\dfrac{B}{B_N} \right)^m$ where B is the unnotched thickness and B_N is the notched thickness.

To determine the value of m, several specimens having different groove depths are tested. If the analysis is valid, a plot of Log K_{nom} vs Log $\left(\dfrac{B}{B_N} \right)$ should produce a straight line with a slope of -m.

This technique was attempted on several specimens of thin-gage material with one slight variation; because it is difficult to machine two opposing grooves in thin sheet, the specimens were grooved on one side only. The grooves were machined with a 45° -Vee milling cutter. A typical 0.010-inch deep groove in a 0.012-inch thick specimen is shown in Figure 30.

Three materials were tested in this manner:

    (1)   0.013-inch thick TZM (center notched)
    (2)   0.012-inch thick 17-7 PH Stainless Steel (symmetrical edge notches)
    (3)   0.008-inch thick L-605 cobalt alloy (symmetrical edge notches)

The results are summarized in Table XII. The specimens were five inches long by 3/4 inch wide and of the thicknesses noted.

Except as noted, all of the specimens listed in Table XII failed in a brittle manner, with no apparent slow crack growth. Log-log plots for the three materials are presented in Figures 31, 32, and 33.

Theoretically it should be possible to extrapolate these curves to $\dfrac{B}{B_N} = 1$ and obtain a true value of K_{IC}. This was done for the materials tested with the results shown in Table XIII. These values seem abnormally low, especially in view of the fact that the extremely brittle Type 301 stainless steel produced a K_{IC} value of 86 ksi $\sqrt{in}$. For comparison, some additional properties of these materials are listed in Table XIV.

50
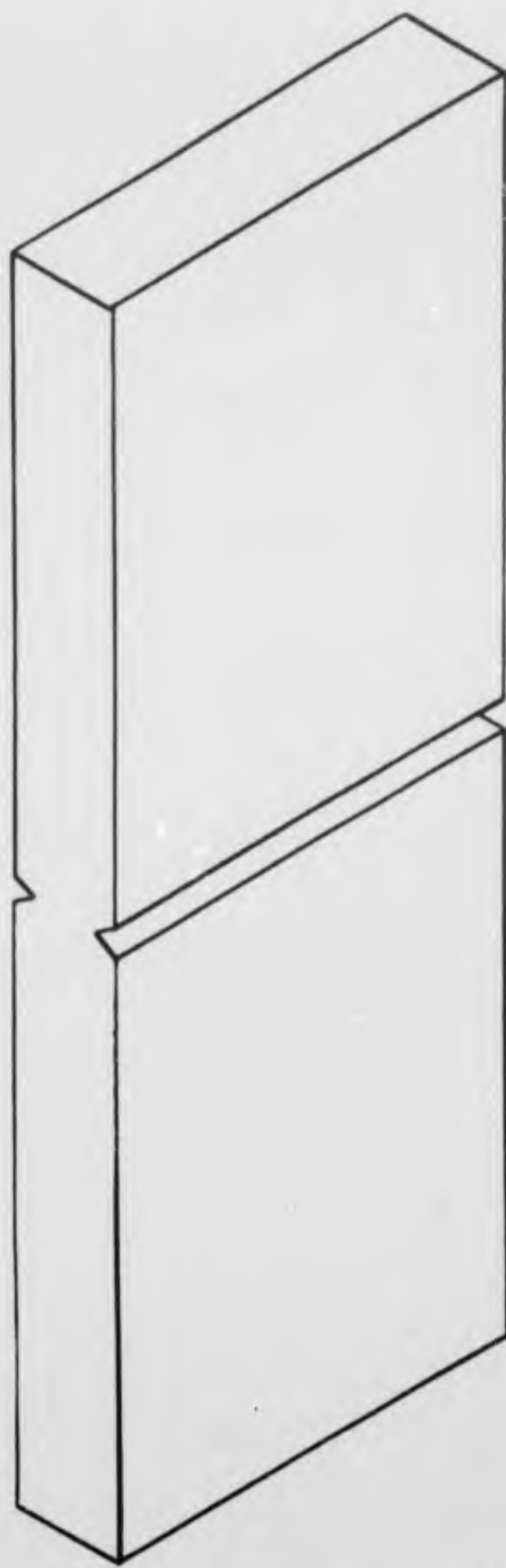
FIGURE 29. SIDE GROOVES IN FRACTURE TOUGHNESS SPECIMEN
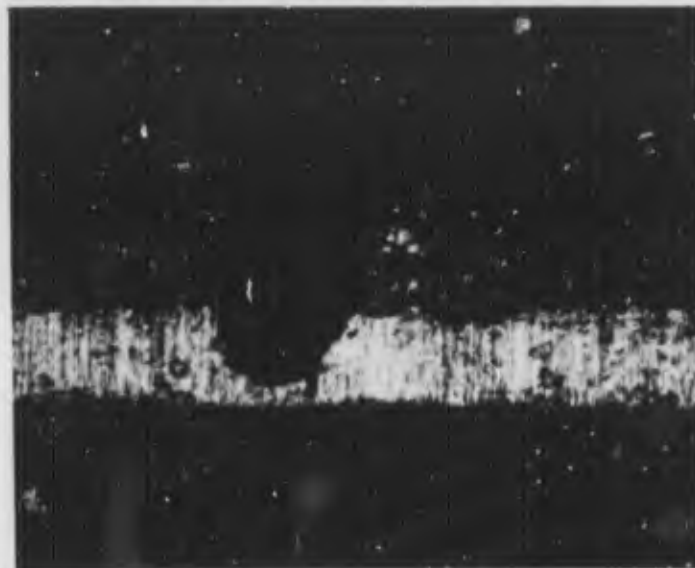
FIGURE 30. 0.010-INCH DEEP SIDE GROOVE IN 0.012-INCH THICK FRACTURE TOUGHNESS SPECIMEN

TABLE XII

DATA OBTAINED FROM SIDE-GROOVED FRACTURE-TOUGHNESS SPECIMENS

Material	Groove Depth	$\frac{B}{B_N}$	$2a_0$ Inches	P_{max} Pounds	σ_{Gross} (ksi)	K_{nom}* ksi $\sqrt{in}$
TZM (0.013 Inch)	0.002 In.	13/11	0.170	832	83	43.8
	0.004 In.	13/9	0.147	682	70	34.2
	0.006 In.	13/7	0.136	418	43	57.6
	0.002**					
17-7 P.H.S.S.	0.004 In.	1.5	0.220	440	49	32.3
(0.012 Inch)	0.006 In.	2.0	0.220	380	42.2	27.8
	0.008 In.	3.0	0.220	280	31.1	20.5
	0.010 In.	6.0	0.220	240	26.7	17.6
L-605	0.002 In.**					
0.008-Inch	0.004 In.	2	0.220	450	73.5	49.4
	0.006 In.	4	0.220	325	53.2	35.7

* $K_{nom} = \left(\sigma \ W \ Tan \ \frac{\pi a}{W} + 0.1 \ Sin \ \frac{2\pi a}{W} \right)^{\frac{1}{2}}$

** Ductile Failures
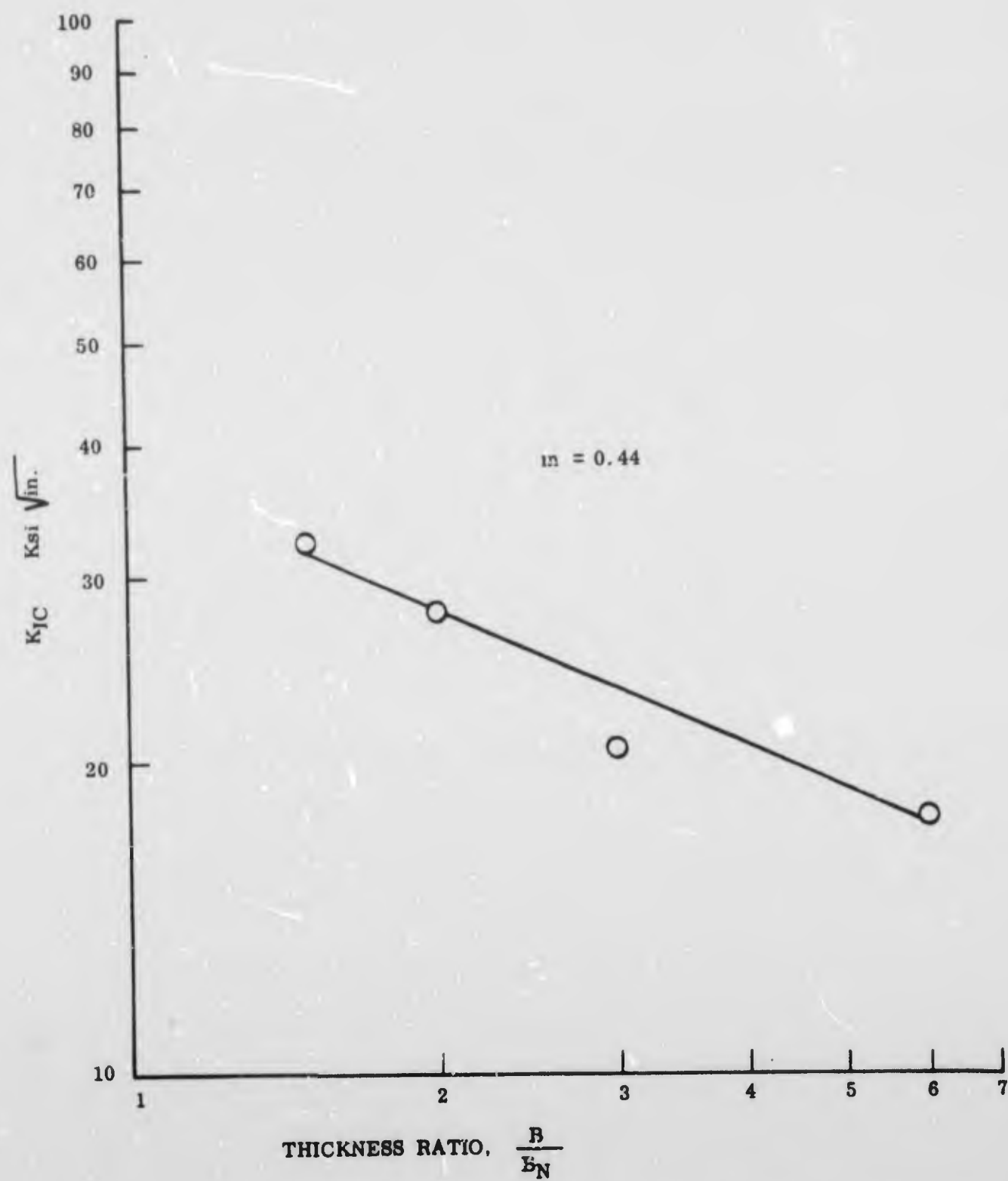
FIGURE 31.   LOG K VERSUS LOG B/BN FOR 0.012-INCH THICK TYPE 17-7 PH
             STAINLESS STEEL
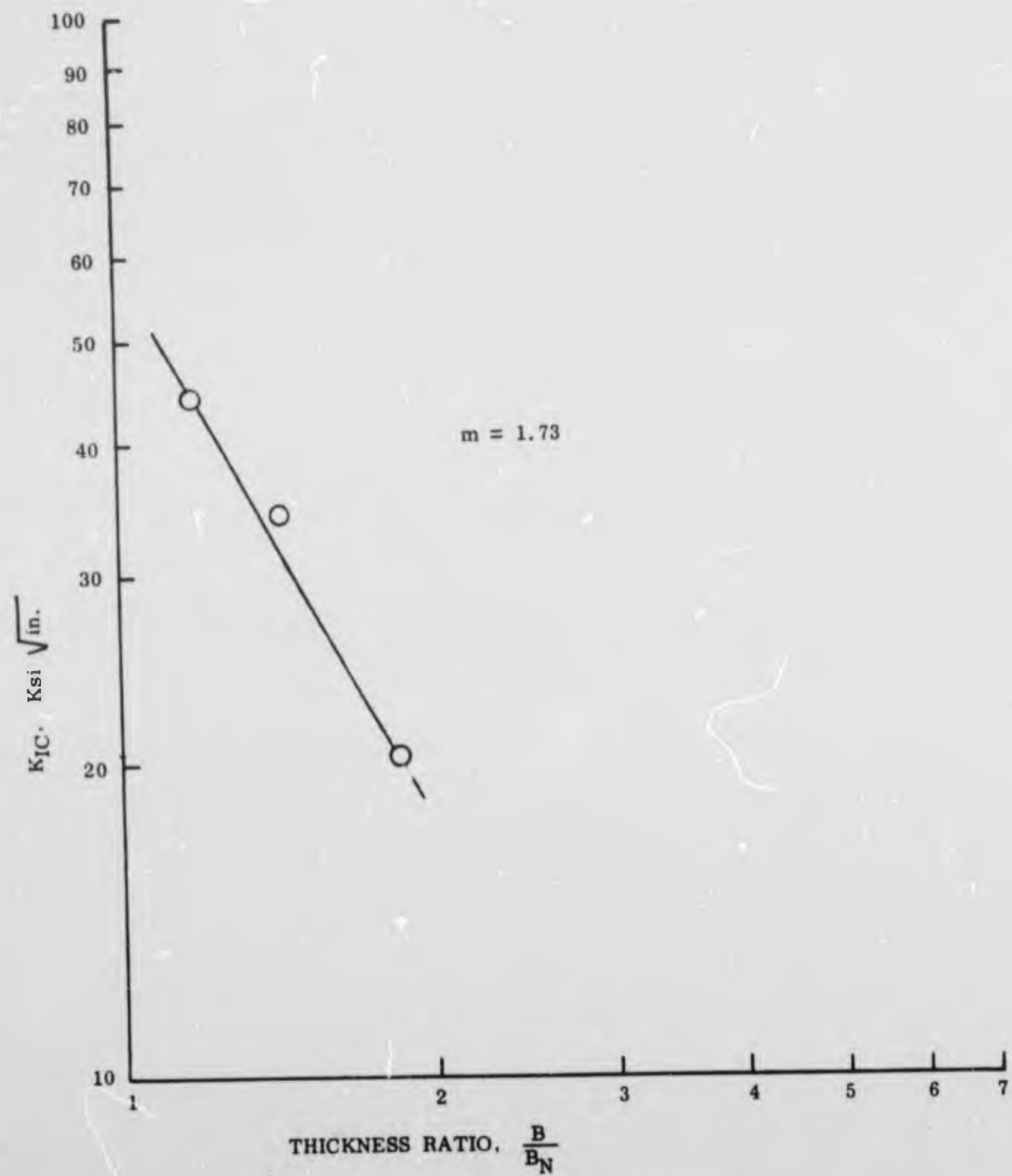
FIGURE 32.   LOG K VERSUS LOG B/BN FOR 0.013-INCH THICK TZM

54
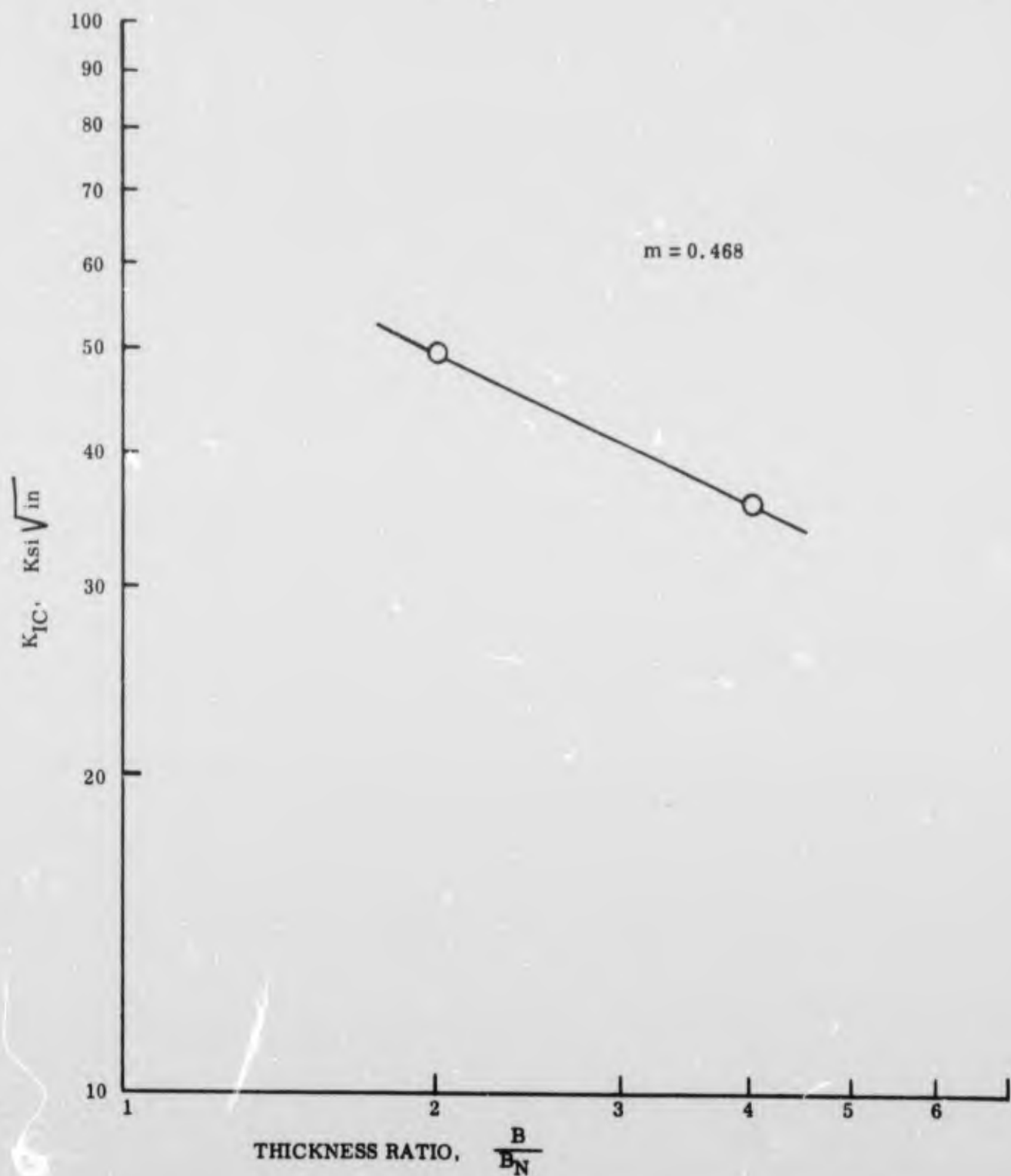
FIGURE 33. LOG K VERSUS LOG B/BN FOR 0.008-INCH L605 ALLOY

TABLE XIII

EXTRAPOLATED K_{IC} VALUES

Material	Slope, m	K_{IC} Extrapolated
17-7 PH SS (0.012-In.)	0.44	38 ksi in.
TZM (0.013-In.)	1.73	50
L605 (0.008-In.)	0.468	69

TABLE XIV

MECHANICAL PROPERTIES OF SELECTED ALLOYS

Material	Yield Strength (ksi)	UTS (ksi)	Notched UTS (ksi)
TZM (0.013 Inch)	81	81	137
17-7 PH s.s. (0.012)	50	110	74
L-605 (0.008 Inch)	83	167	110
430 s.s. (0.006 Inch)	50	65	57
301 s.s. (0.003 Inch)	320	320	183

Gross-ultimate and net-ultimate stresses in the grooved specimens are compared in Table XV. It is interesting to note that for the two ductile materials, 17-7 PH and L-605, the net stresses increased markedly with groove depth, but in the more brittle TZM the net stress decreased with groove depth.

The high values of net ultimate stress indicate that the side grooves are effective in producing a tri-axial stress state. For example, one specimen of PH stainless steel failed at a net stress of 226 ksi. If it is assumed that failure occurred by yielding, the minimum principal stress in the reduced area was 176 ksi (maximum shear-stress theory,

$$\sigma_{max} - \sigma_{min} = \sigma_{ys}).$$

The artificial condition imposed by the side grooves seems unduly severe, and it is doubtful that such conditions are ever encountered in practice. It is concluded, therefore, that side grooving is not a realistic approach to fracture toughness testing of thin gage materials.

TABLE XV

ULTIMATE STRESSES IN GROOVED SPECIMENS

Material	Groove Depth Inches	Net Area $1-^{-3}in^2$	P max. Pounds	Gross ksi	Net ksi
17-7 PH s.s. (0.012 Inch)	0.004	4.24	440	49	104
	0.006	3.18	380	42	119
	0.008	2.12	280	31	132
	0.010	1.06	240	27	226
L-605 (0.008 Inch)	0.004	2.12	450	73	212
	0.006	1.06	325	53	306
TZM (0.013 Inch)	0.002	6.38	832	83	130
	0.004	5.43	682	70	125
	0.006	4.29	418	43	98

3.3 DISCUSSION OF FRACTURE-TOUGHNESS TESTING

The purpose of a fracture-toughness test is to determine the size of the largest crack a material can tolerate without fracturing when loaded to the maximum service load. This problem is most often approached through the use of "sharp-crack" fracture mechanics which is based on a linear elastic stress analysis. If the requirements of this stress analysis are satisfied, the fracture toughness of a material can be measured in terms of the stress-intensity factor K, or the crack-energy release rate $\mathcal{G}$. Unfortunately, the requirements of the stress analysis are quite restrictive. The most restrictive requirement of any such mathematical theory is, of course, that the material be isotropic and homogeneous. It is unlikely that any thin gage metal or alloy will satisfy these requirements completely.

As the thickness of a material is decreased, the fracture mode of the material undergoes a transition from plane-strain to plane-stress. A plane-strain value of fracture toughness is thought to be characteristic of the materials and independent of test specimen size. This is not true of values measured under conditions of plane-stress.

Because almost all thin-gage materials exhibit a plane-stress condition, fracture toughness testing of these materials must be conducted with reference to a particular application, and interpreted in that light.

One very important point that this work has shown is that there can be no such thing as a "routine" fracture-toughness test for thin-gage materials. If one is seeking a routine test to evaluate the fracture characteristics of thin-gage materials, it is more realistic to use a relatively simple notch-tensile test.

57

Fortunately, the problems encountered when one attempts to measure the fracture toughness of thin-gage materials arise because of their high toughness. If a given test does not satisfy the requirements of the stress analysis, one can be confident that the toughness of the material is greater than the value obtained from the test.

IV. TEAR TESTS

Three types of tear tests were evaluated during the program. The significant features of each are discussed below.

4.1 BEAM TESTS

The fixture shown in Figure 34 was used to tear specimens in half lengthwise from a 1 inch long sheared notch. This test requires a rather large load to initiate tearing. As the crack propagates outward from the center of the grips, the moment at the notch root increases and the load falls off correspondingly. Load versus time is recorded on an X-Y recorder and the rate at which the load decreases is a measure of the tear resistance of the material. For instance, the full-hard Type 301 stainless steel fractured catastrophically with an instantaneous decrease in load. One interesting result of these tests is shown in Figure 35. This is a photograph of Type 430 stainless steel showing a plastic zone at the tip of the sheared notch. (The deformed region is actually a Luder's band which initiated at a very low load.)

4.2 PEEL TESTS

The grips shown in Figure 36 were used for this test. As shown in the photograph, a flap is cut in the specimen and bent 180° before attaching the lower grip. The specimen is then pulled in uniaxial tension and load versus time recorded. The significant characteristic of this test is that a very low load is required to initiate tearing, and once initiated, tearing continues at a constant load. As the specimen tears, energy is absorbed by two processes:

(1) Creation of new surface area
(2) Plastic deformation at the flap

An attempt was made to measure the relative magnitudes at these effects but with little success. It was thought that the relative amounts of energy required for these processes could be determined by choosing a material and varying the width of the flap which must be deformed during the test.

Using specimens of 0.012-inch thick 17-7 PH stainless steel, the flap width was varied from 1/2 inch to 3 inches. The results of these tests are presented in Table XVI. There appears to be little correlation between tearing load and flap width.
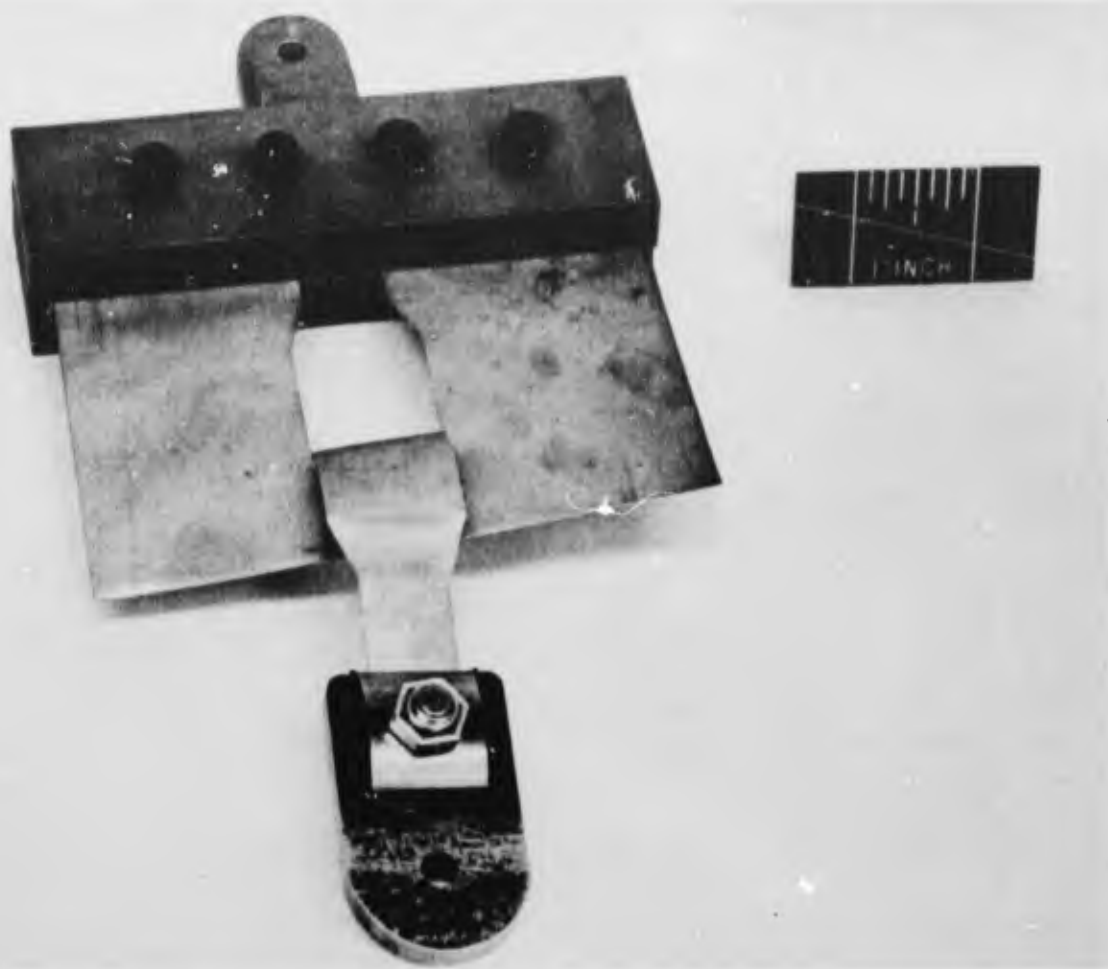
FIGURE 36. GRIPS AND SPECIMEN USED FOR PEEL TYPE TEAR TESTS

TABLE XVI

RESULTS OF PEEL TESTS ON 0.012-INCH THICK
TYPE 17-7 PH STAINLESS STEEL

Initial Flap Width, Inches	Constant Load, Pounds
1/2	46
3/4	50
1	48
1-1/4	48
1-1/2	58
1-3/4	45
2	55
2-3/8	47
3	36

TABLE XVII

TEAR TEST DATA OBTAINED FROM SELECTED THIN-GAGE ALLOYS

Material	Maximum Load Required, Pounds		
	Beam Test	Notch Tensile Test	Peel Test
TD Nickel (0.006 In.)	—	280	16
(0/012 In.)	1125, 1675	—	37
17-7 PH s.s.			
(0.005 In.)	825, 800, 800	210, 200	—
(0.012 In.)	1700, 1425	480, 480, 470	45
TZM (0.006 In.)	—	—	12, 12
(0.012 In.)	Shattered at 1950	850	—
L-605 (0.008 In.)	1375, 1600, 1300	480, 490	42
301 s.s. (full hard)			
(0.003 In.)	700, 425 (very brittle)	200, 250, 387	2
430 S.S. (0.006 In.)	635	—	15

All three methods give a good qualitative indication of the tear resistance of the materials tested, but the notch-tensile test is the most quantitative method available. If an extensometer is placed on the specimen, the area under the portion of the load-elongation curve where load is increasing will represent the energy to initiate tearing, and the area under the decreasing-load portion will represent the energy required to propagate the crack. Furthermore, the net tensile stress can be easily calculated in terms of the maximum load. The beam test and the peel test, on the other hand, both produce complex stress states which cannot be readily analyzed. The notch-tensile test is, therefore, the most useful test for evaluating the tear resistance of thin-gage alloys.
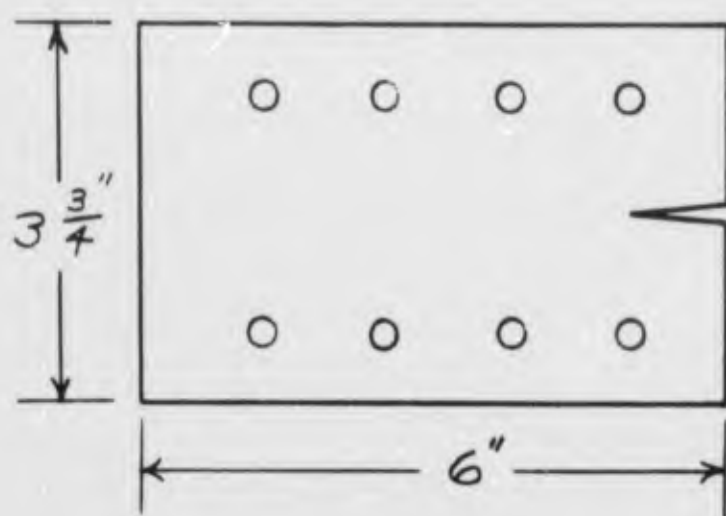
A. Beam Test Specimen
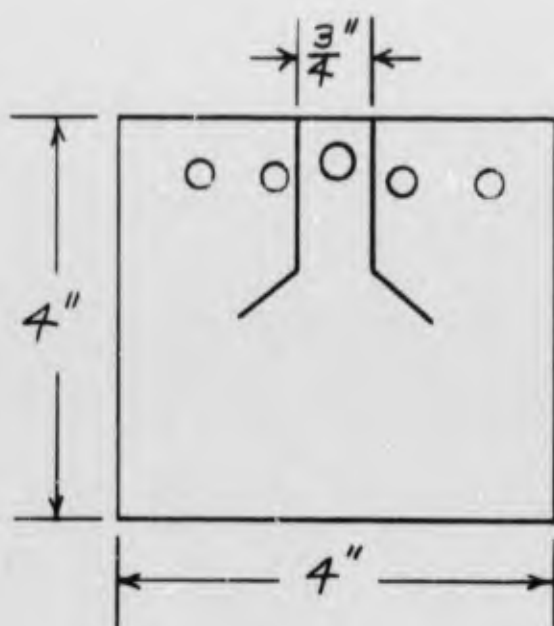
B. Peel Test Specimen
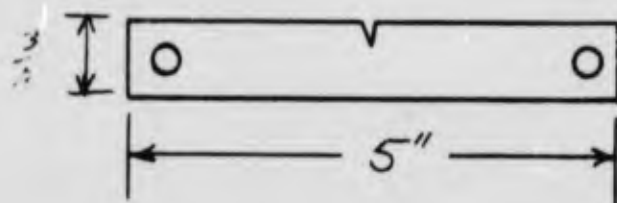
C. Notch Tensile Test Specimen

FIGURE 38. TEAR TEST SPECIMENS

64

V. MECHANICAL TESTING OF THIN GAGE METAL MATRIX COMPOSITES

One objective of this program was to define testing problems and to develop methods for mechanical testing of thin gage metal matrix filament reinforced composites. An example of this type of material is the titanium matrix-boron filament reinforced composite tape which was developed at Solar on Contract AF33(615)-5166. In its present state of development this material is typically 0.015-inch thick by 1/8-inch wide and contains 25 volume percent of 0.004 inch boron filaments in a matrix of commercially pure titanium (Ti75A). This composite tape material, which is made by a continuous roll diffusion bonding process, represents an important class of material as it may be readily used for the fabrication of lightweight structures requiring high strength and stiffness in specific directions. This material has been used exclusively on this program for the development of methods for tensile, creep, stress rupture, and fatigue testing of thin gage composites.

In addition, methods were developed for creep and tensile testing of filaments of boron and high strength wires.

5.1 TENSILE TESTING OF Ti-B COMPOSITE TAPE

When tensile loading uniaxial composite specimens, be it for tensile, creep, stress rupture, or fatigue testing, one problem is to transmit the external load through the matrix to the filaments so that the filaments will be stressed as equally as possible. Another problem is the measurement of average composite strain. Differences between filament strain and matrix surface strain can lead to large errors in elastic and even plastic property determinations. Both of these testing problems are less severe with thin gage composites than with composites of thicker section.

Figure 39 is a sketch showing the components of the composite tape used for this investigation. The tape was made by the continuous feeding of a middle carrier foil, the boron filaments, and two external cover sheet into the wheels of roll diffusion bonding machine. Both the carrier foil and cover sheets were grooved to accept the boron filaments. Typically, 28 filaments were placed in two layers which after edge trimming gave approximately 25 volume percent boron in the test specimens. Figure 40 contains photomicrographs of a tape cross-section after bonding. The good quality of the diffusion bond is illustrated by the continuous structure of the matrix across the bond interfaces. As the bonding operation is very fast, typically 1 second at 1800 F, the very small amount of boride formed at the filament-matrix interface (less than 300 Angstroms) has negligible effect on the mechanical properties of the composite.

Tensile specimens were prepared from composite tape by machining a reduced section 0.110-inch wide by 1.25-inch long, as shown in Figure 41. Each
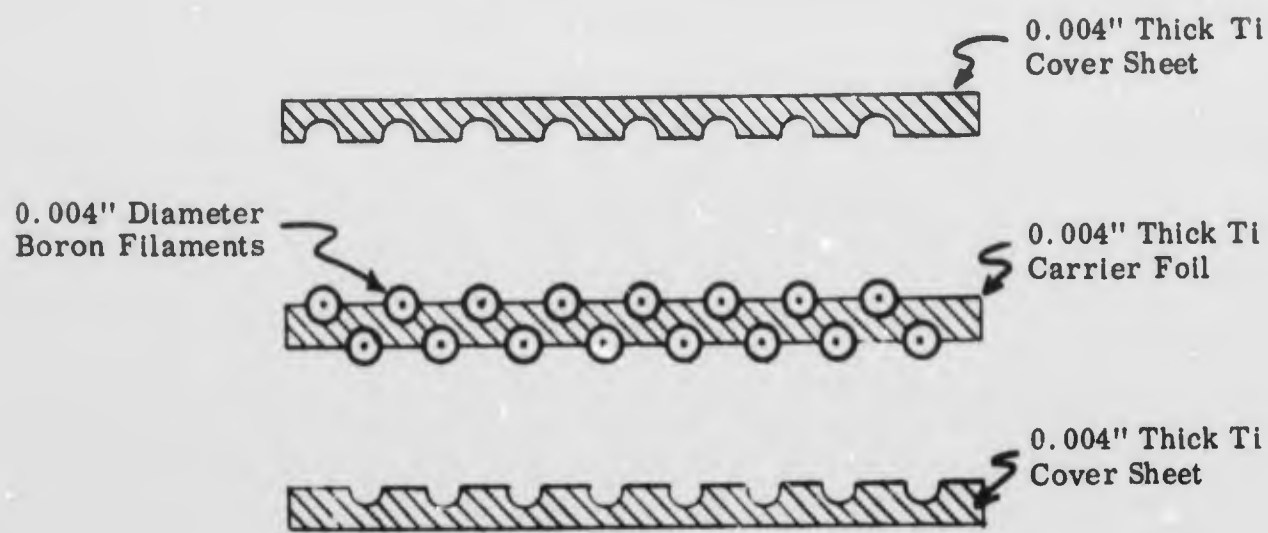
FIGURE 39. COMPONENTS OF A Ti-B COMPOSITE TAPE

A   35X Magnification

B   100X Magnification
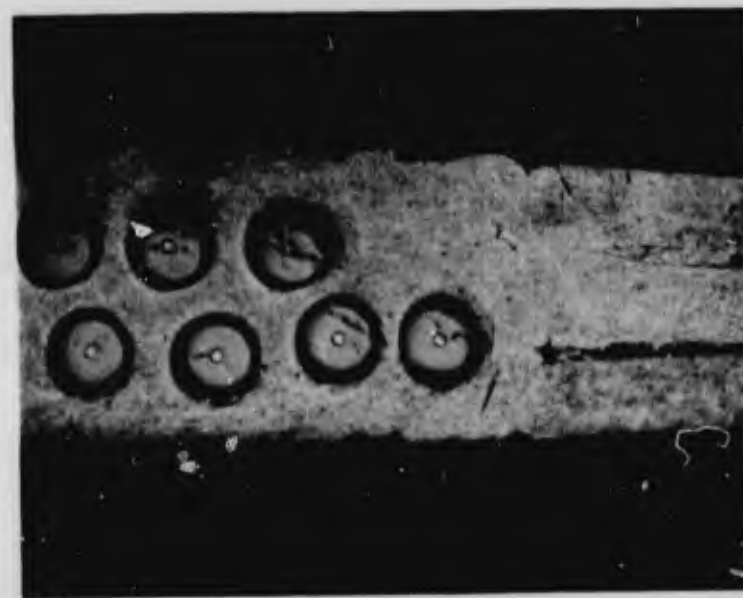
FIGURE 40. PHOTOMICROGRAPH OF Ti-B TAPE AFTER DIFFUSION BONDING
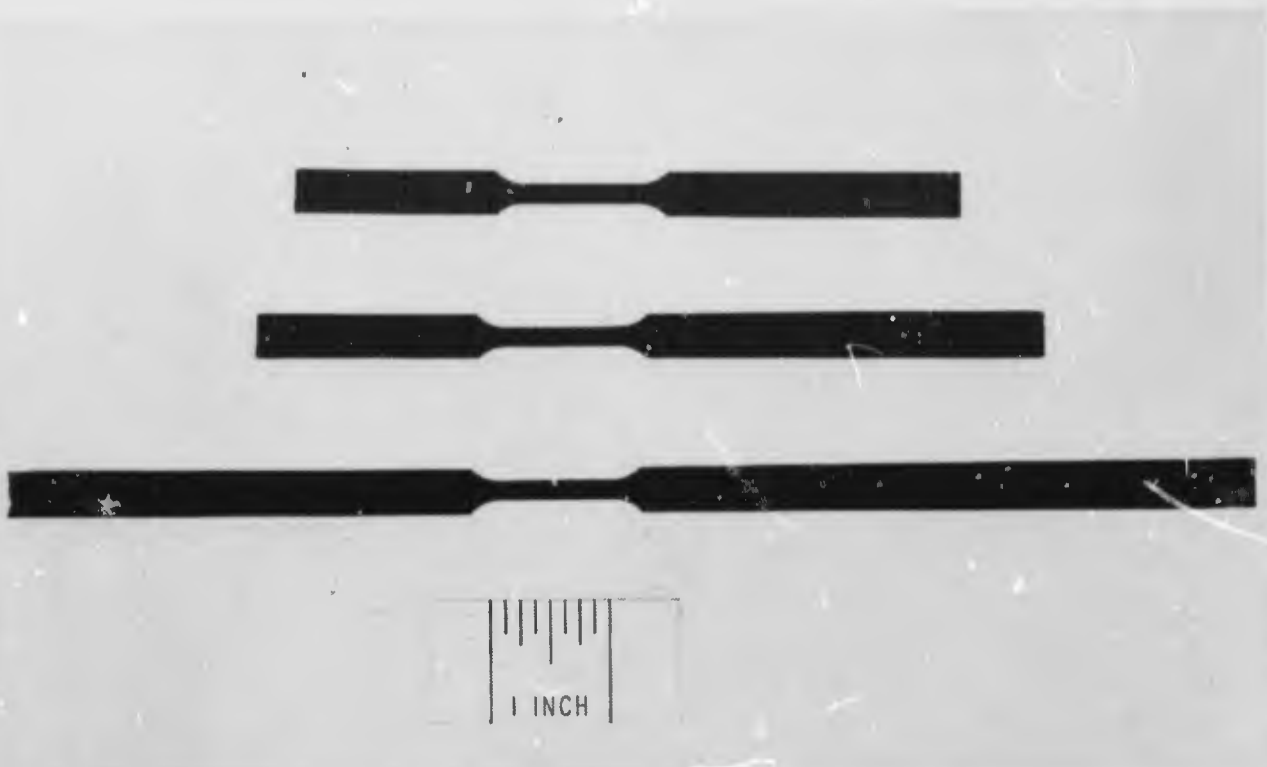
FIGURE 41.   TITANIUM-BORON TAPES AFTER DIFFUSION BONDING AND
TRIMMING

edge of the reduced section was thus machined to within 0.005-inch of the 0.100-inch
wide band that contained the filaments in the center of the tape. The specimens were
machined with a vertical milling machine using the fixture in Figure 42. The procedure
was as follows:

1.   Tape was cut into 10-inch lengths (standard specimen length for
use with thin gage tensile and creep testing machines.

2.   Typically five pieces of tape were stacked into the slot in the milling
fixture and securely clamped in place with the template cover plate.
Back-up strips of 0.030 inch thick stainless steel were used above
and below the stack of specimens to prevent edge rolling of the speci-
mens during the milling operation.

3.   The fixture was aligned in the machine, appropriate machine stops were
set, and the reduced section machined with a 3/4-inch diameter high-
speed steel end milling cutter.

4.   Very little hand finishing of the machined edges was required as little
burr was produced and close control of tolerances was easily attainable.

The specimens were gripped for tensile testing with the grips developed
earlier for testing 3/8-inch wide foils (see Fig. 23 of Ref. 2). This grip is very
similar to the grip developed two years ago for the general tensile testing of thin

·67
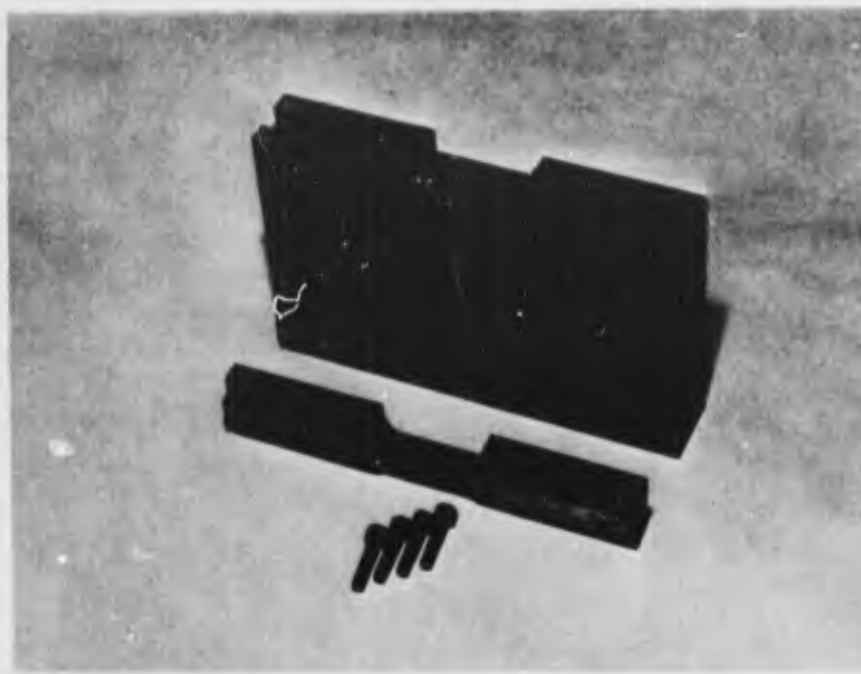
FIGURE 42.   FIXTURE FOR MACHINING REDUCED SECTION OF THIN GAGE
COMPOSITE SPECIMENS

gage materials (Ref. 1).   The principal changes are the decrease in width of the slot
that previously extended through a hole in the end of the specimen.   With the original
grip, specimen alignment was achieved by means of a hole in each end of the speci-
ment. With the new design shown in Figure 43, specimen alignment is achieved by
machining the specimen width to $0.375 \, ^{+0.002}_{-0.000}$ which fits the slot in the grip.   The
grips are attached to the specimen by means of the alignment and torquing fixture
developed earlier.

The tensile strength of the titanium-boron composite tape specimens was
measured at room temperature, at 200 degree intervals over the range 200 F to 1200 F
and at 1500 F.   All testing above room temperature was done in high vacuum (less than
1×10^{-5} Torr). To investigate the effect of strain rate on tensile strength, strain
rates of 0.005 and 0.05 inch/inch/minute were used at each temperature from 800 F
and higher.

The results of these tensile tests on two lots of composite tape are shown
plotted in Figure 44. The two lots of composite tape were made from the same lots of
titanium foil and boron filaments, and both contained the same volume percentage of
filaments.   Tape No. 726 was a preliminary sample produced during optimization of
the manufacturing process.   This tape contained a high frequency of broken filaments
and as a result the elevated temperature strength was lower than for tape No. 808
which was produced after process optimization.
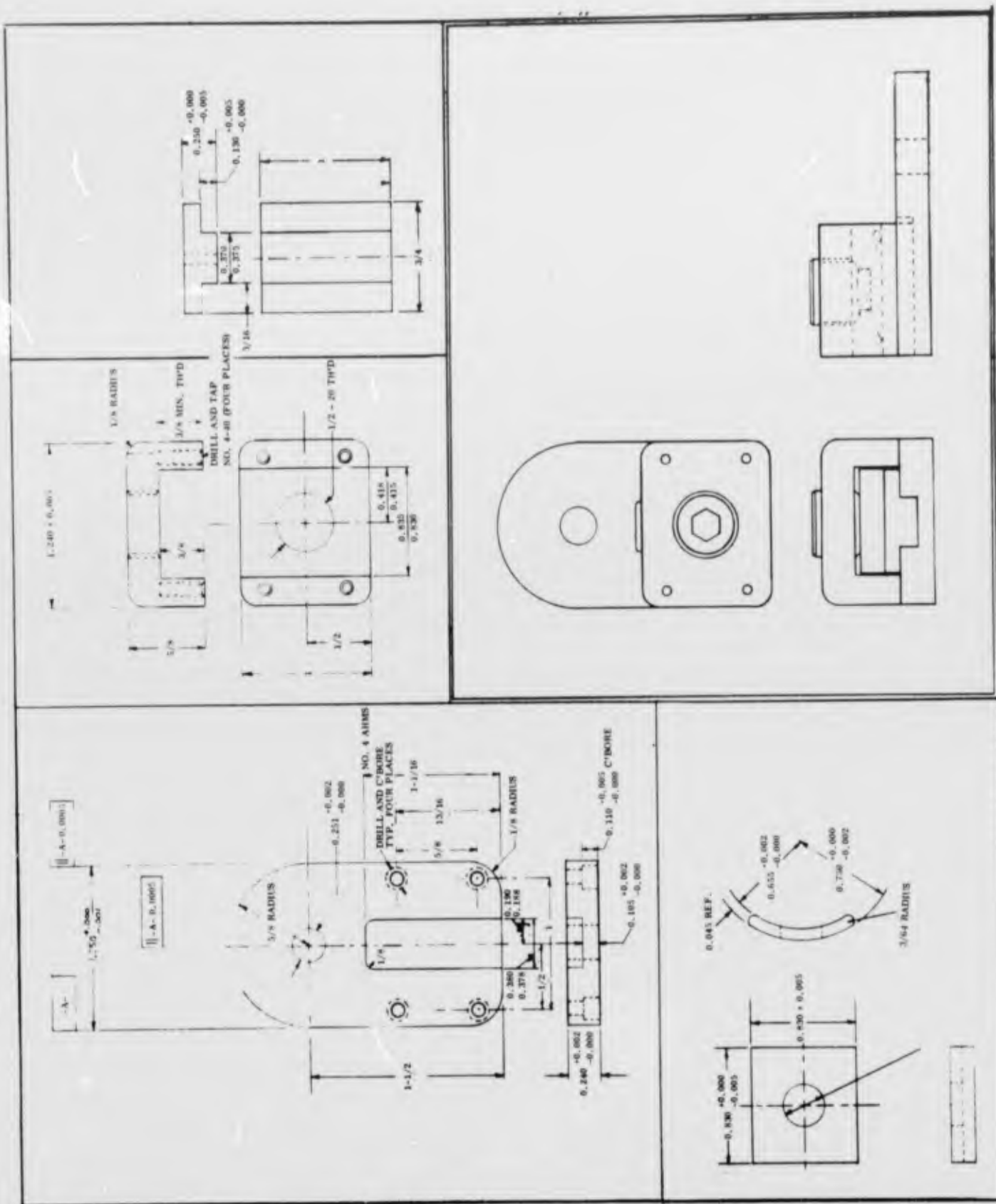
FIGURE 43. GRIP FOR TENSILE AND CREEP TESTING OF THIN GAGE COMPOSITES
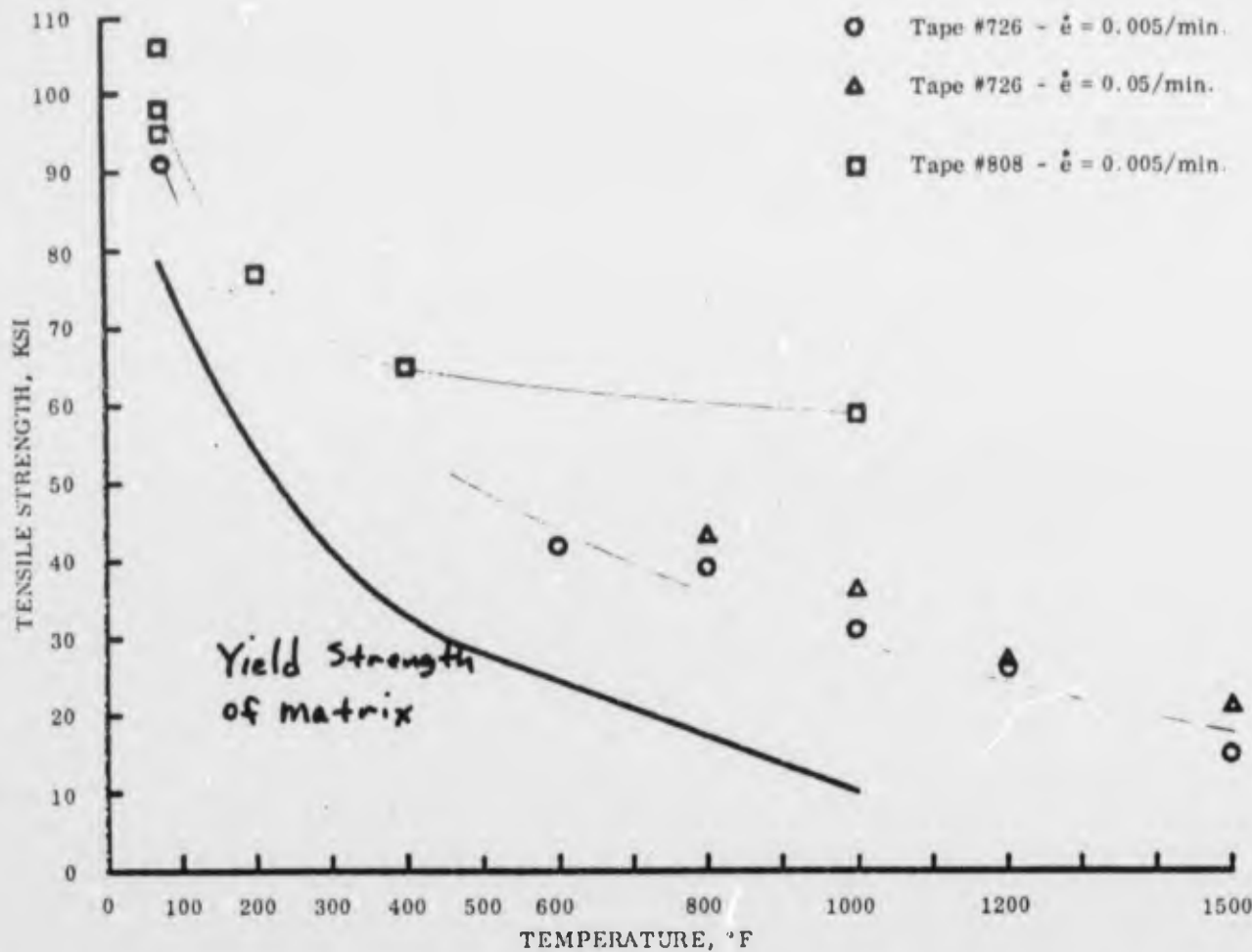
FIGURE 44. TENSILE STRENGTH VERSUS TEMPERATURE FOR Ti-B COMPOSITE TAPES (23 Volume Percent B in Ti-75A Matrix)

5.2 CREEP TESTS ON Ti-B COMPOSITES

Two specimens were tested in the high-vacuum constant-stress creep machine shown in Figure 45. The specimens were 3/8-inch wide by 10 inches long and had reduced sections approximately 1 inch long by 0.125-inch wide by 0.016-inch thick. Both composites were from the same tape and contained approximately 17-volume-percent boron. The thin gage tensile grips shown in Figure 43 were used to grip the specimens. Gage length strain was measured during the tests by means of a double-beam extensometer which was installed in the creep machine. This extensometer is a duplicate of the device developed earlier in the program.

The first specimen was initially loaded to 26.4 ksi at 800 F. The specimen reached a constant strain of 2000 μ-in/in after approximately 30 minutes, at which time the temperature was increased to 1000 F. At this temperature the specimen reached a constant strain of 5000 μ-in/in in approximately 70 minutes. Beyond this point the stress was periodically increased in increments of 2.4 ksi up to a total of 37.6 ksi. After adding each increment of load, the specimen was allowed to reach a constant strain before adding the next increment. Shortly after the specimen was loaded to 37.6 ksi, it broke at a total strain of 7500 μ-in/in. The data from this test are summarized in Table XVIII.

70
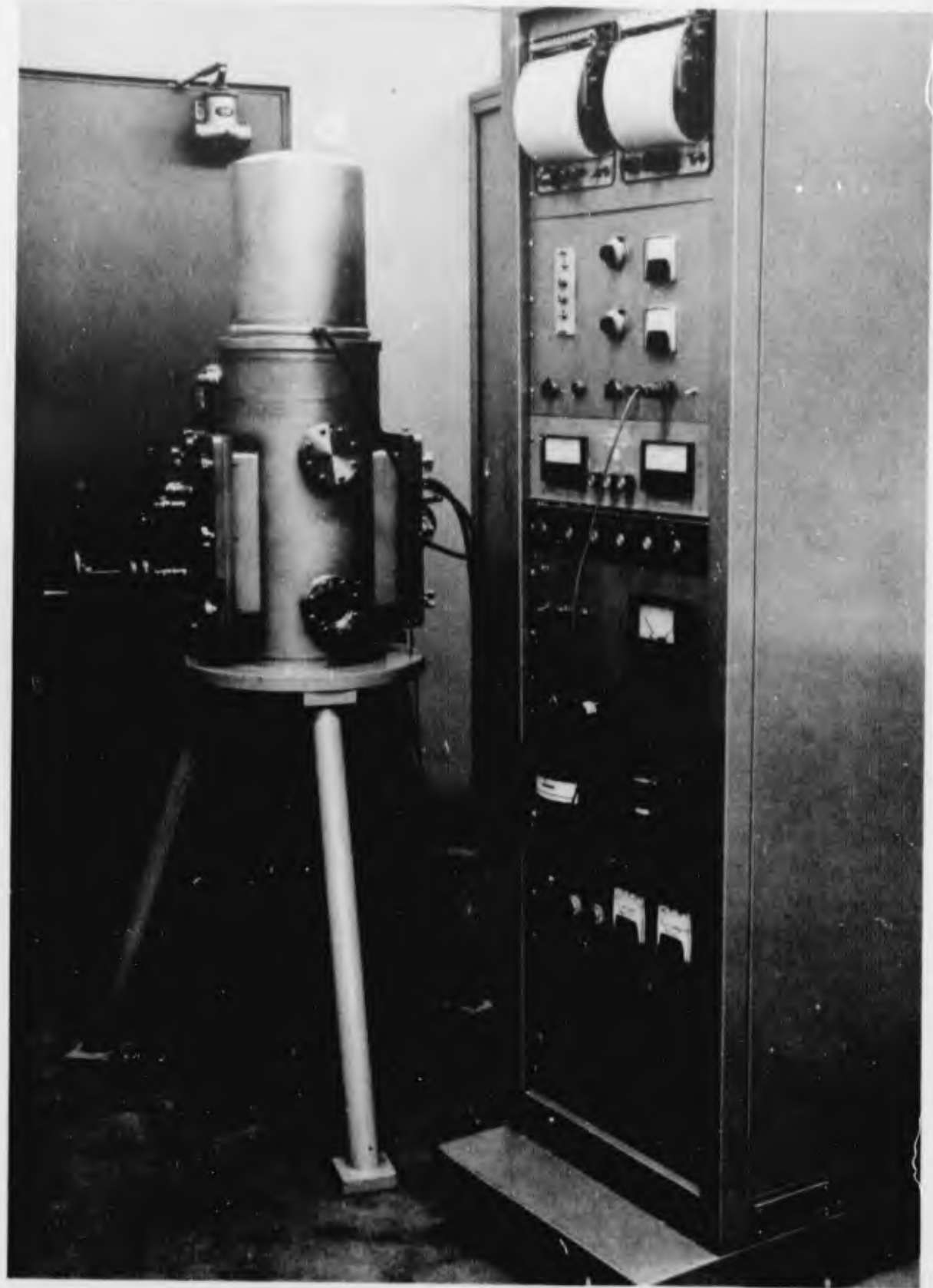
FIGURE 45. HIGH VACUUM CREEP FURNACE

TABLE XVIII

CREEP DATA FROM Ti-B COMPOSITE*

Temper-ature °F	Load Pounds	Composite Stress ksi	Stress in Boron After complete Relaxation of Matrix, ksi	Maximum Strain In Specimen μ-in/in
800	55	26.4	162	2000
1000	55	26.4	162	5000
1000	60	28.8	176	5500
1000	65	31.2	191	5800
1000	70	33.6	206	6500
1000	75	36.2	221	7000
1000	78.35	37.6	230	7500

* 17 volume percent boron in a Ti-75A matrix

The second specimen was initially loaded to 27.2 ksi at 1000 F. After 4 hours the specimen had reached a constant strain of 5000 μ-in/in. After 20 hours no increase in strain was apparent, so the stress was increased to 34.6 ksi and the test continued at this stress for approximately 100 hours. The creep curve obtained from this test is plotted in Figure 46. Analysis of this curve indicates that a minimum creep rate of 10 $\frac{\mu \text{-in}}{\text{in-hour}}$ was reached near the end of the test.

A model showing matrix and filament stresses as functions of time after load-ing and unloading is presented in Figure 47. As shown in the figure, the matrix begins to relax immediately after loading and the stress in the boron filaments increases correspondingly. Given sufficient time, the matrix stress will relax to zero and trans-fer its entire load to the boron. When the composite is then unloaded, the matrix is instantaneously loaded in compression, but again relaxes to zero stress with time. Several times during the test the specimen was unloaded and the matrix allowed to relax before reloading. A typical unloading and reloading cycle is plotted in Figure 48 The shapes of the loading and unloading curves are identical which indicates that the matrix behaves the same in compression as in tension. It appears from Figure 48 that the matrix required about 30 minutes to relax essentially completely. This indi-cates that the boron filaments carried the entire load during most of the creep test. If so, the average filament stress was 206 ksi.

At the end of the 100-hour test at 1000 F the specimen was unloaded and allowed to relax completely at temperature. This portion of the curve showed an instantaneous decrease in strain of 3500 μ-in/in and a slower decrease of 2000 in/in, giving a total decrease of 5500 μ-in/in. The total strain before unloading was 7250

72
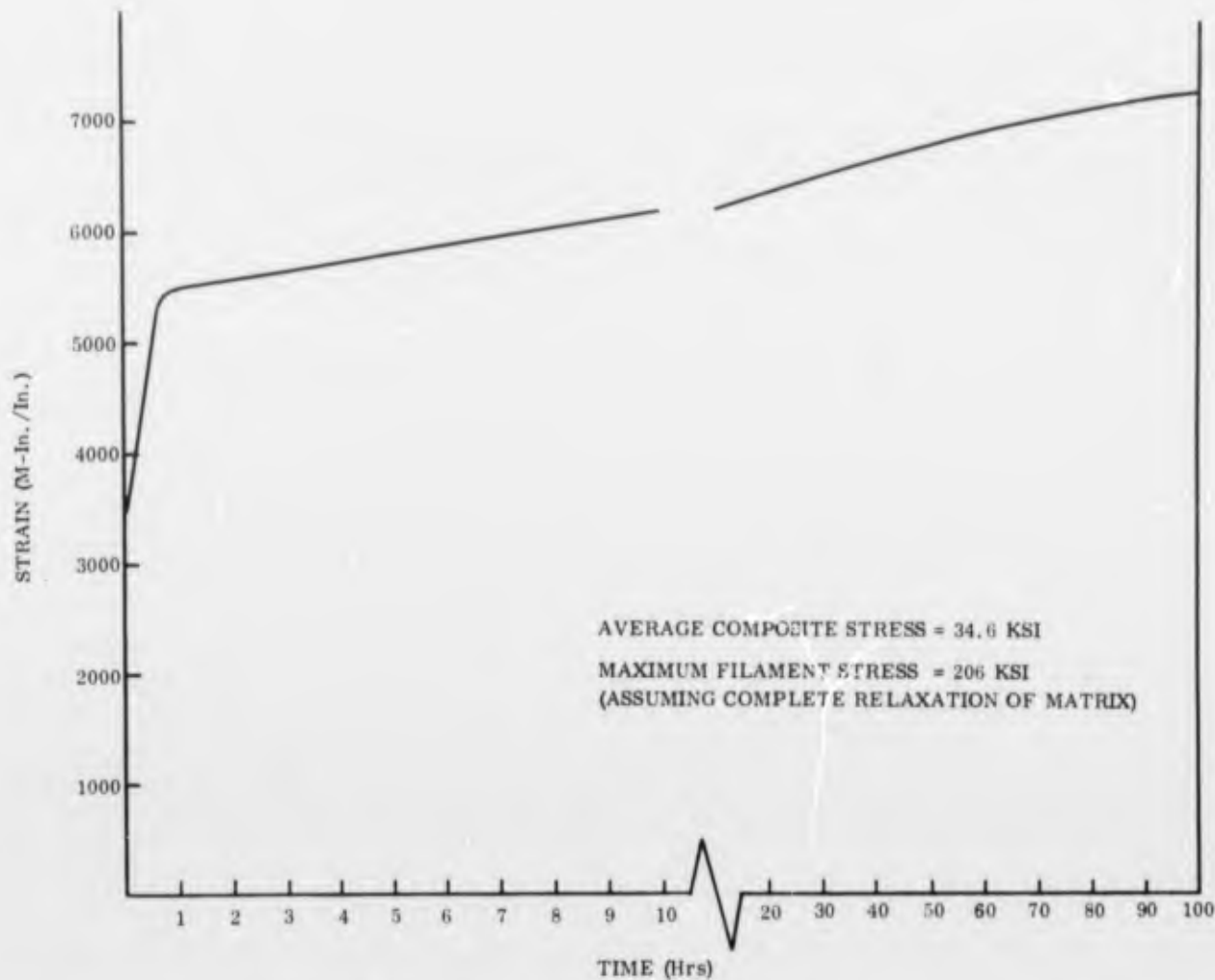
FIGURE 46. CREEP CURVE FOR A Ti-B COMPOSITE (17 Volume Percent Boron in a Ti-75A Matrix) AT A CONSTANT TEMPERATURE OF 1000 F

μ-in/in. These data indicate, therefore, that the specimen underwent a permanent deformation of 1750 μ-in/in during the creep test. If it is assumed that the recoverable strain of 5500 μ-in/in represents the elastic strain in the boron, an elastic modulus can be calculated for boron at 1000 F –

$$E_B = \frac{\sigma}{\epsilon} = \frac{206 \times 10^3}{5.5 \times 10^{-3}} = 37.5 \times 10^6 \text{ psi.}$$

This value is in excellent agreement with the measured values for single filaments reported in Section 5.3.

73
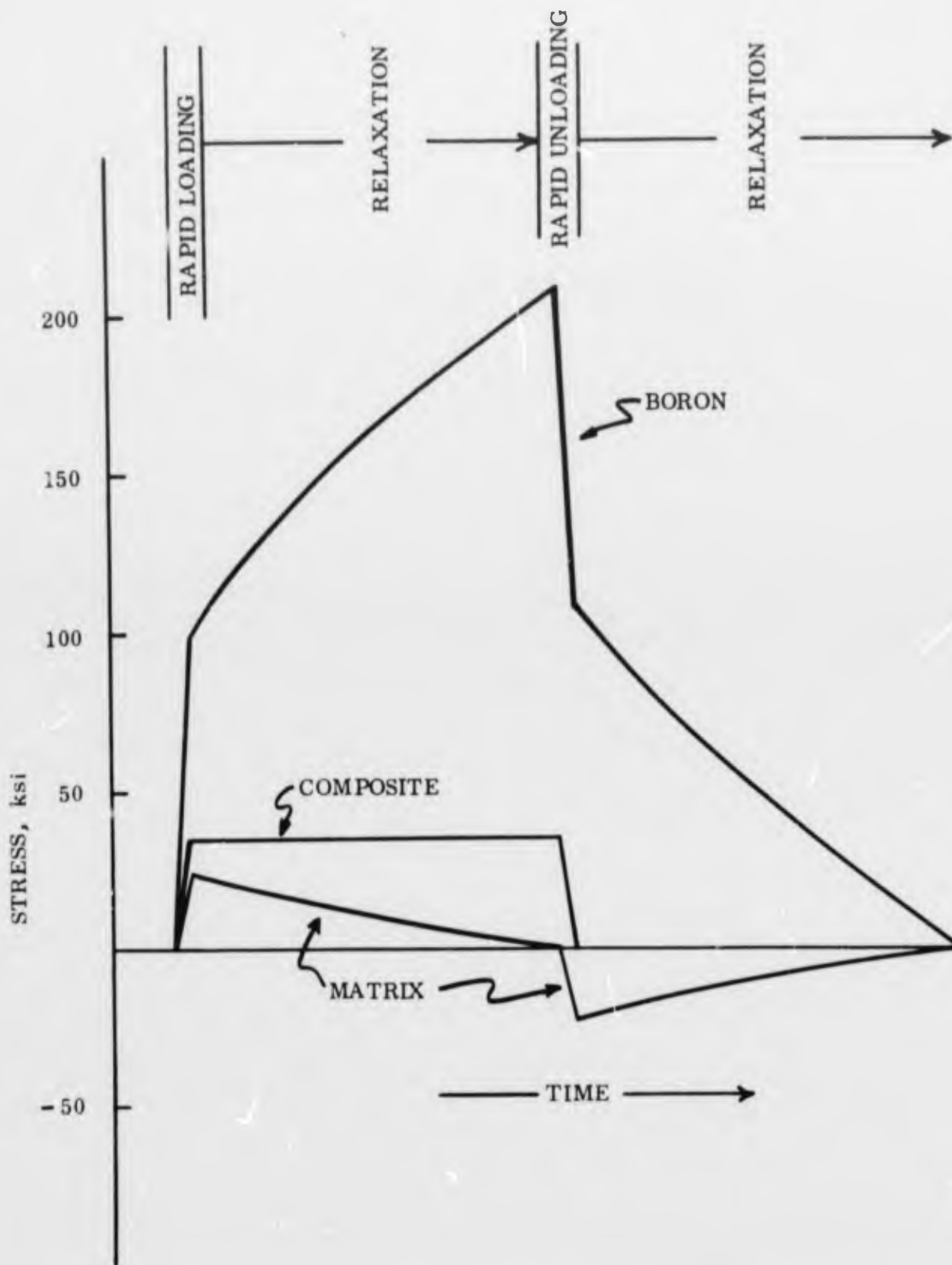
FIGURE 47. STRESS VERSUS TIME CURVES SHOWING LOAD TRANSFER FROM
MATRIX TO FILAMENTS AS MATRIX RELAXES AT 1000 F

74
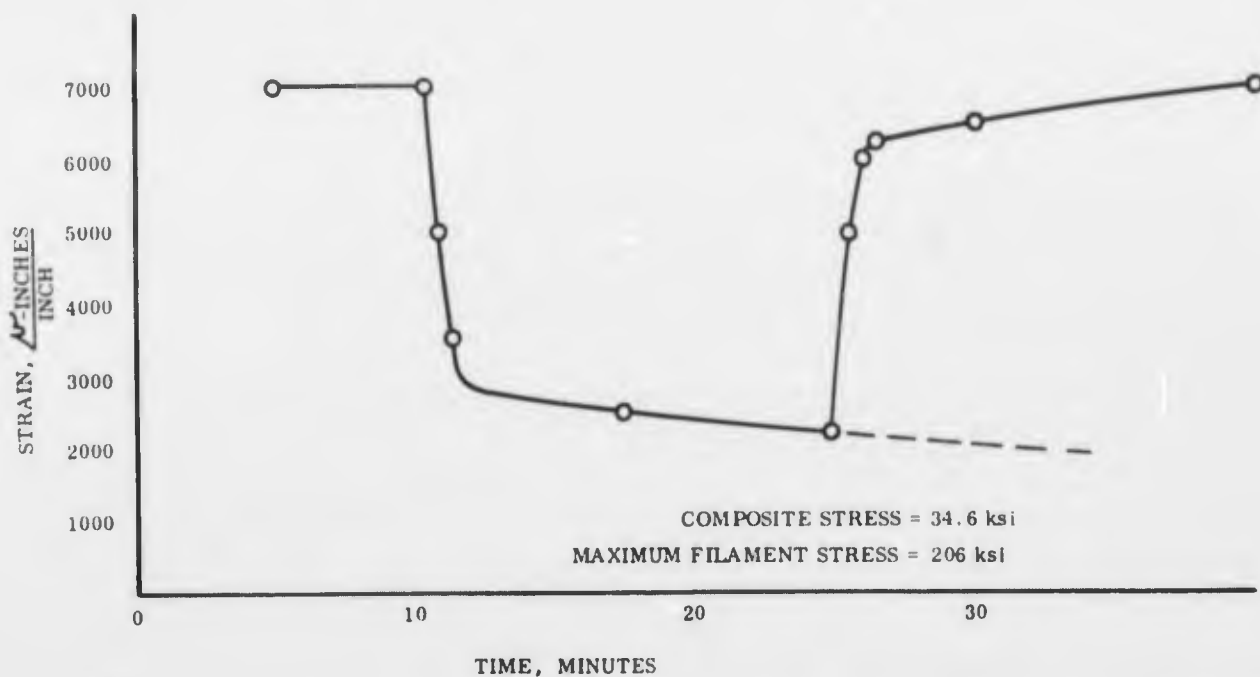
FIGURE 48.   UNLOADING AND RELOADING CURVES OBTAINED AT 81-HOUR STAGE
OF 100-HOUR CREEP TEST

Stress Relaxation and Elastic Modulus Measurements of Ti-75A Matrix Material

A 0.004-inch thick strip of Ti-75A matrix material was tested at 1000 F in the thin-gage tensile machine in order to measure the elastic modulus, and also to observe the stress-relaxation characteristics of the material.

The specimen was loaded rapidly several times in the elastic range to determine the elastic modulus. A value of 8.6×10^6 psi was obtained. The specimen was then loaded slowly $0.005 \frac{in}{in-min}$ to an apparent ultimate tensile strength of 7.44 ksi. The cross-head was locked and the specimen allowed to relax. The data from this test are plotted in Figure 49 as stress vs log time.

The elastic modulus determined from this test can be combined with the calculated value for the boron to give the composite modulus at 1000 F -

$$E_C = E_m V_m + E_B V_B$$
$$E_C = 8.56 \times 0.84 + 37.5 \times 0.16$$
$$E_C = 13.4 \times 10^6 \text{ psi}$$

75
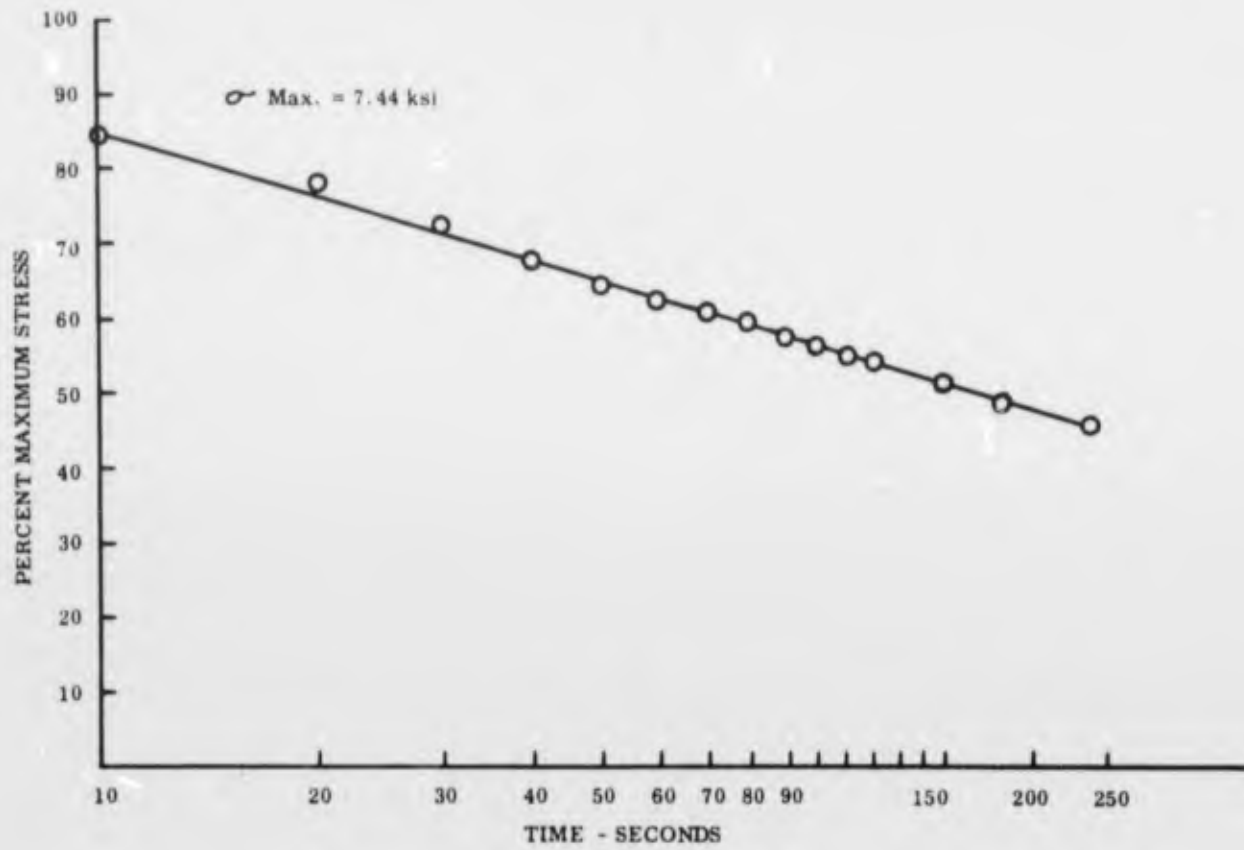
FIGURE 49. STRESS-RELAXATION CURVE FOR Ti-75A MATRIX MATERIAL
AT 1000 F

Room Temperature Tensile Properties of Creep Specimens After 100-Hour Creep
Test

After the creep test, the composite specimen was tested at room temperature
on an Instron testing machine to obtain room temperature tensile properties. The
results of this test are presented below:

Room Temperature Tensile Properties of a
Ti-B Composite after 100-Hr Creep Test

Elastic Modulus	Tensile Strength	Total Strain to Fracture
21.7×10^6 psi	120 ksi	$6600 \frac{\mu\text{-in}}{\text{in}}$

In Figure 50 the experimental stress-strain curve is compared with a theor-
etical curve calculated from the rule of mixtures. A curve for the Ti-75A matrix is
also included for comparison.

76

150 —

Calculated Curve

120 ksi

E = 22.2 x 10^6

STRESS ksi   100 —

Test Curve

E = 21.7 x 10^6

Ti-75A Matrix

50 —

1000   2000   3000   4000   5000   6000   7000

STRAIN $\frac{\text{-in}}{\text{in}}$
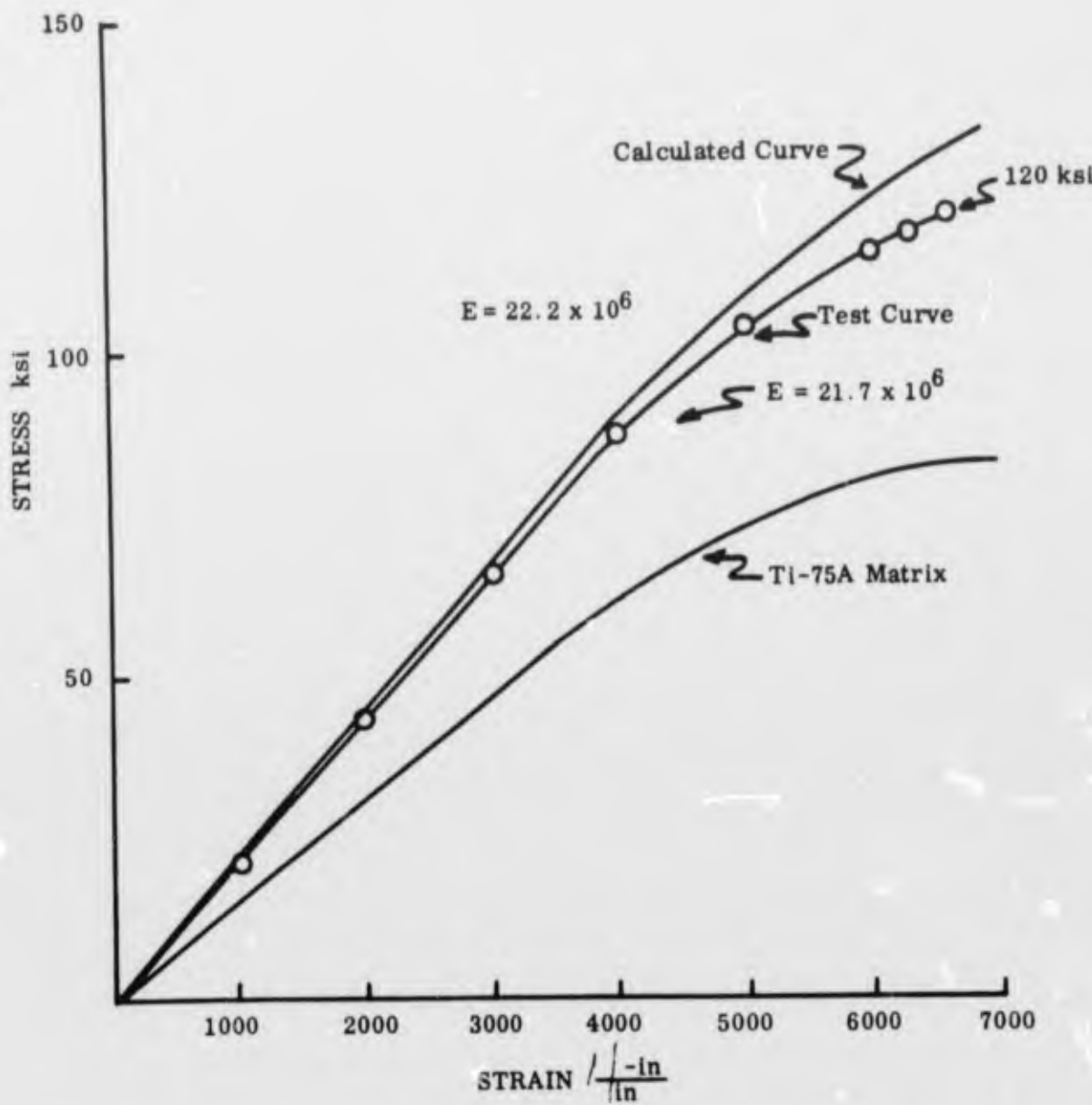
FIGURE 50.   ROOM-TEMPERATURE TENSILE PROPERTIES OF A 17-VOLUME
PERCENT Ti-B COMPOSITE AFTER 100-HOUR CREEP TEST AT
1000 F AND 34.6 KSI CONSTANT STRESS

5.3   TENSILE AND CREEP TESTING OF BORON FILAMENTS

In general, the problems in tensile and creep testing of high strength filaments and wires are similar to those encountered when testing thin gage sheet materials. The problems which are particularly acute with filaments and wires include:

• Method of gripping for application of load

• Measurement of strain

A complex stress concentration occurs at the point of load application with any tensile or creep specimen. For filaments or wires, being of constant section, the stress is thus greater at the gripped ends than in the center. This stress concentration tends to cause failures at the grips.

To minimize stress concentrations, the load must be applied gradually as the filament enters the gripping device. Stated another way, the strain in the filament should decrease gradually from a maximum as it enters the grip to zero value some 20 to 300 filament diameters into the grip, as shown ideally in Figure 51.

As with filament gripping, the principal problem with strain measurement is the avoidance of stress concentration. Mechanical extensometers requiring very low forces for actuation or optical tracking instruments must be used for direct strain measurement. At elevated temperatures the problem becomes more difficult as conventional mechanical extensometers cannot be used and apertures into the hot zone of furnaces, for optical tracking, may result in error due to temperature nonuniformity along the gage section.
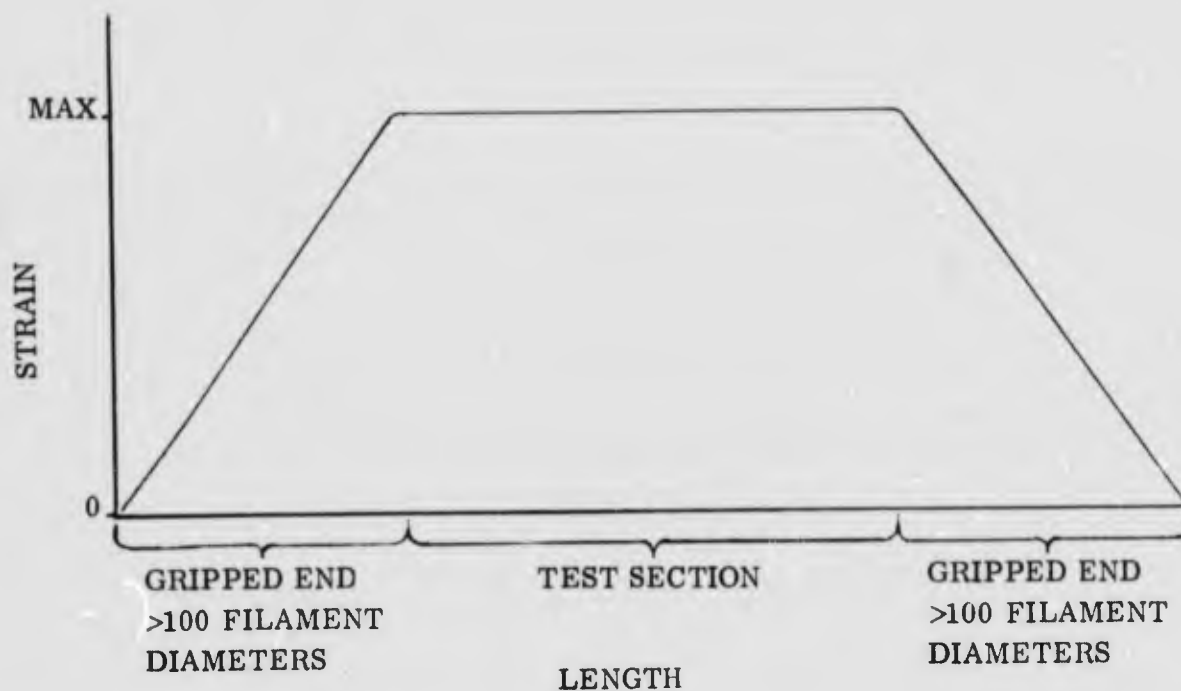
FIGURE 51. IDEALIZED STRAIN ATTENUATION FOR GRIPPING FILAMENTS OR WIRES FOR TENSILE OR CREEP TESTING

The following test methods have been used by various investigators:

Gripping Methods

1. Adhesive bonding of filament to plates gripped by conventional methods.

2. Cementing each end of the filament into a hypodermic needle and then using the enlargements on the needles for gripping, much like gripping a buttonhead type tensile specimen.

3. Clamping between flat grips faced with a thin layer of rubber.

4. Clamping with scissor-action grips lined with soft materials, such as aluminum or silver. Tantalum and graphite linings have been used for elevated temperature testing.

Strain Measurement Methods

1. Light weight bending beam extensometer attached to filament. Useful only near room temperature.

2. Optical tracking of marker flags attached to gage length of filament.

3. Indirect method from cross-head displacement using several different lengths of filaments to determine effects of deformations other than in the test length of the filaments.

5.3.1 Experimental Procedure

The tensile machine, related equipment and procedures developed during the first two years of this program were designed specifically for thin gage sheet metals, alloys, and composites. Methods for gripping boron filaments also were investigated and during this period tensile tests were performed at temperatures ranging from 80 to 2260 F, (see Sec. 3.4 of Ref. 2). During the third year, greater emphasis was placed on thin gage filament reinforced metal matrix composites of less than 0.030 inch thickness, and improved test methods were developed for filaments. The reliability of the gripping method was improved and the double beam extensometer was successfully applied to filaments.

The method for filament gripping is shown in Figures 52A, 52B and 52C. This procedure is modified from the one report earlier (Ref. 2). In Figure 52A the ends of the filament have been positioned to coincide with a line scribe into the center axis of the clamping surface of each grip. (Note that the filament extends through a hole in the bolt to permit clamping of the filament on both sides of the bolt. It is very important that the depth of the scribe line be made gradually deeper toward the free edge of the grip to minimize stress concentration. The depth and width of the line should increase from essentially zero to about two filament diameters in a length of about 20 filament diameters. A quick-setting adhesive was applied as shown, to hold the filament in alignment with the scribe lines on the grips. Good alignment is critical as it minimizes bending stresses in the filament when the test load is applied. Before the adhesive completely hardened, two silver foil pressure pads were placed over the filament and each grip was assembled and tightened as shown in Figures 52B and 52C respectively.

A. Applying Adhesive to Position Filament in Grip
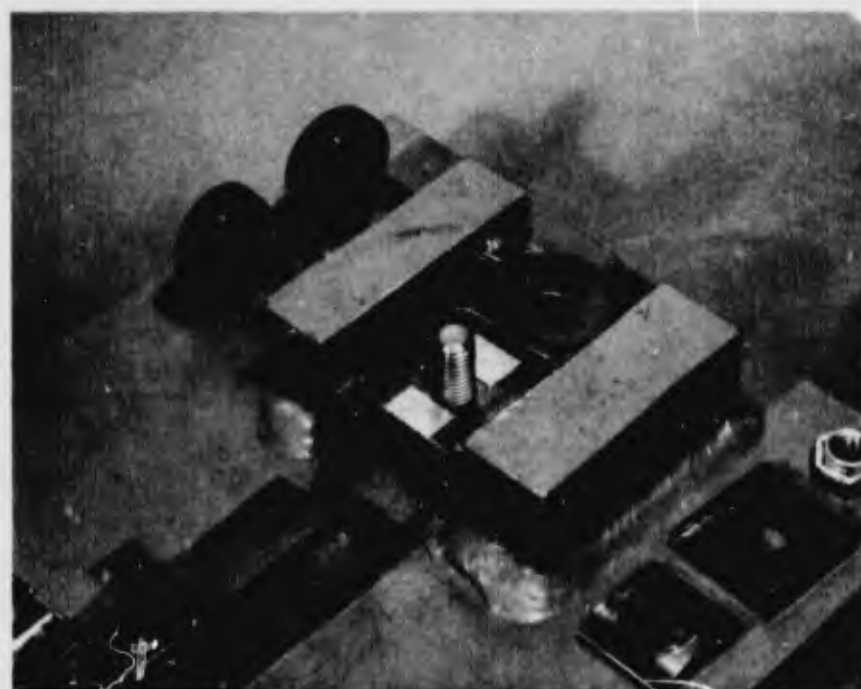
B. Silver Foil Pressure Pads Placed Over Filament

FIGURE 52. METHOD FOR GRIPPING BORON FILAMENTS FOR TENSILE
AND CREEP TESTS (Sheet 1 of 2)

C. Torquing Grip to Proper Clamping Force

FIGURE 52. METHOD FOR GRIPPING BORON FILAMENTS FOR TENSILE
AND CREEP TESTS (Sheet 2 of 2)

The pressure pads consisted of a double thickness of 0.004 inch pure silver foil. Other soft materials, such as aluminum or copper, though not evaluated here, should also be useful. The thickness should be at least 2 filament diameters and the foil must extend to the edge of the grip to avoid stress concentrations in the filament. The grips were tightened with a torque of 30 inch pounds which produced a clamping force of about 300 pounds.

The extensometer clips were attached to the filament as shown in Figure 53. For accurate control of gage length (2.00 inches) and to avoid damage to the filament, the extensometer clips were held in the proper position by a spring actuated fixture. The grips and extensometer clips thus attached, the test filament was then transferred to the test machine by means of the special handling device shown in Figures 54A and 54B.

The extensometer clips developed for filament (and wire) testing are shown in Figure 55. This clip is similar to the one developed earlier for testing thin gage sheet, (see Fig. 11 of Ref. 2). The molybdenum pad and cone-point of the earlier clip have been replaced with two copper pads with slightly convex surfaces. The spring clip and retainer were made from 0.010 inch thick by 3/16 inch wide molybdenum strip. The choice of materials depends upon test temperature and materials compatibility considerations. For example, when testing tungsten wires at higher temperature, columbium pads and tantalum alloy clips could be used. The copper pads have proven satisfactory for boron testing as no increased frequency of filament fracture was experienced for temperatures to 1000 F for durations to 70 hours.

FIGURE 53.   INSTALLING EXTENSOMETER CLIPS TO BORON FILAMENT

The high elastic recoil of a filament at the end of a tensile test typically caused multiple fracturing so that it was generally impossible to determine the initial site of fracture.   The claim of no increase frequency of filament fracture is based on the fact that normally a short length of filament would be found intact within each extensometer clip after the tensile or creep test.

The test load was applied to the filaments in two stages with the weights shown in Figure 56. A preload consisting of the lower grip and a small initial weight was applied to straighten the filament and to permit positioning of the extensometer pushrods.   The combined weight of the lower grip and initial weight was 0.49 pound which produced an initial stress of 39,000 psi in the filament.   The upthrust of each extensometer pushrod was approximately 0.02 pound. (With a 0.004 inch diameter filament, the resulting stress would be 1.6 ksi, which is negligible in the case of boron.)   After the test temperature had been attained, the test load was applied to the filament by lowering the final weights which were supported on a platform attached to the lower pullrod of the tensile machine as shown in Figure 57.   Stress levels of 219, 264, and 316 ksi were produced with various combinations of the weights shown in Figure 56.

A boron filament installed in the test machine is shown with the extensometer attached in Figure 58. (The sheet of paper was inserted to make the filament more discernable in the photograph.)   The extensometer pushrods extend downward out of the furnace and transmit the motion of the gage marker clips to the double-beam extensometer.   For a description of the double-beam extensometer see Section 2.3 of Reference 2.

82
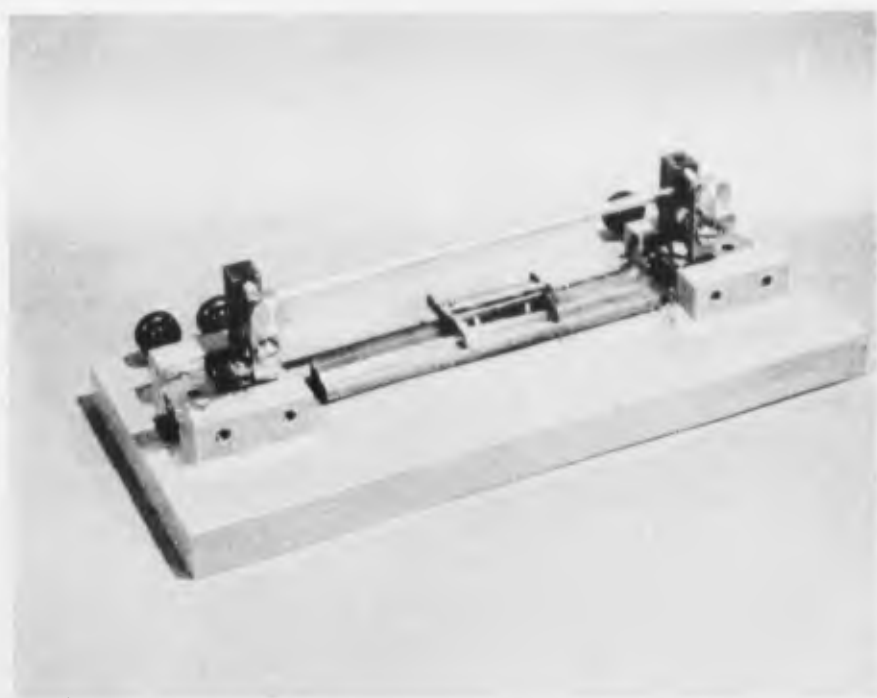
A. Transfer Fixture Attached to Gripped Filament
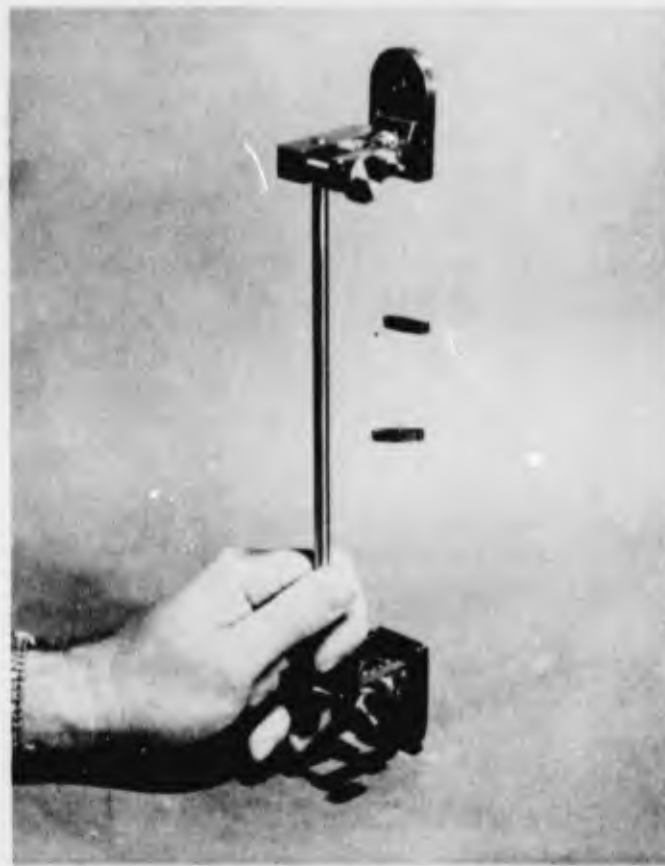
B. Gripped Filament Being Transferred From
Torquing Fixture to Test Machine

FIGURE 54.   METHOD USED TO TRANSFER GRIPPED FILAMENT
TO TEST MACHINE

83
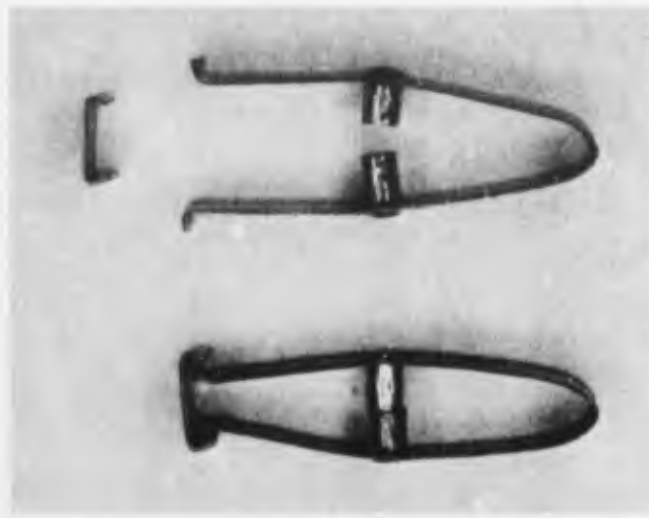
Magnification: 2X

FIGURE 55. EXTENSOMETER CLIPS FOR FILAMENTS AND WIRES

FIGURE 56. WEIGHTS AND WEIGHT PLATFORM USED FOR CREEP
TESTING BORON FILAMENTS

The procedure for creep testing of filaments was as follows:

1. Cut filament to length (10 inches) and measure diameter to within
   50×10^{-6} inches

2. Install grips and extensometer clips

3. Transfer to test machine and apply preload
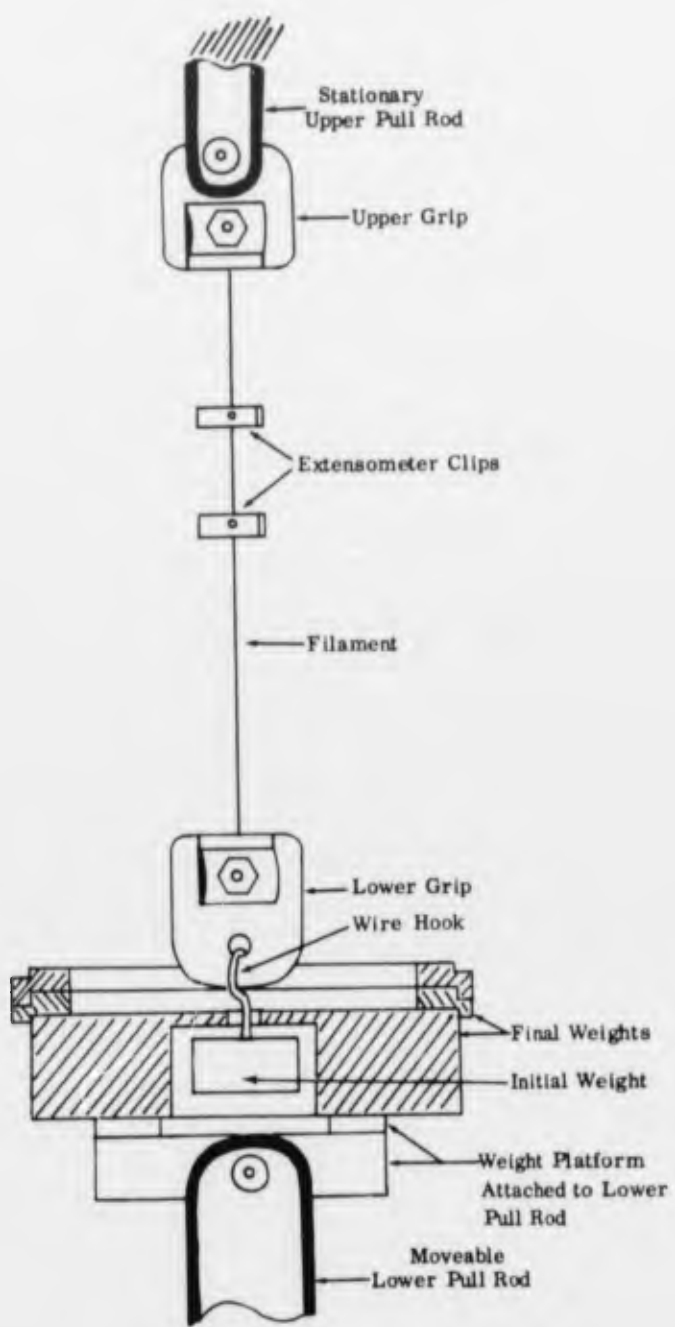
FIGURE 57.   METHOD FOR LOADING BORON FILAMENTS FOR
TENSILE AND CREEP TESTS
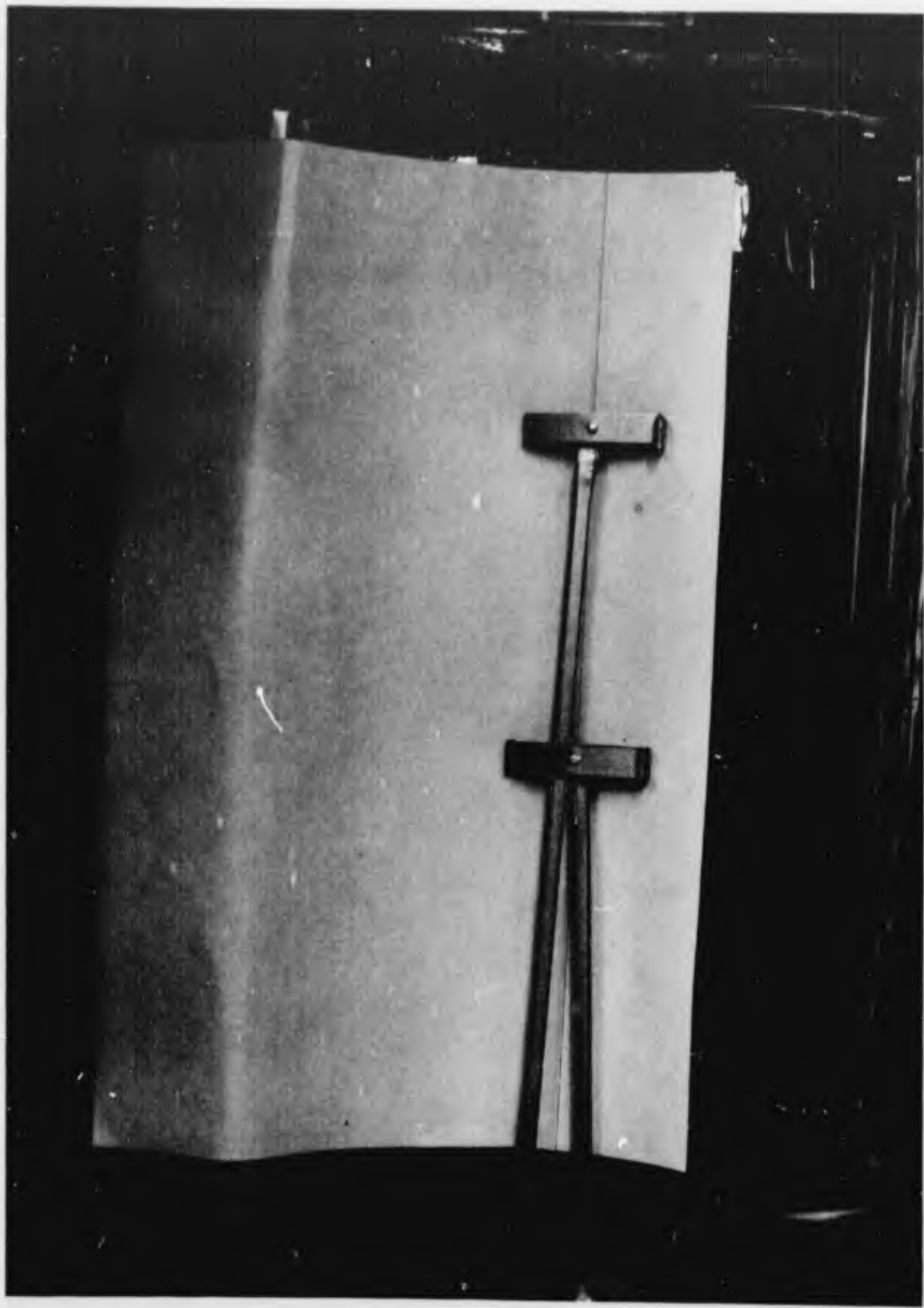
FIGURE 58. CLIPS AND PUSHRODS OF DOUBLE BEAM EXTENSOMETER
ATTACHED TO BORON FILAMENT

4. Attach and electrically balance extensometer

5. Evacuate chamber and heat specimen to desired temperature

6. Lower the weight platform and apply the full test load with dead weights

7. Record gage length strain as a function of time

The procedure used for tensile testing filaments and wires was as follows:

Steps 1 through 5 were the same as for creep testing, listed above.

Step 6 - With weight sufficient to exceed the ultimate strength of the filament on the weight platform, lower the weight platform and apply the test load at a predetermined rate until filament fracture occurs.

Step 7 - Record stress (load) as a function of gage length strain.

The principal advantages of these procedures are:

1. Filament buckling or overloading during periods of furnace heating or cooling are avoided by use of the small dead-weight preload.

2. High sensitivity and precision in strain measurement with excellent stability over extended periods of time.

3. All gage length strain, even that which occurs on loading and unloading during a creep test, can be measured and recorded.

5.3.2 Creep Test Results

The results of creep tests on boron filaments conducted at 1000 F in high vacuum (10^{-6} Torr) at stress levels of 219, 264, and 316 ksi are shown in Figures 59, 60 and 61 respectively.

The creep test at 219 ksi ran for 15 hours and resulted in a permanent creep strain of 1490 μ inches/inch. The creep rate decreased from 200 μ inches/inch/hour at the first hour to a nearly steady state rate of 14 μ-inches/inch/hours at the fifteenth hour. An unload-load cycle was made after 15 hours of constant load testing to determine the amount of plastic deformation which had occurred during the creep test. As shown in the insert of the figures, the stress was cycled from 219 to 39 to 219 ksi by lifting and reapplying the final weight (see Fig. 59). As nearly steady state conditions had been attained at the end of 15 hours, the change in strain corresponding to the 180 ksi stress reduction during the unloading cycle was almost entirely elastic. This technique is effective in determining the elastic and plastic components of the total strain, and is also a convenient method for determining the elastic modulus. The elastic modulus on unloading calculated to be 37.3 x 10^6 psi (at 1000 F).

Another test shown plotted in Figure 60 ran for 65 hours at a stress of 264 ksi. The creep rate decreased from approximately 250 μ-inches/inch/hr at the first hour, to 27 μ-inches/inch/hour at the fifteenth hour to a nearly steady state creep rate of 10 μ inches/inch/hour after 65 hours. The permanent creep strain was determined

87
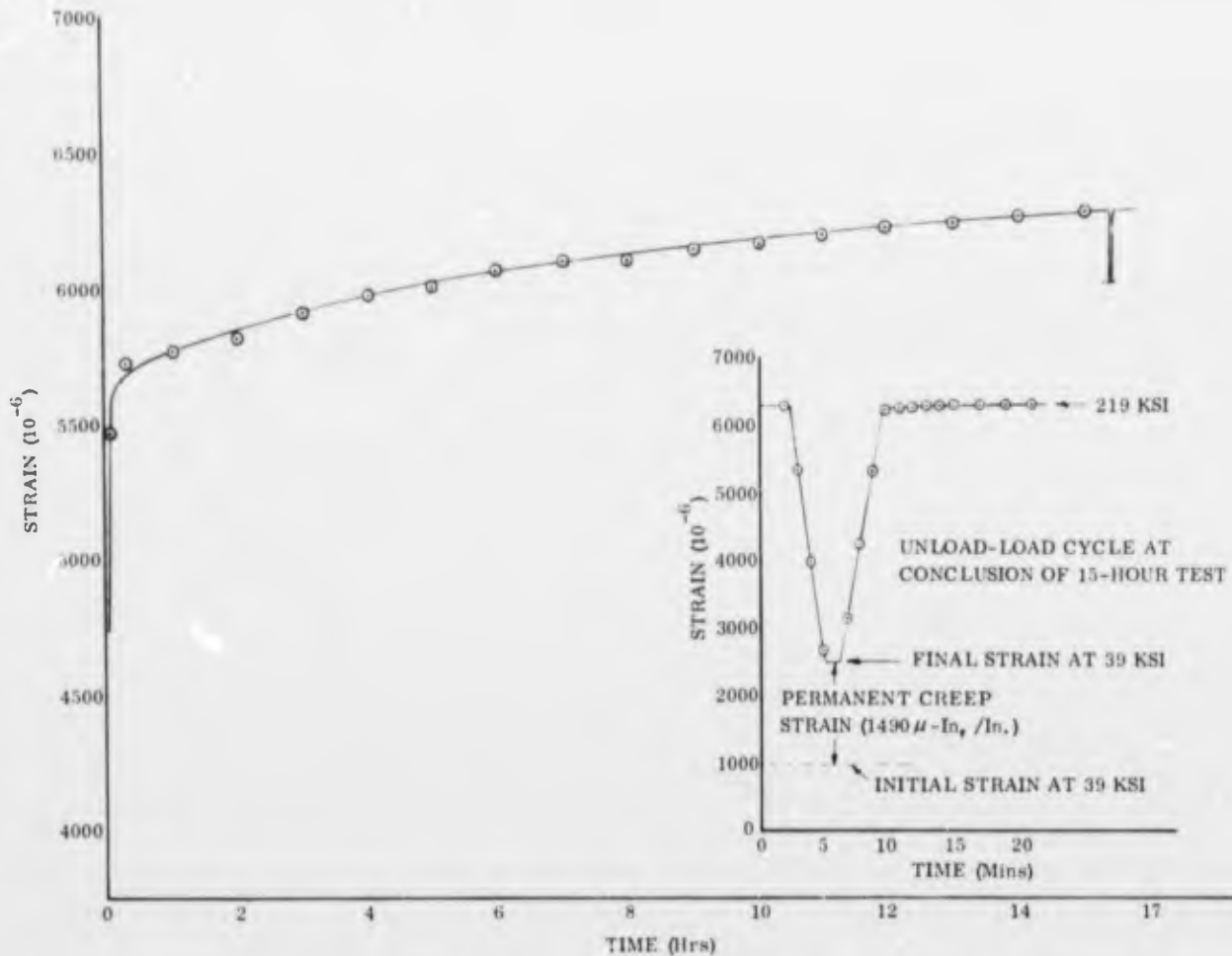
FIGURE 59.   CREEP OF 0.004-INCH DIAMETER BORON FILAMENT AT 1000 F IN
HIGH VACUUM AT 219 KSI STRESS

at the completion of the test by measuring the change of strain as the stress was de-
creased from 264 to 39 ksi.   The permanent creep strain which had occurred in 65 hrs
at 264 ksi at 1000 F was 3470 μ inches/inch.

The strain during the initial loading of the above test was also measured and
is shown in the insert of Figure 60.   The weight platform was retracted at a rate of
0.05 inch per minute which resulted in a strain rate of only 2000 μ inch/inch/min.
Note that the strain continued at the same rate for about 500 μ inch/inch beyond the
point where the test load had been fully applied.

The final creep test of a boron filament was conducted at 316 ksi at 1000 F.
This test shown plotted in Figure 61 ran for over 16 hours when fracture occurred after
a total strain of 11,300 μ-inches/inch.   For this test the weight platform was retracted
at a rate of 0.4 inch per minute which resulted in an initial strain rate of about 37,000
μ-inches/inch/minute.   The constant load strain rate at the end of the first hour was
about 250 μ-inches/inch/hour (4.2 μ-inches/inch/min).   The creep rate reached a
minimum value of 30 μ-inches/inch/hour after fifteen hours and then increased until

88

fracture occurred at 16.3 hours. This rise in creep rate indicates that a defect was growing within the 2 inch gage section of the filament for over one hour prior to fracture.

5.3.3 Tensile Test Results

The results of tensile tests of boron filaments and René 41, AFC-77, and AM355 wires are presented in Table XIX. These data should be considered somewhat preliminary as insufficient tests were performed to permit statistical analysis. For example, just the uncertainty of filament diameter of $\pm 50 \times 10^{-6}$ inch results in a corresponding uncertainty of ± 2.5 percent on the elastic moduli and stress values. As was demonstrated on Contract AF33(615)-5166, large numbers of tests are required on filaments to accurately characterize their mechanical properties.
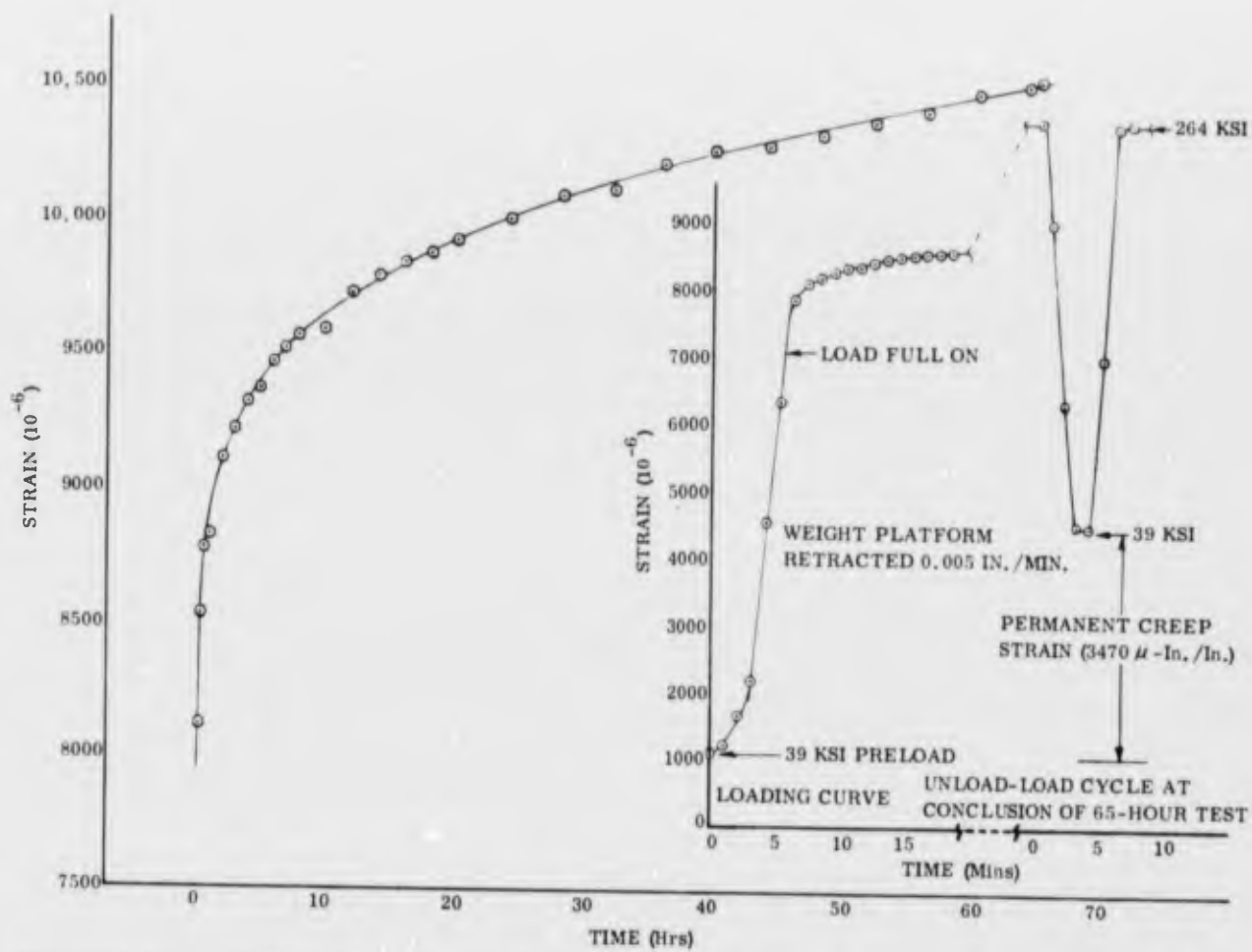
FIGURE 60.   CREEP OF 0.004-INCH DIAMETER BORON FILAMENT AT 1000 F IN HIGH VACUUM AT 264 KSI STRESS
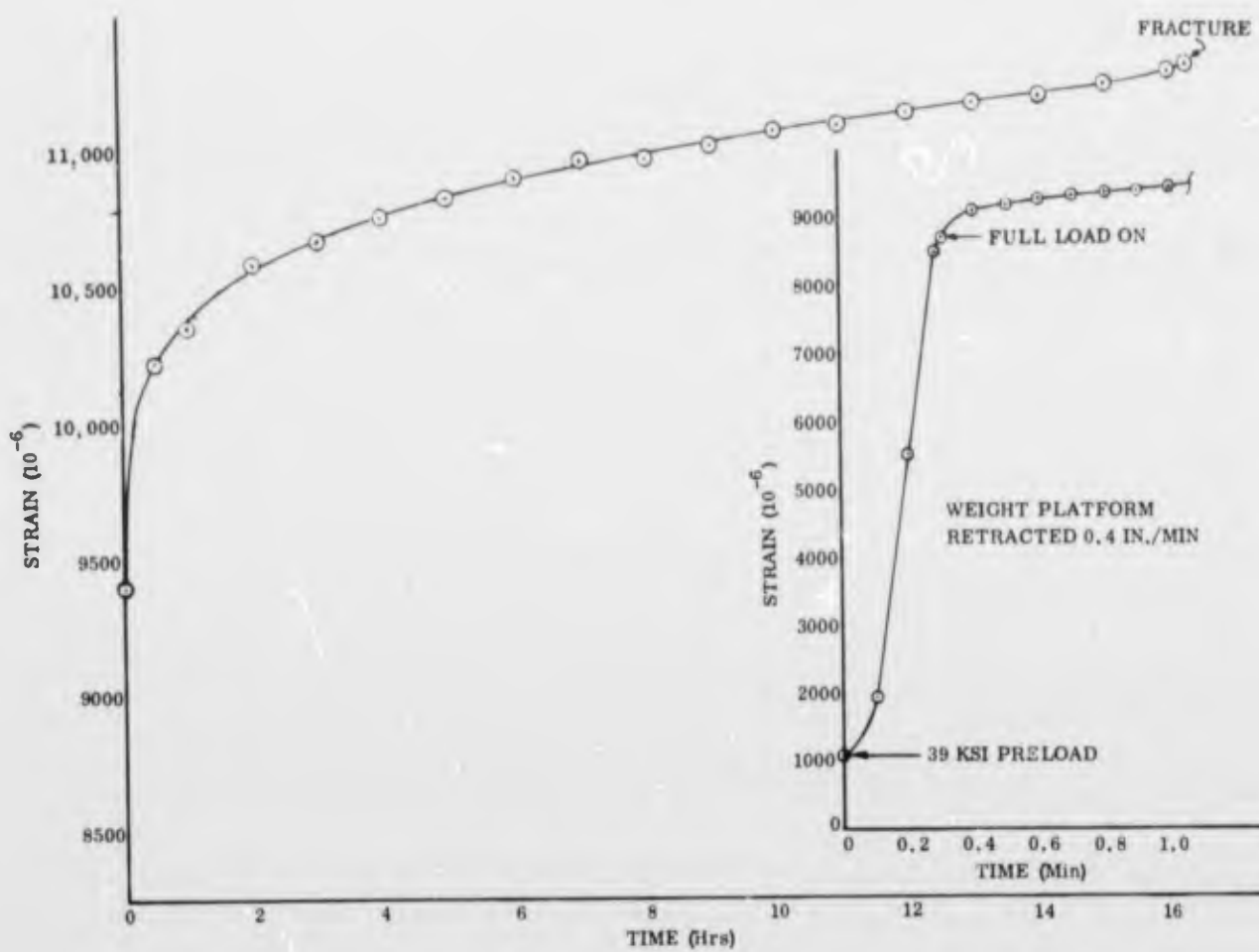
FIGURE 61.   CREEP OF 0.004-INCH DIAMETER BORON FILAMENT AT 1000 F IN
HIGH VACUUM AT 316 KSI STRESS

5.4 EFFECT OF LENGTH ON THE STRESS-RUPTURE STRENGTH OF Ti-B
COMPOSITES

According to the shear-lag theory of composites, the ineffective length of a
broken filament will be small as long as the matrix efficiently transfers the load from
the end of the broken filament to adjacent filaments. (The ineffective length is the
length over which the load carried by a broken filament is appreciably below that car-
ried by an intact filament.) Elastic analysis shows that the ineffective length depends
on $\dfrac{E_f}{G_m}$, where E_f is the filament modulus and G_m is the shear modulus of the
matrix (Ref. 14).

Broken filaments can be tolerated in a composite as long as the distance
between breaks is large compared to the ineffective length.   This is usually the case
at room temperature. At elevated temperatures, however, the properties of the
matrix become extremely time-dependent. The ineffective length then depends on the
ratio $\dfrac{E_f}{G_{m(rel)}}$ where $G_{m(rel)}$ is the relaxed modulus of the matrix (the ratio of
stress to strain after the matrix has relaxed to its equilibrium value).

90

TABLE XIX

TENSILE TESTS OF BORON FILAMENTS AND METAL WIRES

Material	Diameter $(10^{-3}$ In)	Temperature (F)	$\dot{\epsilon}$ (Min^{-1})	E $(10^6$ psi)	Prop. Limit $(10^3$ psi)	0.2% Offset Yield Strength $(10^3$ psi)	Ultimate Strength $(10^3$ psi)
Boron[1]	4.0	1000[3]	0.005	38.1	156	—	403[5]
Boron	4.0	1000	0.010	36.4	211	—	396
Boron	4.0	1000	0.050	39.9	213	—	393
René 41[2]	3.9	1000	0.005	22.9	190	270	324
AFC-77	5.9	80[4]	0.005	33.2	213	475	478
AFC-77	4.3	80	0.005	33.8	248	462	>565[6]
AFC-77 Oxidized	5.5	80	0.005	29.8	283	466	506
AM-355	3.8	80	0.005	30.4	382	496	543

(1) Supplied by Texaco Experimental, Inc.
(2) René 41, AFC-77 and AM-355 wires supplied by AFML
(3) All 1000 F tests made in 10^{-6} Torr vacuum
(4) All 80 F tests made in air at 1 atmosphere
(5) Boron filaments elongated about 0.1 percent at ultimate strength
(6) Wire slipped in grip and did not fracture

At high temperatures the relaxed stress, and hence $G_{m(rel)}$ approaches zero, and the ineffective length approaches infinity. Under these conditions the ineffective length should be equal to the length of the specimen which is heated, or in effect, the length of the hot zone of the furnace.

To investigate this effect, several stress-rupture tests were run at 1000 F on Ti-B tapes with hot sections varying in length from 5 inches to 54 inches. The results of this work are shown in Figure 62. The decreasing rupture stress with increasing specimen length indicates that the number of broken filaments is proportional to specimen length, as might be expected.

5.5 ROOM TEMPERATURE FATIGUE TESTS ON Ti-B COMPOSITES

Tension-tension fatigue tests were run on Ti-B tapes at stress ratios of A = 0.1, 0.33, and 0.67 (A = σ alternating/σ mean), on an MTS testing machine with a sinusoidal output at 30 cps. The tensile grips shown in Figure 43 were used to grip the specimens.

Figure 63 shows the S-N curve determined from these tests, and Figure 64 shows the shape of the modified Goodman diagram. The results seem to follow the
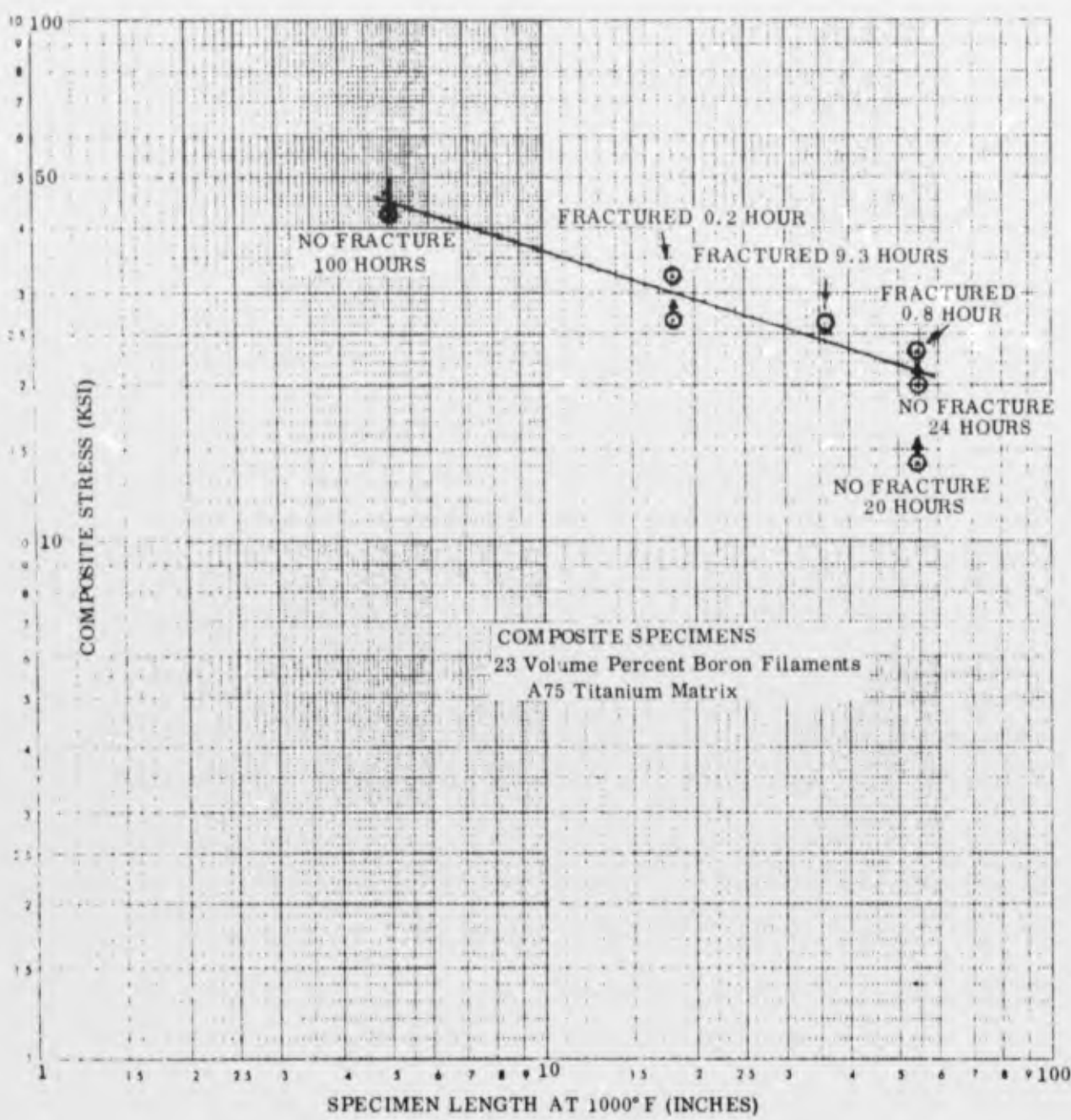
FIGURE 62.   EFFECT OF GAGE LENGTH ON RUPTURE LIFE OF TITANIUM-
BORON COMPOSITE TAPE AT 1000 F

STRESS RATIO $\quad A = \dfrac{S_{ALT}}{S_{MEAN}}$
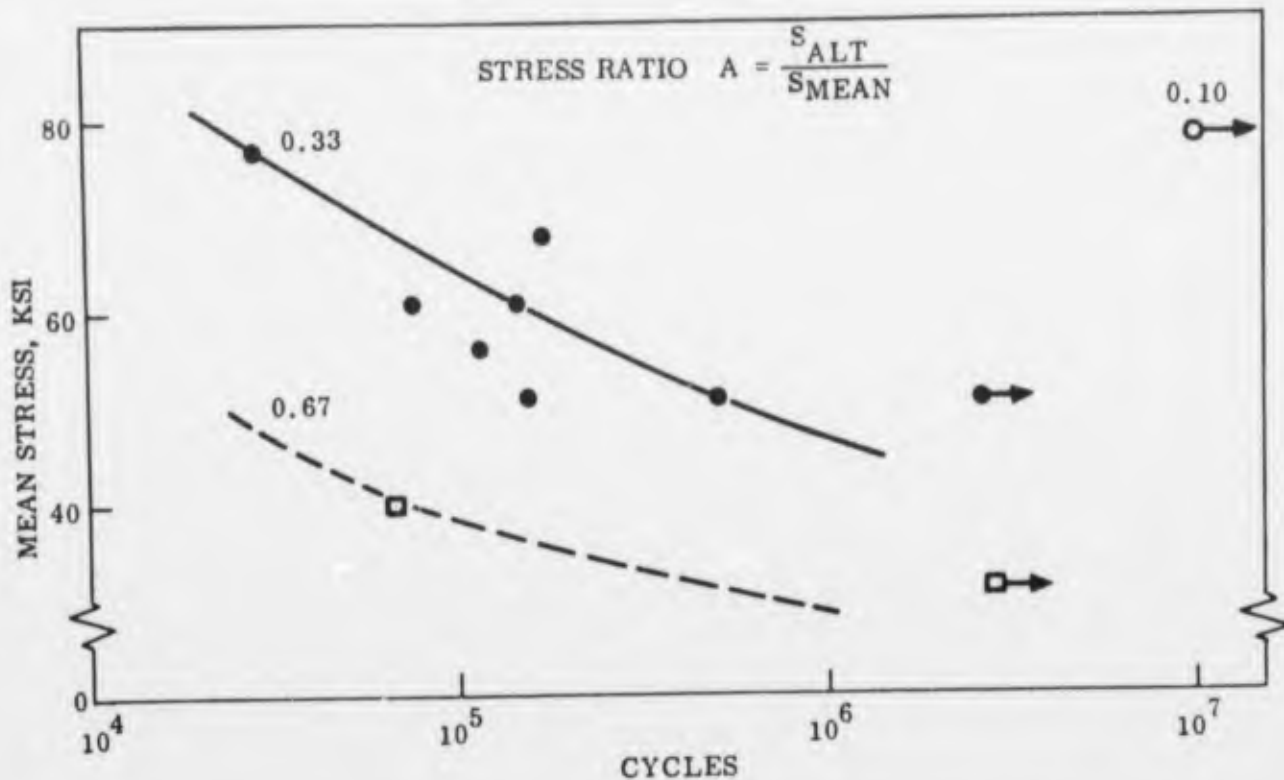
FIGURE 63. TENSION-TENSION FATIGUE TESTS OF TITANIUM-23 VOLUME PERCENT BORON TAPE
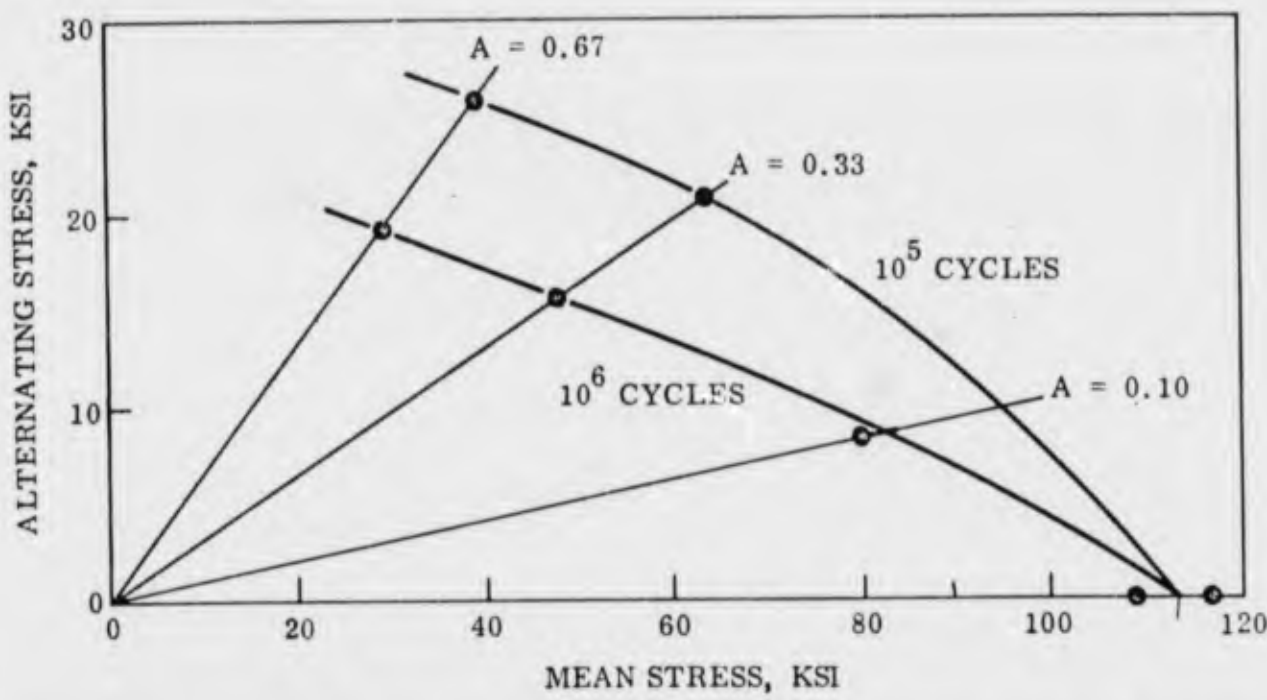
FIGURE 64. GOODMAN DIAGRAM FOR TITANIUM-23 VOLUME PERCENT BORON TAPE

93

Goodman line characteristic of brittle or notched materials rather than the Gerber parabola characteristic of ductile metals.

The tensile properties of runout specimens are listed in Table XX. These values indicate that the tensile strength was unchanged by fatigue exposure.

TABLE XX

TENSILE STRENGTH AFTER FATIGUE EXPOSURE
OF TITANIUM-23 PERCENT BORON TAPE

Fatigue Exposure Stress (ksi)		Cycles	Tensile Properties	
			Strain to Fracture (10^{-6})	UTS (10^3 psi)
	None		4680	108.5
	None		5280	116.5
78 ± 7.8		10,000,000	4400	102.5
52 ±17.7		2,621,000	4380	114.0
31 ±20.7		2,836,000	4940	115.0

5.6 DISCUSSION - COMPOSITE TESTING

Although a considerable amount of valuable data were generated during the composite testing phase of the program, it is difficult to draw conclusions regarding composite testing in general. The techniques developed were entirely satisfactory for testing titanium-boron tapes, and it is expected that the same techniques will be applicable to other composite systems having the same geometry. However, at the present time there is no such thing as a standard composite, or a standard test method for composites.

The mechanics of composite materials are very complex. The components of a composite are chosen because they have different properties which can be combined to give a material with better overall properties than either of the components alone. These individual differences complicate the stress analyses. The more the components differ in mechanical properties the further the composite deviates from the homogeneous, isotropic material required for so many elasticity and strength of materials solutions.

The rule of mixtures has been used throughout the program to calculate stresses and elastic moduli, but there are at least two reasons why this approach may not be entirely realistic.

1. The rule of mixtures does not account for residual stresses introduced during fabrication.

2. The rule of mixtures does not account for triaxial stresses due to differences in the Poisson's ratios of the components.

94

Unfortunately, the effects of both of these conditions are very difficult to predict quantitatively or to measure experimentally.

It is virtually impossible to make a metal-matrix composite without introducing residual stresses. All such composites are fabricated at elevated temperatures in order to bond the filaments securely into the matrix. Unless the coefficients of thermal expansion are identical, which is not likely, residual stresses are produced as the composite cools to room temperature. The result is that at room temperature the component with the higher coefficient of expansion is in tension and the component with the lower coefficient of expansion is in compression. When the composite is tested in tension, the apparent proportional limit of the matrix is lower than actual because of the residual tensile stress which was present in the matrix at the start of the test.

Furthermore, the equal-strain concept is not valid for computing stresses in the components because neither component was at zero strain at the beginning of the test.

As an example, the approximate coefficient of thermal expansion for boron filaments and titanium are $2.5 \frac{\mu - in}{in-deg. F}$ and $5 \frac{\mu -in}{in-deg. F}$ respectively. When these materials are diffusion bonded at 1700° F and cooled to room temperature, appreciable residual stresses can be expected. The magnitudes of these stresses cannot be predicted, however, because stress relaxation occurs rapidly in titanium above 1000° F.

It is equally difficult to predict the results of the Poisson effect. In the case of titanium-boron, Poisson's ratio for boron filaments is not known, but it is thought to be between 0.1 and 0.15. Since Poisson's radio for titanium is about 0.3, a triaxial stress state will be produced when the composite is loaded uniaxially.

In addition to these factors, one must be aware of the statistical nature of composite strengthening to interpret test data properly. One of the reasons why it is difficult to predict the strength of a composite is that the "strength efficiency" of the fibers is reduced in making a composite. That is, the average strength of the fibers in the composite will be less than the average strength of the fibers tested individually .

Sutton and Chorne (Ref. 15) have introduced the term, β, to compare the strength of fibers before and after composite fabrication.

$$\beta = \frac{\bar{S}_f^*}{\bar{S}_f} ,$$ where $\bar{S}_f^*$ is the average filament strength before fabrication and $\bar{S}_f$ is the average filament strength in the composite. The strength of the composite can then be written

$$S_C = \left[\beta \, S_f \right] V_f + \sigma_m V_m .$$ This gives a good indication of how much of the fibers' potential strength was lost in the fabrication.

The effect of length is another complicating factor. If the strength of a fiber decreases with length, then any given fiber will fracture into two or more stronger fibers. Rosen (Ref. 14) discusses the problem of composite length in terms of the "ineffective length" of the broken fiber as already mentioned in Section 5.4. According to Rosen, the ineffective length, δ, is defined by the following expression:

$$\delta = \frac{d_f}{2} \left[\frac{\left(1 - V_f^{\frac{1}{2}} \right)}{V_f^{\frac{1}{2}}} \left(\frac{E_f}{G_m} \right) \right]^{\frac{1}{2}}$$

where d_f is the fiber diameter, V_f is the volume fraction of fibers, E_f is the fiber elastic modulus, and G_m is the shear modulus of the matrix. The strength of the composite will then be a function of δ :

$$\sigma_c = V_f \left(a \delta \beta e \right)^{-\frac{1}{\beta}} + V_m \sigma_m$$

where a and β are constants which are determined from tests on the as-received fibers. Rosen points out, however, that the strength predicted by this expression cannot be expected in a real composite because the character of the fibers are usually changed by the fabrication process. The expression can be used, therefore, to determine how much of the composite's potential strength was lost in fabrication.

The strongest conclusion to be drawn from the composite-testing work presented in this report is that much additional work needs to be done in the area of composite testing. Two areas which should be studied in considerably more detail are, (1) the effect of length on composite strength, and (2) the effects of temperature and time on the mechanical properties of composites.

REFERENCES

1. Metcalfe, A. G. and Rose, F. K., "Advanced Methods to Test Thin Gage Materials". Summary Technical Report AFML-TR-65-259, Solar Division of International Harvester Company (July 1965).

2. Rose, F. K. and Metcalfe, A. G., "Advanced Methods to Test Thin Gage Materials". Summary Technical Report AFML-66-318, Solar Division of International Harvester Company (October 1966).

3. Lee, G. H., "An Introduction to Experimental Stress Analysis". Wiley and Sons, New York (1950) p. 55.

4. Pickett, G., "Equations for Computing Elastic Constants from Flexural and Torsional Resonant Frequencies of Vibration of Prisms and Cylinders". Proc. ASTM (1945) p. 846.

5. Dieter, G. E., "Mechanical Metallurgy". McGraw-Hill, New York (1961) p. 195.

6. Orowan, E., "Fatigue and Fracture of Metals". John Wiley and Sons, New York (1950).

7. Irwin, G. R., Naval Research Laboratory Report 4763 (May 1956).

8. Srawley, J. E. and Brown, W. F., "Fracture Toughness Testing and its Applications". ASTM STP 381 (1965) p. 158.

9. Boyle, R. W., Sullivan, A. M. and Krafft, J. M., "Determination of Plane Strain Fracture Toughness With Sharply Notched Sheets". Welding Research Supplement (September 1962) pp. 428-5.

10. ASTM Special Committee on Fracture Testing, "Fracture Testing of High-Strength Sheet Materials". ASTM Bulletin (January 1960) p. 29.

11. Weiss, V. and Yukawa, S., "Fracture Toughness Testing and its Applications". ASTM STP 381 (1965) p. 7.

12. Anctil, A. A., Kula, E. B. and Di Cesare, E., "Electric Potential Method for Determining Slow Crack Growth". ASTM Proc., Vol. 3 (1963) p. 799.

13. Freed, C. N. and Krafft, J. M., "Effect of Side Grooving on Measurements of Plane Strain Fracture Toughness". ASTM Journal of Materials, Vol. I (December 1966).

14.   Rosen, B.W., "Mechanics of Composite Strengthening". Fiber Composite Materials, ASM (1964) p. 37.

15.   Sutton, W.H. and Chorne', J., "Potential of Oxide Fiber Reinforced Metals". Fiber Composite Materials", ASM (1964) p. 173.